EI 110

ACTA POLYTECHNICA SCANDINAVICA

Reluctance Network for Analysing Induction Machines

JARMO PERHO

Helsinki University of Technology
Laboratory of Electromechanics
P.O.Box 3000
FIN-02015 HUT
Finland

Dissertation of the degree of Doctor of Science in Technology to be presented with due permission of the Department of Electrical and Communications Engineering, for public examination and debate in Auditorium S3 at Helsinki University of Technology (Espoo, Finland), on the 12th of December, 2002, at 13 o'clock.

ESPOO 2002

ABSTRACT

This thesis presents the components, the construction rules and the equations of the reluctance network used in the analysis of an electrical machine. It defines the equations to form the components of a single-phase electric equivalent circuit from the results of a reluctance network. As part of the study, a computer program has been developed to solve a two-dimensional reluctance network. As a result, the flux and current distributions are calculated for a cage induction motor. The rotor construction with a single-cage and double-cage winding is studied. From the analysis results, a single-phase equivalent circuit is defined to calculate the locked-rotor current of the motor in the steady-state period after the inrush current, at the moment when the rotor starts to rotate.

The target in the study is to develop a single-phase equivalent circuit for a starting motor with the effects of iron saturation and eddy-current losses included. The leakage-flux paths of the core in the rotor have their own reactances and iron-loss resistances in the single-phase equivalent circuit. The cumulative influence of the main and leakage fluxes on the magnetic saturation of the machine cross-section is taken into account by using a reluctance model covering the whole cross-sectional area of the machine. The components for the equivalent circuit are defined from the energy distribution over a period in steady-state condition.

In the analysis program, damping caused by leakage reactance of the end-windings in the stator and rotor is excluded from the model equations. Only the resistances of the windings are included to limit the supply current.

PREFACE

This research work was carried out in the Laboratory of Electromechanics of Helsinki University of Technology. The work is applied to the research field to accomplish the need of a universal magnetic model for an electrical machine. The work started from my licentiate studies, and gained new impetus from Aalborg University, Denmark.

Helsinki, May 2002

Jarmo Perho

CONTENTS

6

LIST OF SYMBOLS

A	cross-sectional area
$\mathbf{A}$	time-dependent square-matrix, (page 95)
a_i	constants in the flux-density polynomial, defined in Eq. (55)
B	flux density, defined in Eq. (23)
B	border node
C_m	magnetic capacitance, defined in Eqs. (79), (82) and (88)
$\mathbf{D}$	derivative matrix, defined in Eq. (124)
E	electromotive force
$E_{P\mathrm{fe}}$	electromotive force, equivalent in accordance with the iron losses, (page 81)
$E_{z,e}$	EMF source of a slot region, defined in Eqs. (8) and (11)
E	flux-path region, reluctance element
e	index of elements
F	force
F_m	magnetomotive force
ΔF_m	difference of magnetomotive force, defined in Eqs. (6) and (10)
$\mathbf{F}$	time-dependent vector of the sources, (page 95)
f	frequency
H	magnetic field strength
h	height
I	current
i	index, iteration-step index, imaginary unit $\sqrt{-1}$ for space coordinate
j	index, imaginary unit $\sqrt{-1}$ for time coordinate
k	time-step index
L	inductance
l	length
$\mathbf{M}$	coefficient matrix, (page 97)
m	index, number of phases, weight
N	number of time steps in period
N	number of turns, number of wires
N_eff	number of effective turns, defined in Eq. (6)
N_a	number of parallel wires
N_τ	number of pole pitches
n	quantity
n	maximum value for index
P	electric power
P_fe	iron losses

P_h	hysteresis losses, defined in Eq. (24)
P_r	eddy-current losses, defined in Eq. (24)
p	number of pole pairs
p_h	factor for hysteresis losses, defined in Eq. (24)
p_r	factor for eddy-current losses, defined in Eq. (24)
Q	number of slots
Q_c	number of slots in sector, defined in Eq. (5)
q	index of slot pitches
R	resistance
$R_{z,e}$	resistance of a slot region, defined in Eq. (7)
R_{Pfe}	resistance, equivalent in accordance with the iron losses, defined in Eq. (87)
R_m	reluctance
R_{mr}	radial reluctance, defined in Eqs. (1) - (4)
$R_{m\varphi}$	circumferential reluctance, defined in Eqs. (1) - (4)
$\mathbf{R}$	residual vector, (page 97)
r	radius
r_{in}	inner radius
r_{out}	outer radius
r_m	reluctance factor independent on reluctivity, defined in Eq. (52)
s	slip
T	time of period
T_δ	air-gap torque, defined in Eq. (45)
t	time
Δt	length of the time step, time difference
U	phase voltage
V	volume, electric voltage
ΔV	electric voltage drop
V_m	magnetic scalar potential
w	width
W_b	iron-loss energy, defined in Eq. (135)
W_e	heat-energy of winding, defined in Eq. (129)
W_m	magnetic energy, defined in Eqs. (18) and (144)
X	reactance
$\mathbf{X}$	vector of the unknowns, (page 95)
x	quantity
Z	impedance

α	angle
δ	radial length of the air gap
ε_h	loss factor of material, for hysteresis losses
ε_r	loss factor of material, for eddy-current losses
η_{fe}	fill factor of the iron sheet
Λ	permeance
λ	permeance factor independent of reluctivity, defined in Eq. (53)
ν	reluctivity, defined in Eqs. (52) and (54)
Φ	flux
φ	phase shift
Ψ	flux linkage
ω	angular frequency

Subscripts

ave	average
c	calculation sector
eff	effective
equi	equivalent
fe	iron
h	main field
(i)	iteration step
L	supply line
N	rated value
pc	sheet package of iron core
R	rotor
r	radial
S	stator
s	slot
t	tooth
v	ventilation duct of iron core
y	yoke
z	axial
δ	air gap
ε	connected to loss factor of material
Φ	flux flow
φ	circumferential

10

σ	leakage field
τ	pole pitch

Superscripts

(k)	time step
T	transposed vector, (page 96)
*	referred to stator (quantity in single-phase equivalent circuit), (page 100)

Operators

Im{}	operator giving the imaginary part of a complex number, (page 90)
Re{}	operator giving the real part of a complex number, (pages 64 and 90)
Δ	difference

Abbreviations

EMF	electromotive force
FEM	finite element method
MEC	magnetic equivalent circuit
MMF	magnetomotive force

Method of presentation for the variable type

X	the quantity
$\mathbf{X}$	vector of the quantity
$X(t)$	instantaneous value of the quantity
$\vec{X}$	complex phasor for the time-sinusoidal approximation of the quantity, (page 64)

$x(t)$	the time-sinusoidal quantity
$\hat{x}$	amplitude of the time-sinusoidal quantity, (page 64)
$\vec{x}$	complex phasor of the time-sinusoidal quantity, (page 64)

1 INTRODUCTION

1.1 Background of the work

The reluctance model has been the principal design tool for electrical machines since the beginning of the last century. The reluctance model is constructed for the main-flux path only, at first because of manual calculation, and later because of the speed of the solution. The accuracy of the main-flux path model is acceptable when we use it to determine the no-load condition. The model defines the magnetic state of the main-flux path at the maximum magnetic stresses of the mean main-flux branch. The calculation takes into account the state of side branches to the main-flux path using correction factors. To solve the loading condition, the design routine converts the quantities of the reluctance model into the components of a single-phase equivalent circuit. The leakage-flux path has its own equivalent components in the single-phase equivalent circuit. The definition of the leakage-flux components is based on the averaging formulae for every single leakage-flux path.

A reluctance model using electric components was developed to solve the magnetic state in the machine before the development of digital computers. This analogue technique was presented in the 1950's, and included the interacting electric and magnetic fields (Atkins 1958). The definition of the quantities, flux, current, energy, and torque, has been collected in (Oberretl 1963). The analogue model was used, for example, to solve the eddy-current problems (Roberts 1960). Iron saturation was taken into account in these solutions (Roberts 1962). The size of the analogue models was limited to small regions such as one slot pitch. The problems arising because of electric components are discussed in (Silvester 1967).

The rapid development of digital computers since the 1980's has led to the use of such mathematical analysis tools as FEM (Finite Element Method) in the research into magnetic fields. The reluctance model has remained part of daily design routines. The reasons for the use of the reluctance model have been the reasonable accuracy of the model and the experimental knowledge and statistics of behaviour of the model.

The reluctance model represents the geometry of the machine's cross-section. It saves the information of geometry within reluctances. We can connect reluctances in parallel or in series and create a block having only one common reluctance. However, the information of geometry remains. The reluctance model has future potential as an analysis tool in research, in particular, in the operational simulation of an electrical

machine. A simple model can solve simulation accurately enough more quickly than a small FEM model.

In the Laboratory of Electromechanics at Helsinki University of Technology, the development of a computer program using a reluctance network was started in 1989. The development was part of a two-years project, "Development of an inverter driven electrical motor". The result of the development was a computer program calculating a single-phase equivalent circuit for a cage-induction motor.

The development of the new computer program-package for this study began at Aalborg University, Denmark. In the summer of 1994, Prof. Ewen Ritchie of Aalborg University organised a PhD course in the use of reluctance networks and proposed co-operation to create a universal program by using the reluctance network method (Magnetic Equivalent Circuit, MEC). The aim of the co-operation was that both of the laboratories might develop a program that would be suitable for their own area of interest and add to the knowledge of the program.

In the Laboratory of Electromechanics, the main target in the development of the new MEC model has been flexibility of modelling. The computer program package is made up of separate and independent subprograms. To analyse the magnetic field and electric quantities, the program package includes the system equations for the quantities in the reluctance model. In the analysing program, e.g. time-stepping method, the necessary subprograms form the system equation matrices. The system equation matrix can be solved by an external solver. The user can choose from the alternatives to the flux-path element definitions, the reluctance model construction, and the reluctance network definitions. The definition rules form the rules of a universal reluctance network. The alternatives to the rules are a collection of variations concentrating on a particular type of electrical machine.

1.2 Conventional reluctance model

The conventional reluctance model has only one branch, the mean branch of the main-flux path. At the no-load condition, a supply voltage causes a current in the excitation winding of the machine. The amplitude of the flux caused by the current, and the flux distribution inside the machine depend on the magnetic circuit of the machine. The time variation of the flux distribution follows mainly the time variation of the supply voltage in an ac-excited machine and the rotational speed of the rotor in a dc-excited machine. The flux causes a magnetic saturation of the core of the machine. This causes a non-sinusoidal space variation of the flux distribution over the machine's

cross-section. The reluctance model takes into account the side branches of the main-flux path using correction factors. The flattened air-gap flux-density distribution, the flux leakage along the tooth, and the uneven flux distribution in the yoke have their own correction factors to modify the components of the reluctance model. The correction factors are partly empirical and reflect the manufacturers working routine. They are often in the form of a diagram or table.

By the use of computers, conventional reluctance models can have extra branches (Vogt 1983). When the machine has a distributed excitation winding, the reluctance model may be widened to the entire pole pitch. The branches have identical elements to the mean branch, but the model gives better agreement than the mean branch alone. Certain correction factors may be omitted, and the flux distribution at the no-load condition improves.

1.3   A short review of the use of the conventional reluctance model

The routine to design an electrical machine uses the reluctance model to determine the properties of the machine in different loading conditions. The quantities of the reluctance model are converted into the components of a single-phase electric equivalent circuit. The magnetic circuit of the machine and the losses generated in the machine have their own equivalent components in the equivalent circuit (Arnold & la Cour 1909, Richter 1951, Vogt 1983, Perho 1993). In the conventional machine design, the variation of the quantities is assumed to be sinusoidal. The non-sinusoidal variations of quantities are approximated by the sinusoidal fundamental-harmonic components. The currents and voltages in the single-phase equivalent circuit are phasors.

The permeances from the main-branch reluctance-model are converted into the main reactance of the single-phase equivalent circuit. The losses of the reluctance model are converted into the resistances of the single-phase equivalent circuit. The main reactance is an average value over the machine cross-section. The components comprising the main reactance are the permeances along the main-flux path

- the permeance of the yoke in the stator,
- the permeance of the tooth in the stator,
- the permeance of the air gap,
- the permeance of the tooth in the rotor, and
- the permeance of the yoke in the rotor.

The values of the permeance components in all regions are defined at no-load and the excitation of the machine at the rated voltage. By the use of computers, the permeance components may also have a flux dependence or a current dependence defined as a function of the current or voltage in the equivalent circuit.

The leakage-flux paths have either their own equivalent reactances or a common equivalent reactance in the single-phase equivalent circuit. The values of these reactances must be calculated from averaging formulae for every single leakage-flux path. The leakage-flux paths are taken into account as separate and independent flux paths. Every flux path has an experimental equation for its permeance depending only on the machine's dimensions (Richter 1936).

1.4   A short review of research using the reluctance network method

The MEC model has been used to analyse electrical machines such as an asynchronous machine fed by an inverter (Hrusovsky & Hrabovcova 1995, Perho 1993, Perho & Ritchie 1995), a permanent magnet motor (Perho & Ritchie 1996, Rasmussen & Ritchie 1997), and a linear stepping motor (Wang & Gieras 1998). The possibility to simplify the MEC model and to minimise the system equations has lead to new approaches such as a solution of a three-dimensional magnetic field for a disk induction motor (Ciosk & Gierczak 1998), the coupling of an MEC model with FEM analysis (Gyselinck et al. 1998), a vibration and noise analysis for an electrical machine (Vandevelde et al. 1998), and an analysis of skewing in a three-dimensional MEC model (Sewell et al. 1998).

The size of the MEC model depends on the analysis. For the simulation of a motor operation, the MEC model should be small in order to minimise calculation time. For example, in the simulation of the transient state under local magnetic fault conditions (Ah-Jaco et al. 1998), the reluctance model of an asynchronous motor used consists of slot pitches with a reduced number of reluctances. The main flux path has a circumferential saturable reluctance for the yoke and a radial saturable reluctance for the tooth. The leakage flux path has a circumferential unsaturable reluctance branch for the wound slot part and a circumferential saturable reluctance branch near the air gap, with a series reluctance of the tooth tip and the slot opening reluctances. The reluctance model in the air gap consists only of the radial reluctances between the opposite stator and rotor teeth. Using the reluctance combination method of Ostovic (Ostovic 1989b), the unknown variables are four potentials in a connected slot pitch. A minimal number of elements are similarly necessary when modelling skewing in three-dimensional analysis (Sewell et al. 1998).

The theory for a numerical solution of an MEC model and its components has been presented by (Ostovic 1989a), (Gagnon et al. 1993), and (Xiaogang et al. 1995), and in combination with FEM model analysis (in discussion of Mukherjee et al. 1989). The problems with the three-dimensional MEC model are presented by (Sewell et al. 1998).

1.5   Magnetic saturation in a single-phase equivalent circuit

To simulate machine reliability in action, the user needs a single-phase electric equivalent circuit of the machine. It must be simple to make the simulation fast. A problem arises when the machine parameters are unknown. Not all of the necessary parameters can be defined by standard measurements. Alternative methods to provide standard definitions and to determine machine parameters have been developed (Ganji et al. 1996). Problems relating to the small size and the accuracy requirement remain. Different single-phase equivalent circuits for a cage induction machine have been presented, with eddy current branch (Fujimaki & Miyashita 1985, Hamels 1984), with leakage-flux path losses (Jagiela 1985, Perho 1993), with multi-branch impedance of rotor bar (Paszek 1981, Paszek & Pawelek 1984), and with separation of stator and rotor iron losses (Udayagiri & Lipo 1989).

In the simulation of electrical machines, the need for a simple saturation model in the single-phase equivalent circuit is obvious. The conventional analysis of magnetic paths is not popular when investigating the saturation of iron in flux paths. There are different variations for the saturation model to use in the operational simulation. A common feature among these models is the problem solving method. The single-phase equivalent circuit is standard in form, and the new effect, saturation, is applied to it by force. The modelling of the saturation is done using mathematical functions. Examples include the saturated equivalent circuits for a cage induction machine (Ferreira de Jesus 1988), for an inverter fed cage induction machine (Andria et al. 1986, Hasuike 1984), for a switched reluctance motor (Athani & Walivadekar 1994), and for a cage induction machine with a solid steel or copper layer rotor (Gibbs 1948). A new saturation term has also been applied in the single-phase equivalent circuits of space-vector theory, 'cross-saturation' (Brown et al. 1983, Kamoun & Popoujadoff 1986, Li 1996, Levi 1997), which takes into account the saturation of the real main-flux path on the two orthogonal axes of d and q. Special equivalent circuits have also been published with a divided rotor cage model calculated by FEM analysis (Healey et al. 1994).

The saturation of the main flux path in the yoke has been investigated using classical theory (Gynt & Schuisky 1958, Fritz 1989, Weh 1957), the MMF (magnetomotive force) harmonics (Qishan 1986), and a layer division in the reluctance model (Dudzikowski 1994). The saturation of the main-flux path in the teeth is investigated using classical theory (Gynt & Schuisky 1958).

The saturation of the leakage-flux path has been studied by many authors. Different solutions have been presented to take into account the slot form near the air gap. The conventional method is the analysis of the real flux paths. An analysis for open and semi-closed slots with an iterative process has been presented by (Agarwal & Alger 1961, Akbaba & Fakhro 1987). The saturation of the closed slot has a model of a variable fictitious slot opening (Akbaba et al. 1987, Savelainen 1980). The saturation of the zigzag flux path is studied by (Beier, 1964). The saturation factors for different slot types are presented by (Angst 1963, Chalmers & Dodgson 1969, Mouly et al. 1983). Another approach has involved leakage-flux calculation using FEM analysis and a single rotor slot (Richter et al. 1981). An analysis using the Fourier series in magnetic field components is presented in (Rogers & Benaragama 1978).

The starting current of a cage-induction motor has been calculated taking into account the current distribution in the rotor bar without saturation by (Bolte 1981), and by using FEM analysis (Andresen & Müller 1983). The problems of electromagnetic fields in the rotor slot are presented by (Iwata 1984, Sliwinski 1987).

The calculation of the special iron-loss components has been studied for a cage-induction motor with frequency-converter supply (Andresen et al. 1986), for a permanent magnet motor (Atallah et al. 1992), for pole shoes of a salient pole machine (Gibbs 1947, Moriyasu & Endo 1980), and tested with a special machine for a cage induction motor (Chalmers & Richardson 1966). The stray-load losses of a cage induction motor have been discussed widely and a wide overview is provided by (Jimoh et al. 1985) and a report of the test results of calorimetric measurements by (Löser & Sattler 1986).

1.6   Reluctance network of the study

The deficiency in the conventional reluctance model is that the main-flux path is separated from the leakage-flux path. In a real machine, the magnetic saturation of the material in the main-flux path affects the magnetic state of the leakage-flux path. On the machine cross-section, the real flux paths include the same regions of material, and their fluxes have a cumulative influence on the magnetic saturation of the region.

The leakage-flux paths may be taken into account more effectively by using a more sophisticated reluctance model covering the whole cross-sectional area. The time dependence of the flux paths may be taken into account more precisely by using a special reluctance model for the air-gap region when the rotor is rotating.

In the present study, the magnetic model of a cage-induction motor is constructed using a reluctance model. The model describes the cross-section of the motor. The electric models for the windings of the motor, the magnetic model, and the mechanical model of the motor are connected according to Fig. 1 to a reluctance network model. The voltage or current supply is connected to the terminals of the primary winding. The primary winding is the distributed stator winding. Every coil of the primary winding has a connection to the reluctance model as a current source. The reluctance model operates as an electromotive-force source for every coil. The secondary winding is supplied from the reluctance model. The secondary winding is the cage winding of the rotor. Every bar of the secondary winding has a connection to the reluctance model as a load. The reluctance model operates as an electromotive-force source for every bar. The rotational angle of the rotor is solved from the air-gap torque calculated from the reluctance model. In this study, the rotor is locked.
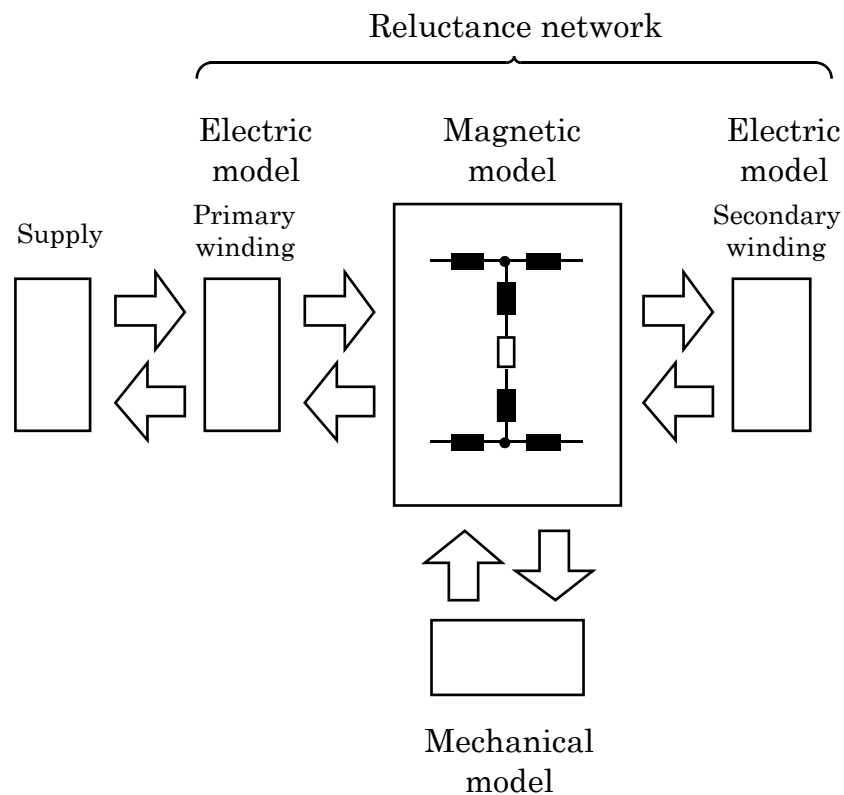
Fig. 1   Construction of the reluctance-network model in the study.

In the machine cross-section, the main-flux path includes all the side branches parallel to the mean main-flux branch. All the other elementary flux paths belong to the leakage-flux path. The reluctance model of the study consists of reluctance elements in which the flux path is divided into two main perpendicular directions. The elements model flux paths when the flux flows through an element along either direction alone or along both directions on the same time. The saturation of iron in an elementary flux path is taken into account defining the magnetic properties of the equivalent reluctance element by using the total flux density of element.

1.7   Single-phase equivalent circuit of the study

In this study, the reluctance network model will be used to define the components of a single-phase equivalent circuit. The equivalent circuit is standard in form, Fig 2. The rotor model is constructed as for a double-cage rotor. The components of the equivalent circuit are defined using the flux-path definitions of the reluctance model (Perho 1993). The magnetic energy of an elementary flux-path is modelled in a reactance X. The iron losses of the same elementary flux-path are taken into the equivalent circuit using a resistance R_{fe} connected parallel to the reactance X. The modelling of the winding losses follows the reluctance network definitions, too. The losses of the conductor connected to a reluctance element are modelled as a part of resistance R.

An energy component of an elementary flux-path has to be named to belong to a main-flux or a leakage-flux component in the single-phase equivalent circuit. The decision will be made according to the flux routes on the machine cross-section. The naming is clear in the elementary paths of the yoke region. The routes of both the flux
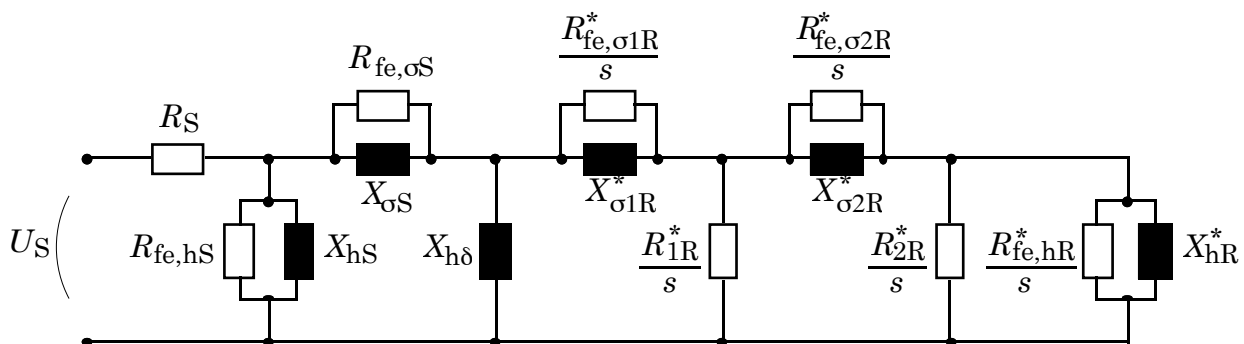
Fig. 2   The single-phase equivalent circuit of the cage-induction motor (Perho 1993). The components of the main flux path have an index h and the components of the leakage flux path an index σ. The components of stator, rotor and air gap have indices S, R and δ,. The asterisk indicates that the quantity is referred to the stator.

components join in the elements of yoke. The effect of the leakage flux will be included in the reactance X_h of the main-flux path. In the tooth region, the routes of the flux components deviate. Both the deviating routes need their own component in the single-phase equivalent circuit. The effect of the leakage flux will have an own component X_σ in the equivalent circuit in series with the reactance X_h of the deviating main-flux path. In the air-gap, the energy is concentrated to one reactance of main-flux path in this study.

1.8 The aim of the study

This thesis introduces the structure of the universal reluctance network used in the computer-program package developed. It specifies the rules for the construction of the network, the definitions of the material properties used in the modelling, and the system equations. It describes the method for the construction of a single-phase equivalent circuit from the results of the reluctance network. It presents the rules for the universal reluctance network by solving as an example a cage-induction machine. It further provides alternatives of the rules for this machine type.

The applied part of this study concentrates on the leakage-flux paths on the machine cross-section. The principal intention is to model the magnetic field distribution near the air-gap region with a small reluctance network. The target machine type is a cage-induction motor. The emphasis is on the locked-rotor current in the steady-state period after the inrush current, at the moment when the rotor starts to rotate. The currents and the magnetic fluxes have their steady-state values. In practice, this happens when the input voltage of the stator winding is increased slowly and the rotor is locked at stand-still. The major purpose is to develop a single-phase equivalent circuit for a starting motor with the effects of iron saturation and eddy-current losses included. Two cage-induction motors will then be analysed, a single-cage 15 kW and a double-cage 37 kW four-pole motor.

The aim of the study is to introduce a single-phase equivalent circuit and a reluctance network model working together. The components of the equivalent circuit are defined from the results of analysis using the reluctance network model. The components of the equivalent circuit have the properties of the flux paths modelled by the reluctance network.

In this study, the reluctance network is limited so as to model only two-dimensional flux distributions. The three-dimensional leakage-flux paths of the coil ends of the windings are outside the scope of this study. The reactances of these paths can be

included as extra leakage inductances to the single-phase equivalent circuit presented in this study.

1.9 Outline of the thesis

This thesis consists of ten chapters. In Chapter 1, a brief introduction about methods of modelling magnetic fields, problems of single-phase equivalent circuits and a summary of previous studies to connect special demands to the single-phase equivalent circuit are given. The purpose of this research is described and the outline of the thesis is sketched.

In Chapter 2, the basic reluctance element for the reluctance model will be introduced. The construction rules of the reluctance model for the machine cross-section will be given. The reluctance network will be constructed by connecting the reluctance model and the electric circuits of the machine windings. The components and the specifications of the reluctance network will be given.

In Chapter 3, the equations of magnetic and electric circuits of the reluctance network will be introduced. The equations of magnetic energy, flux density, iron losses, and air-gap torque will be given. All the equations will be defined for a reluctance element.

In Chapter 4, the material properties will be introduced. The definitions of magnetic axial length of the reluctance model will be given. The reluctivity of a reluctance element has a definition basing on the material data and on the total flux density of the reluctance element. In this chapter, the reluctivity definition will be shifted according to the flux density component of the main direction of the flux flow. The redefinition is meant to be used only in certain special cases discussed in the chapter.

In Chapter 5, a magnetic capacitance will be introduced as an analogue for the resistive losses in the magnetic circuits. The capacitance may be used for conductor losses or partly for iron losses of the reluctance element (eddy-current losses). It will give the same phase shift and energy loss as the resistive current circuit of the conductor.

In chapter 6, the equations introduced in Chapter 3 are collected as a matrix equation for the reluctance network. The principle of solution of the matrix equation will be shown.

In Chapter 7, the method to define the components of a single-phase equivalent circuit will be introduced. The method bases on the energy distribution in the reluctance network. A reference slot-pitch model will be used as an energy equivalent for the reluctance network. The energy of the reluctance network will be collected to the equivalent regions of the reference slot-pitch model. An equivalent region will have an analogue component in the single-phase equivalent circuit. The component will include the material properties of the slot-pitch region. The saturation of iron will have an effect to the flux-density variation in the reluctance element. The same effect will be seen in the energy of the reluctance element and its analogue component in the single-phase equivalent circuit.

In Chapter 8, a computer program package will be introduced. The program was developed to solve a reluctance network model. The program bases on a universal reluctance network. The universal reluctance network is a tool to analyse magnetic field and electric circuits connected to the reluctance model. The target of the analysis can be any electrical machine or magnetic component.

In Chapter 9, two squirrel cage motors will be analysed, a 15 kW single-cage and a 37 kW double-cage asynchronous motor. A two-dimensional reluctance model will be defined for both the motors using the presented methods in earlier chapters. The reluctance networks will be defined and solved, and the results will be introduced. Both the motors will have same kind of single-phase equivalent circuit where the values of the components will be defined from the energy distribution of the analysis in the reluctance model.

Chapter 10 will summarise the research and assess the method proposed for suitability for analysis and design of electrical machines and magnetic circuits.

2 MESH GENERATION

The aim of this chapter is to specify a universal reluctance network for use with the electrical machines. The version of the network presented in this chapter will be magnetically two-dimensional. The principles of network construction will be solved in the context of a radial-flux slotted machine with either a concentrated or cage winding in the stator and rotor.

In a rotating radial-flux electrical machine, the axial dimension of the machine is greater in comparison with the circumferential dimension of the machine. The core of the machine may be treated magnetically as infinitely long. This assumption means that the flux distribution is constant in the axial direction of the machine and that the flux has no component in the axial direction. The flux distribution may be defined for the cross-section of the machine and using a two-dimensional magnetic model.

The reluctance network is a magnetic equivalent circuit that describes magnetic flux paths on the cross-section of the target electrical machine. The reluctance network includes the reluctance models of the stator, rotor and air gap, and the electric models of the stator and rotor windings.

The chapter is divided into main topic sections: reluctance element, elementary mesh for the core and the air gap, reluctance model of machine cross-section, and connection between magnetic and electric models.

2.1 Reluctance element

This section introduces the basic component of the reluctance model, a reluctance element for a flux-path region.

The reluctance model is based on the flux paths over the machine cross-section. The flux path has an equivalent circuit component in the reluctance model, a reluctance element, as in Fig. 3. When the flux-path is divided into smaller parts, every flux-path division has its own reluctance element. The reluctance elements of the divisions form a chain of elements as an equivalent for the flux path.

The reluctance element has its own branches among the flux components flowing through the flux-path region. A three-dimensional region has a circumferential, a radial, and an axial branch in its reluctance element. To minimise the reluctance
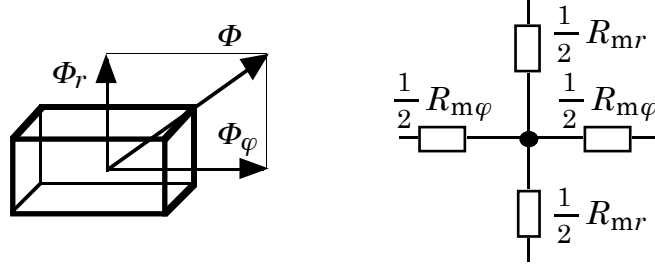
Fig. 3   A flux-path region and its equivalent two-dimensional reluctance element.

model, two-dimensional modelling is selected in this study, and only the circumferential and radial branches are taken into the reluctance element.

The circumferential branch of the reluctance element has a reluctance $R_{m\varphi}$ defined for the circumferential flux component Φ_φ. The radial branch of the reluctance element has a reluctance R_{mr} defined for the radial flux component Φ_r. Both branches are connected in a scalar magnetic potential node. The reluctance components in the main directions are divided to both sides of the node, as in Fig. 3. In the simulation, the magnetic state of the reluctance element is defined as a function of the total flux density of the flux-path region. The values of the branch reluctances depend on each other according to the reluctivity of the entire flux-path region.

2.2   Elementary mesh for the core region

This section defines the basic unit of the reluctance model, an elementary mesh for the slot pitch. The definition of the elementary mesh is based on the flux-region layers where every layer is a portion of the flux path. The construction of the elementary mesh and the problems in the refinement of the elementary mesh will be discussed in this section.

The machine cross-section may be divided into repetitive areas according to the slotting. The natural division of the cross-section is the unslotted and the slotted areas. For the flux-path regions, those areas are dealt with in circular layers. The layers are referred to as the layers of the yoke, and the layers of the slotting. Every circular layer has the same circumferential base-division according to the slotting.

The stator and rotor have different divisions of the circular layers in the circumferential direction. The basis of the division is the minimum circumferential repetitive unit, the slot pitch. This is a sector of the core that includes one tooth and

one slot. The symmetry division of the stator and rotor depends on the windings and on the positions of the stator teeth and stator slot openings compared with the rotor teeth and rotor slot openings. The symmetry division is the smallest collection of slot pitches in which the properties of the machine can be comprehensively studied. The symmetry division is a repetitive construction division that includes only one pole pitch or a collection of pole pitches as a minimum.

To define the reluctance model for the flux path, a collection of reference flux-path regions is used. The basis for the reference regions is a sector. All other reference regions are used to model the slot or the pole depending on the machine type. The slot or pole dimensions define the type of the flux-path regions, a rectangle, a trapezium, or a circular region. A flux-path region may also be a combination of reference regions.

2.2.1 Reference flux-path regions

The present study uses the reference flux-path regions to construct the reluctance model. The base region is a sector layer, Fig. 4. The others are a rectangle, a trapezium, and a circular region modelling the slot regions, Fig. 5.

The radial and circumferential reluctance components of the sector, $R_{\mathrm{m}r,e}$ and $R_{\mathrm{m}\varphi,e}$, are

$$
\begin{cases}
R_{\mathrm{m}r,e} = \dfrac{\nu_e}{l_e} \dfrac{1}{\alpha_e} \ln\!\left(\dfrac{r_{\mathrm{out},e}}{r_{\mathrm{in},e}} \right) \\[4ex]
R_{\mathrm{m}\varphi,e} = \dfrac{\nu_e}{l_e} \dfrac{\alpha_e}{\ln\!\left(\dfrac{r_{\mathrm{out},e}}{r_{\mathrm{in},e}} \right)}
\end{cases}
\tag{1}
$$

where the quantities are, as in Fig. 4,
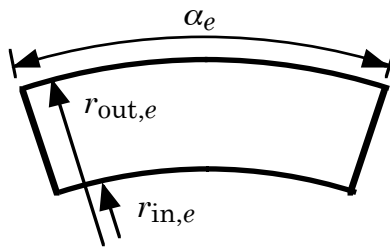
Fig. 4   The basic reference flux-path region, a sector.

v_e reluctivity,

l_e axial length,

α_e angular width,

$r_{\text{out},e}$ outer radius, and

$r_{\text{in},e}$ inner radius.

The radial and circumferential reluctance components of the slot region are

- for a rectangle, Fig. 5a,

$$
\begin{cases}
R_{\mathrm{m}r,e} = \dfrac{v_e}{l_e}\dfrac{h_e}{w_e} \\[3mm]
R_{\mathrm{m}\varphi,e} = \dfrac{v_e}{l_e}\dfrac{w_e}{h_e}
\end{cases}
\tag{2}
$$

- for a trapezium, Fig. 5b,

$$
\begin{cases}
R_{\mathrm{m}r,e} = \dfrac{v_e}{l_e}\dfrac{h_e}{w_{e2}-w_{e1}}\ln\!\left(\dfrac{w_{e2}}{w_{e1}}\right) \\[4mm]
R_{\mathrm{m}\varphi,e} = \dfrac{v_e}{l_e}\dfrac{w_{e2}-w_{e1}}{h_e}\dfrac{1}{\ln\!\left(\dfrac{w_{e2}}{w_{e1}}\right)}
\end{cases}
\tag{3}
$$

- for a circular region, Fig. 5c,
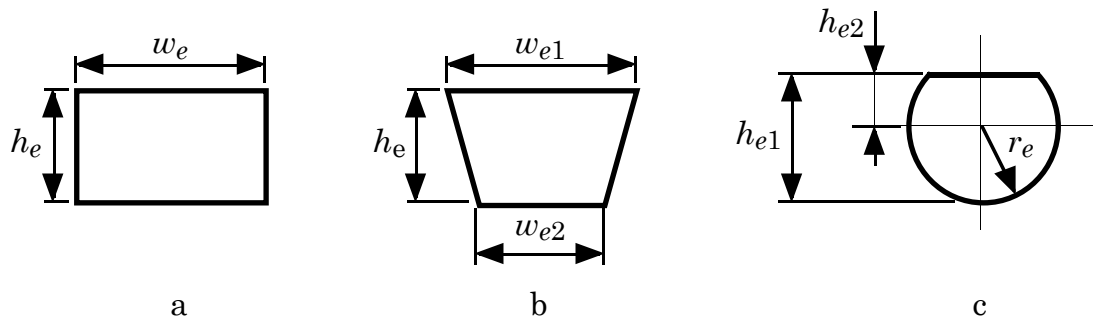
Fig. 5   The reference regions of the slot are
a) rectangle, b) symmetric trapezium, and c) segment of a circle.

$$\begin{cases} R_{\mathrm{m}r,e} = 0.5 \dfrac{v_e}{l_e} \left[\arcsin\left(\dfrac{h_{e2}}{r_e}\right) + \arcsin\left(\dfrac{h_{e1} - h_{e2}}{r_e}\right) \right] \\[4ex] R_{\mathrm{m}\varphi,e} = \dfrac{v_e}{l_e} \dfrac{2}{\arcsin\left(\dfrac{h_{e2}}{r_e}\right) + \arcsin\left(\dfrac{h_{e1} - h_{e2}}{r_e}\right)} \end{cases} \tag{4}$$

2.2.2 Generation of the slot-pitch mesh

A slot-pitch region includes four flux-path regions, as in Fig. 6. The flux-path regions of the yoke (E_{y1} and E_{y2}) are the circumferential divisions of the circular layer of the yoke. The flux-path regions of the slotting (E_s and E_t) are the circumferential divisions of the circular layer of the slotting. Each region can have a circumferential and a radial subdivision inside its sector without any response from neighbouring regions. The flux transfer between the regions crosses at the borders of the regions.

The slotting layer has the regions of the slot E_s and the tooth E_t. The circumferential division between the regions E_s and E_t bases on the slot dimensions. The main subdivision in the radial direction is the same in both the regions. The radial division is based on the slot definitions. The divisions are the opening, the top, the middle, and the bottom of the slot.

Flux-path regions are defined together with the neighbouring regions. The circular layer of the slot-pitch division has an equivalent reference region of a sector, as in
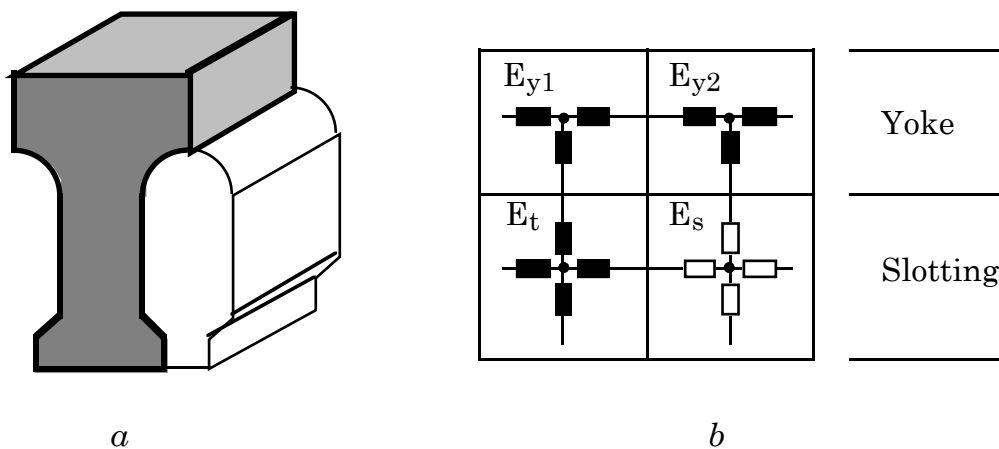
Fig. 6 A slot pitch model.
a) A slot pitch of an electrical machine with the tooth and slot sectors.
b) The equivalent reluctance model. The white-coloured reluctance components are of constant reluctivity. The black-coloured ones are of flux dependent reluctivity.

Fig. 7. This is the base for determining the flux-path regions. In the slot E_s, the portion of the slot has a form of a reference region, as in item 2 of Fig. 7. To construct the flux-path region for the tooth E_t, as in item 1 of Fig. 7, the region of the slot is separated from the sector region. The divisions of the bottom, middle, top, and opening of the slot are separated independently, Fig. 8. The yoke layer has the same circumferential division as the slotting layer. The circumferential division of the yoke layer, E_{y1} and E_{y2}, is made by dividing the slot-pitch sector between the regions according to the neighbouring regions E_{s1} and E_{t1}.
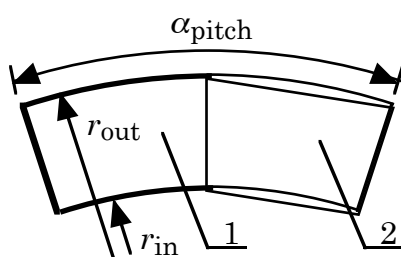
Fig. 7   A division of the sector flux-path region on the slot pitch division.
Item 1 is a flux-path region of the tooth E_t and Item 2 a region of the slot E_s.

a

b
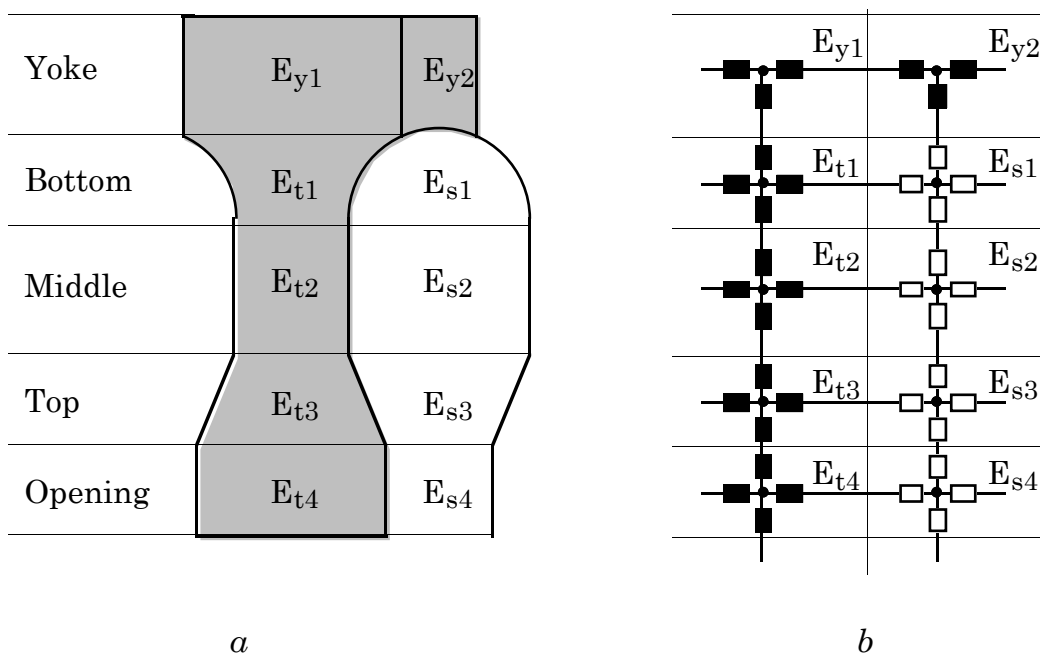
Fig. 8   The divisions of the slot-pitch sector.
a) The flux-path regions E_s and E_t are divided into radial divisions according to the slot definitions. The divisions of the bottom, middle, top, and opening of the slot are separated independently according to Fig. 7.
b) The reluctance model of the slot-pitch sector.

2.2.3 Refinement of the mesh

To analyse the properties of the flux-path region, the basic subdivision according to the slot dimensions does not always be accurate enough. The basic subdivision has to be divided to smaller regions. The new division may be done inside the target region maintaining the neighbouring regions unchanged. The division may not change the flux flow to the neighbouring regions. The connections to the neighbouring regions must be secured by using a border node. The border node presents the magnetic potential at the border line between the regions.

The correct division does not affect the flux flow through the divided region. Fig. 9a presents a model of the region before division. Fig. 9b presents the same region after an incorrect division. The reluctance value of the route between border nodes B_1 and B_3 differs from the reluctance value before division. The division provides a new parallel route through the border nodes B_2 and B_4. The corrected model is presented in Fig. 9c. The model is constructed using two divisions in radial and two in circumferential direction. Only the possible flux routes are presented. Every subregion has its own reluctivity value according to the flux flow through the subregion.

The smallest division in refinement is two to all directions. When using a larger number of divisions in a region to radial or circumferential direction, it will happen that the branches to the border node short-circuit divisions. If the division of the neighbouring region may not be subdivided to the same direction, the only possible solution is to increase the subdivision of the target region also to the other direction.

a   b   c
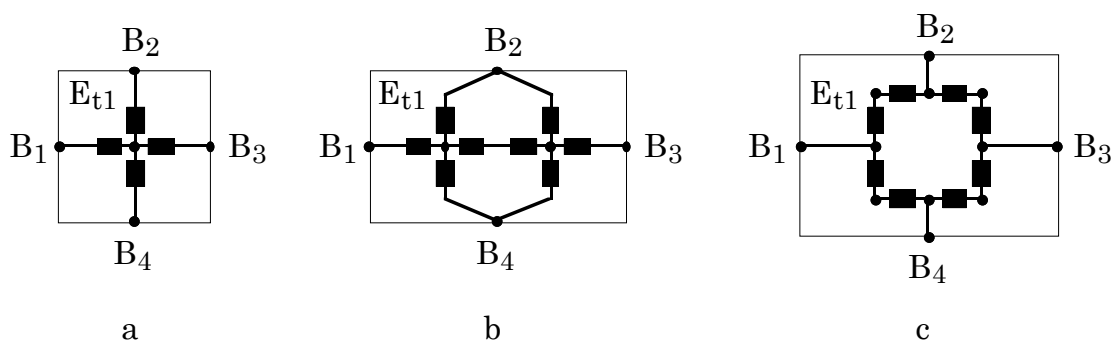
Fig. 9 Subdivision alternatives inside the flux-path region.
a) The basic division of region E_{t1} before subdivision.
b) An incorrect subdivision: the reluctance of region E_{t1} changes because of the passing routes through the border nodes B_2 and B_4.
c) A corrected subdivision of b: the division of region E_{t1} without changes to the flux paths.
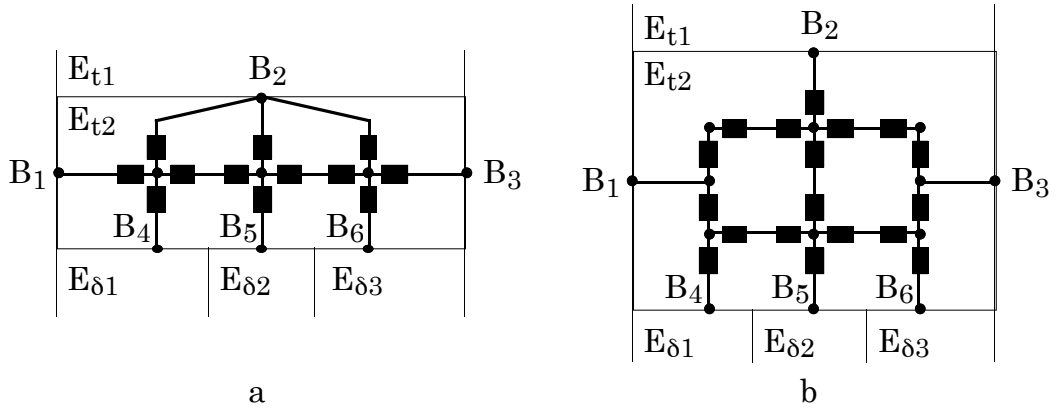
Fig. 10 Subdivision alternatives inside the flux-path region.
a) An incorrect subdivision: the reluctance of region E_{t2} changes because of the passing routes over the middle subdivision, presented in Fig. 2.11 (Rasmussen 1996).
b) A corrected subdivision: the division of region E_{t2} without changes to the flux paths.

Rasmussen (Rasmussen 1996) used a special circumferential division at the top of the tooth to obtain a more accurate air-gap model, as in Fig. 10a. Three circumferential divisions of region E_{t2} (the top of the tooth) are connected to region E_{t1} (the main tooth) using the common border node B_2 and to region E_δ (the air gap) using border nodes B_4, B_5 and B_6. There is a short-circuit to the circumferential flux path from the neighbouring teeth over the middle division of region E_{t2}. A corrected subdivision is presented in Fig. 10b. There the radial division of region E_{t2} is two.

2.3   Elementary mesh for the air-gap

This section defines the construction rules for the air-gap elementary mesh. The air-gap reluctance model is not constant; it will change according to the rotor position.

The air gap has its own circular layer between the stator and rotor. The layer has a circumferential width defined by the common symmetry division of the stator and rotor. The axial length of the layer is the magnetic length of the air gap. The opposite positions of the stator slot pitches and the rotor slot pitches give the number of divisions in the flux-path region E_δ. The minimum repetitive construction division in region E_δ is one pole pitch or a collection of pole pitches. The air-gap reluctance model differs from the stator and rotor reluctance models only in the manner of renovation at each time step when the rotor is rotating.

The air-gap reluctance model connects the stator and rotor reluctance models. The circumferential subdivision of the air-gap layer is based on the positions of the stator

slot pitches relative to the rotor slot pitches. The opposite positions of the slot pitches change when the rotor rotates. To simplify the construction of the reluctance model of the entire machine, the stator and rotor reluctance models have border nodes on all tooth and slot opening elements on the borderline of the air gap. This ensures that the stator model and the rotor model may be independent of the construction of the air-gap model.

To ensure modularity, the definition of the air-gap flux-path regions is of constant dimensions. The air-gap region E_δ is divided radially into two regions. One region is connected to the stator, $E_{\delta,S}$, and the other to the rotor, $E_{\delta,R}$, as in Fig. 11a. Regions $E_{\delta,S}$ and $E_{\delta,R}$ are defined according to the slot pitches of the connected machine parts. The basic circumferential divisions of regions $E_{\delta,S}$ and $E_{\delta,R}$ are based on the circumferential divisions of the reluctance models of the tooth and slot opening.

The air-gap region E_δ is the union of regions $E_{\delta,S}$ and $E_{\delta,R}$. The circumferential division of region E_δ is based on the opposite positions of the divisions in regions $E_{\delta,S}$ and $E_{\delta,R}$, as in Fig. 11a. When a division in region $E_{\delta,S}$ has a common sector with a division in region $E_{\delta,R}$, the common sector between the air-gap borders of the stator

a   b
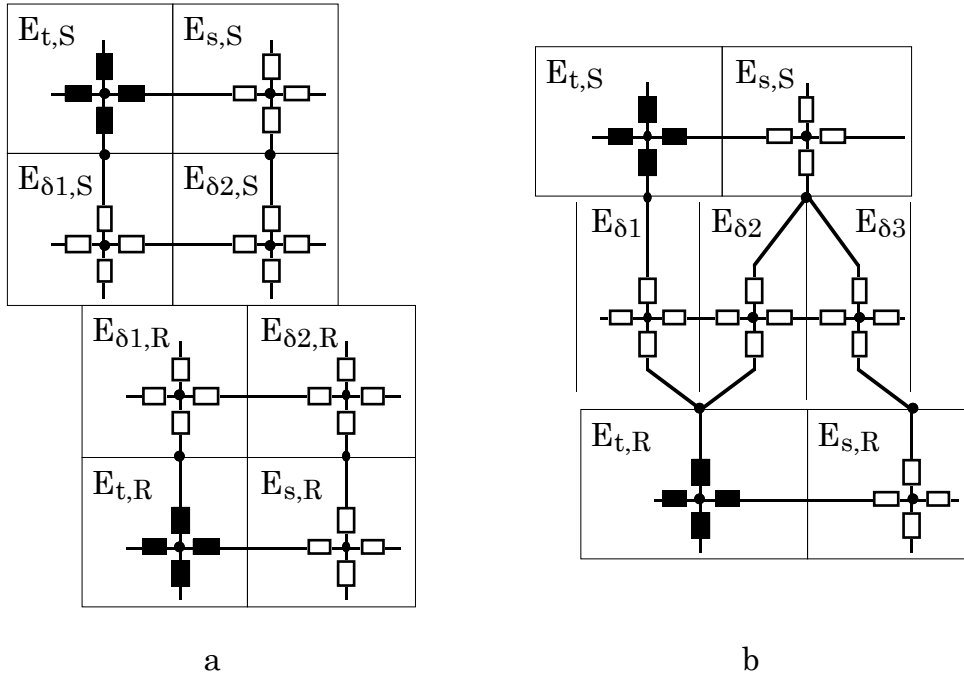
Fig. 11   The construction of the air-gap region E_δ.
a) The opposite positions of the divisions in the regions $E_{\delta,S}$ and $E_{\delta,R}$, and
b) the resulting division of the air-gap region E_δ connecting the stator and rotor models.

and rotor forms a division in region E_δ, as in Fig. 11b.

In the air-gap model, the border node may have multiple branches, Fig. 11b. Under the tooth, the short-circuiting route of the circumferential air-gap flux does not represent a significant error. When two flux-path regions pass each other in the air gap (through the border node on the tooth), it may be considered as a real flux passing along the tooth top with an infinite permeability.

Under the slot opening, the short-circuiting route of the circumferential air-gap flux causes a more significant error in the analysis. The error grows when the proportion of the width of the slot opening to the pole pitch increases. These cases are e.g.

-       an open slot opening in a large machine using preformed preinsulated coils, and
-       a small number of slots for pole and phase or
        a small pole pitch in a machine with open or semi-closed slot opening.

The reason for the error is that the short-circuited and the neighbouring regions are of same material and the degree of saturation of material is the same. The error changes when the air-gap model is rebuild because of the rotation of rotor. The error affects to the magnetic width of the tooth. The size of the error depends on the degree of magnetic saturation of the machine. A solution is to divide the border layer on the slot opening into smaller regions.

The accuracy of the simulation may demand a further subdivision of the air-gap region E_δ both in the radial and in the circumferential directions. To solve a no-load condition or a loading condition, the simulation may be sufficiently reliable when using a simple air-gap model, as in Fig. 12b, in which the connection between the stator and rotor has radial components only (Ostovic 1989a, Perho 1993). The simulation of the leakage fields, as in the short-circuit condition, requires a better model with the possibility to model the circumferential flux components in the air gap (Perho & Ritchie 1995), as in Fig. 12c and 12d.

The only way to increase the circumferential division in the air-gap region E_δ is to increase the circumferential divisions in the stator and rotor reluctance models. The stator tooth and slot regions, $E_{t,S}$ and $E_{s,S}$, could have a circumferential subdivision, e.g. three and two in Fig. 12a. The rotor tooth and slot regions, $E_{t,R}$ and $E_{s,R}$, could have a circumferential subdivision, e.g. two for both the regions in Fig. 12a.
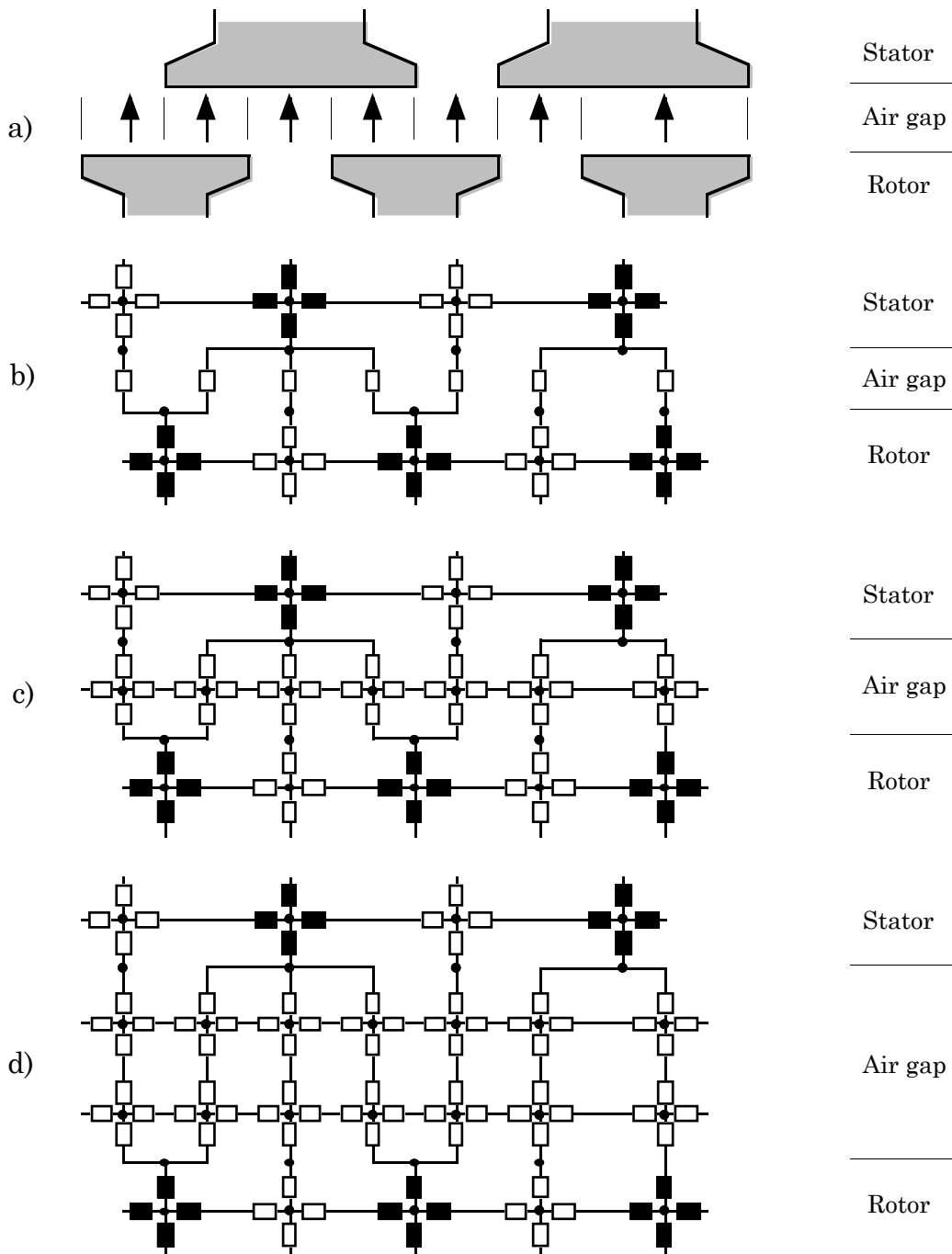
Fig. 12 Definition of the reluctance model for the air gap.
a) The flux paths between the stator and rotor.
b) Reluctance model has only radial flux paths.
c) Reluctance model has radial and circumferential flux paths.
d) Reluctance model has a radial division of two in radial and circumferential flux paths.

2.4 Reluctance model of the machine cross-section

This section defines the smallest reluctance model of the machine cross-section. The definition depends on the symmetry of the stator and rotor constructions.

The complete models for the stator and rotor include the flux-path regions E_s, E_t, and E_y of all the slot pitches. The flux-path regions of the slot pitches are combined. As a result, there are separate stator and rotor reluctance models. The flux-path regions are of constant form during the computation. The stator and rotor reluctance models with the air-gap reluctance model form the reluctance model of the machine.

It is possible to reduce the size of the reluctance model. The stator and rotor reluctance models are constructed using the repetition of the slot pitches. The resulting reluctance model of the machine cross-section has a repetition depending on the number of pole pitches and on the symmetry of the windings. This repetitive sector defines the number of flux-path regions required in the comprehensive analysis.

The smallest possible repetitive sector of the reluctance model is the sector of one pole pitch. The boundaries of the repetitive sector reflect the calculated properties as an image over the boundaries. The boundaries act as property mirrors when the number of pole pitches in the repetitive sector, $N_{\tau c}$, is not an even number. The results of the analysis using the repetitive sector may be copied over the entire machine cross-section taking a mirroring if needed.

The numbers of slots included in the repetitive sector, $Q_{c,S}$ for the stator and $Q_{c,R}$ for the rotor, are

$$
\begin{cases}
Q_{c,S} = N_{\tau c} \dfrac{Q_S}{2p} \\[2mm]
Q_{c,R} = N_{\tau c} \dfrac{Q_R}{2p}
\end{cases}
\tag{5}
$$

where

Q_S is the number of slots of the stator,
Q_R is the number of slots of the rotor, and
p is the number of pole pairs.

2.5   Connection between magnetic and electric models

This section specifies an extended definition for the basic reluctance element presented in Chapter 2 and defines an electric element with a connection between the reluctance and electric models of the flux-path region.

A flux-path region of conductor has an equivalent element both in the magnetic model and in the electric model. In the reluctance model, the conductor is as a current source presented there with a magnetomotive force (MMF) source F_m. In the electric model, the flux-path region operates as a voltage source for the conductor, and is presented with an electromotive force (EMF) source E. The EMF source is caused by the flux variation in the flux-path region. The MMF source of the reluctance model and the EMF source of the electric model transfer the energy between the models.

The extended reluctance element will take on a source component. The new extension is an equivalent for the flux-path region with an MMF source F_m divided to both sides of the node, as in Fig. 13b. The MMF may be caused by a permanent magnet or by a current. The study concentrates only on the MMF caused by a current.

a   b   c
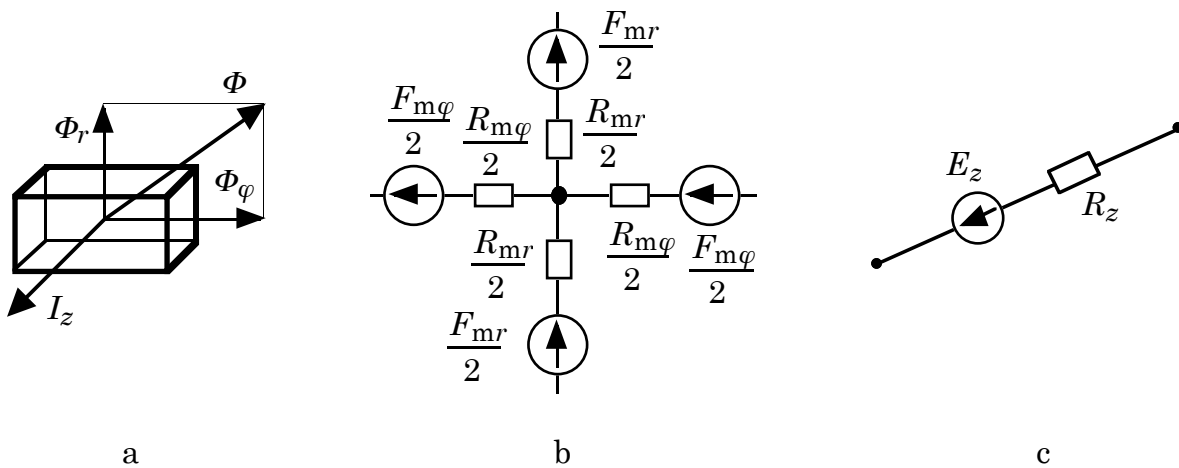
Fig. 13   A flux-path region of conductor and the equivalent magnetic and electric elements of the region.
a) A flux-path region of conductor has the flux components Φ_r and Φ_φ, and the axial current I_z flowing through the region.
b) The extended reluctance element consisting of branch reluctances and MMF sources divided to both sides of the node. The components F_{mr} and $F_{m\varphi}$ are assumed not to be present simultaneously.
c) The electric element consisting of an EMF source E_z induced from the flux variation and an axial resistance of conductor R_z.

An electric element is a model of a conductor in an electric model. In the two-dimensional reluctance model, the current of the conductor has only the axial component I_z on the machine cross-section. The electric model can still be three-dimensional, only the axial branch of the electric element can have connection to the reluctance model. The axial component of the electric element consists of the branch resistance of the conductor R_z and an EMF source E_z, as in Fig. 13c.

2.5.1 Electric element

The MMF source of the reluctance model is caused by a flux-path region of an axial conductor in which a current flows, as in Fig. 13a. The current density is assumed to be constant over the flux-path region. In the reluctance element, the MMF source caused by the current in the region can be modelled only to one main direction, in either a radial or circumferential direction. The placement and the value of the MMF source F_m depend on the other MMF sources of the reluctance model.

The winding of the machine may have a three-dimensional electric model consisting of three-dimensional electric elements, as in Fig. 14. The electric model of the conductor presented in Fig 13c is the axial branch of the whole three-dimensional electric element. The radial and circumferential conductors of the winding are outside of the flux-path regions modelled by the two-dimensional reluctance model. The electric element, in Fig. 14, has nodes on the both ends of the axial branch. The resistance R_z and the EMF source E_z of the axial branch are between the nodes. The resistances of the radial and circumferential branches, R_r and R_φ, modelling the radial and circumferential conductors are divided to both sides of the nodes.
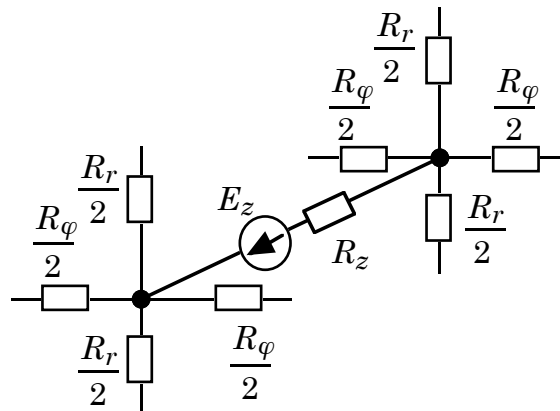
Fig. 14   A three-dimensional electric element of a winding.
The axial branch models the flux-path region with a conductor, a part of a winding.
The radial and circumferential branches model the part of the winding outside of the flux-path regions modelled by the two-dimensional reluctance model.

2.5.2 Distributed winding

In a distributed winding, the current flows in parallel and serial wires. In the reluctance model, the assumption made in the modelling of the winding is a uniform current density distribution over the entire coil area in the slot.

The current of a coil side forms a group of MMF sources distributed to all the reluctance elements on the sector of the slot region E_s, and of the neighbouring yoke region E_{y2}, as in Fig. 15. The distributed winding causes the MMF sources in the reluctance model only on the circumferential branches of the reluctance elements. The MMF increase $\Delta F_{m,e}$ in an element of the slot region is

$$\Delta F_{m,e} = \frac{A_{z,e}}{A_{coil}} \frac{N_{coil}}{N_{a,coil}} I_{coil} = \frac{A_{z,e}}{A_{coil}} N_{eff,coil} I_{coil} \tag{6}$$

where

a   *b*

Fig. 15   The MMF sources from the slot current in the slot-pitch model.
a) The division of the slot-pitch sector to layers. The yoke layer E_y is divided according to the slotting layer divisions E_t and E_s. Both the slotting layer divisions are divided according to the slot dimensions. The current is flowing in the regions E_{s1} and E_{s2} of the slot.
b) The reluctance model of the slot-pitch sector. The regions E_{y2}, E_{s1} and E_{s2} have the MMF sources only in the circumferential branches of the reluctance elements divided to both sides of the nodes.

$A_{z,e}$ is the axial current-carrying area of the element,

A_{coil} is the total area of the coil in the slot,

N_{coil} is the number of wires in the coil and

$N_{\text{a,coil}}$ the number of parallel wires in the coil.

$N_{\text{eff,coil}}$ is the number of effective turns of the coil, and

I_{coil} is the current of the coil.

The value for the MMF source is cumulative starting from the air-gap border-regions to the yoke. The MMF value grows linearly within the flux-path region where the current flows, as in Fig. 16. The value of the MMF source associated with the reluctance element is an average value of the cumulative MMF acting on the element.

To define the electric model of the distributed winding, the coil side may be replaced with an equivalent coil wound around the yoke in the slot sector, as in Fig. 17a. In the reluctance model, the wound area of the slot will be divided according to the slot dimensions, as in Fig. 15. The same division shall be done in the electric model, too. The equivalent coil will be divided according to the slotting division, in Fig. 17a to a coil of flux-path region E_{s1} and to a coil of region E_{s2}. Both of the region coils have their own electric elements in the electric model. The electric elements have a EMF source $E_{z,s1}$ or $E_{z,s2}$ on the axial branch of the electric element. The EMF source is supplied from the flux-flow variations inside the region coils in flux-path regions E_{s1}, E_{s2} and E_{y2}. The EMF value grows linearly within the flux-path region, as in Fig. 16.
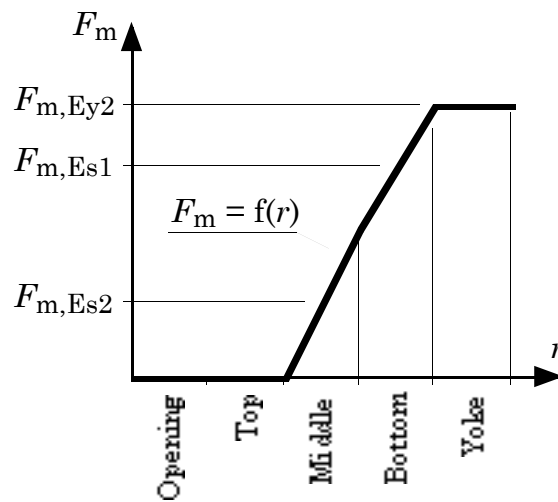
Fig. 16   The MMF distribution of the coil side as a function of radius from the air gap to the yoke.
The MMF sources for the reluctance elements E_{s2}, E_{s1} and E_{y2} in Fig. 15 have an average value from the cumulative MMF value acting on the reluctance element.

Fig. 17 Definition of the electromotive force for a distributed winding.
a) Two equivalent coils of the slot regions E_{s1} and E_{s2} are wound around the yoke and connected in series forming the real coil side.
b) The electric model of the real coil side connecting the electric elements of the slot-region coils in series.

The electric model of the coil side is in Fig. 17b. Only the axial branch of the basic electric element is used. The resistance $R_{z,e}$ of the slot-region coil is

$$R_{z,e} = \frac{1}{2} \frac{A_{z,e}}{A_{\text{coil}}} R_{\text{coil}}$$

(7)

and the EMF source of the branch is

$$E_{z,e} = \frac{A_{z,e}}{A_{\text{coil}}} \frac{N_{\text{coil}}}{N_{\text{a,coil}}} \left[\frac{1}{2} \left(\frac{\mathrm{d}\Phi_{\varphi,e}}{\mathrm{d}t} \right) + \sum_{i=1}^{e-1} \left(\frac{\mathrm{d}\Phi_{\varphi,i}}{\mathrm{d}t} \right) \right]$$
$$= \frac{A_{z,e}}{A_{\text{coil}}} N_{\text{eff,coil}} \left[\frac{1}{2} \left(\frac{\mathrm{d}\Phi_{\varphi,e}}{\mathrm{d}t} \right) + \sum_{i=1}^{e-1} \left(\frac{\mathrm{d}\Phi_{\varphi,i}}{\mathrm{d}t} \right) \right]$$

(8)

where the summation goes from the flux of the yoke region to the neighbouring region corresponding to the target electric element E_e.

The coil-side EMF is the sum of the EMF sources of all the elements of the coil side

$$E_z = \sum_e E_{z,e} \qquad\qquad (9)$$

2.5.3   Cage winding

In a cage winding, the current flows in single conductors in each slot. The divisions of slot region, E_s, divide the single conductor into a multiple cage winding comprising a collection of elementary bars connected parallel, as in Fig. 18a. In the reluctance model, the assumption made in the modelling of the winding is a uniform current density distribution over the elementary bar.

The currents of the elementary bars form a group of MMF sources distributed to all the reluctance elements on the sector of slot region E_s and of the neighbouring yoke region E_{y2}, as in Fig. 18b. The value for the MMF source is cumulative starting from the air-gap border-region to the yoke, as in Fig. 19. The cage winding causes the MMF sources only on the circumferential branches of the reluctance elements. An axial

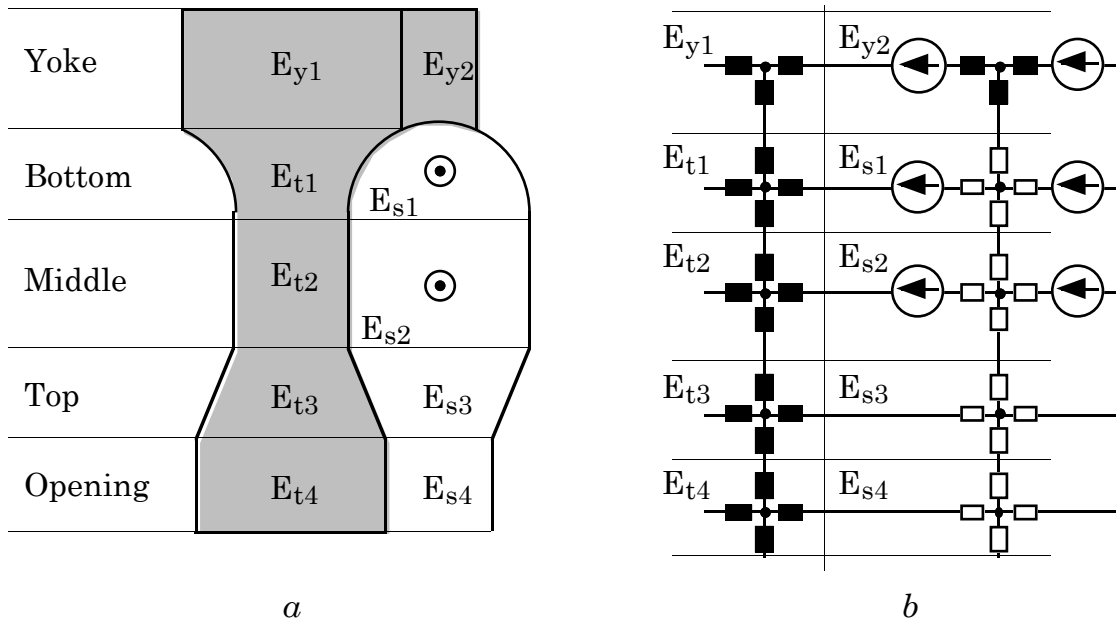*a*   *b*
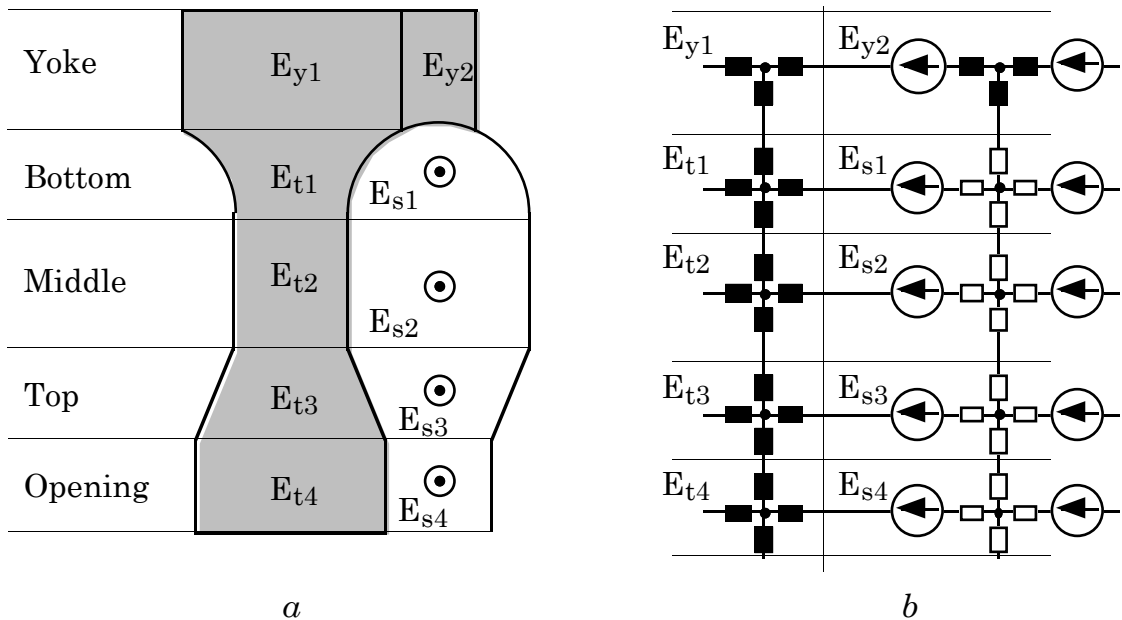
Fig. 18   The MMF sources from the slot current in the slot-pitch model.
a) The division of the slot-pitch sector to layers. The yoke layer E_y is divided according to the slotting layer divisions E_t and E_s. All the slotting layer divisions are divided according to the slot dimensions. The current is flowing in all the regions of the slot.
b) The reluctance model of the slot-pitch sector. All the regions in the slot sector have the MMF sources in the circumferential branches of the reluctance elements divided to both sides of the nodes.
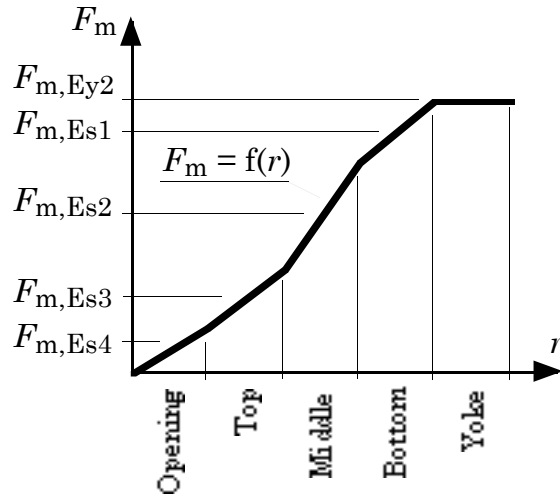
Fig. 19   The MMF distribution of the cage-winding bar as a function of radius from the air gap to the yoke.
The MMF sources for the reluctance elements in Fig. 18 have an average value from the cumulative MMF value acting on the reluctance element.

current $I_{z,e}$ flowing in the elementary bar causes an increase $\Delta F_{m,e}$ in the MMF distribution

$$\Delta F_{m,e} = I_{z,e} \tag{10}$$

The value of the MMF source associated with a reluctance element is an average value of the cumulative MMF acting on the element, as in Fig. 19.

To define the electric model of the cage winding, the end-ring of the winding has to be divided circumferentially into sectors of slot pitches and radially into parts according to the height of the elementary bars. In the electric model of the winding, the elementary bar and the division of both the end-rings have a common three-dimensional electric element, as in Fig. 14. To define the EMF source on the axial branch of an electric element, the elementary bar may be replaced with an equivalent coil, having one effective turn, wound around the yoke in the slot sector, as in Fig. 20a. The equivalent coils are separate and connected together in the electric model of the slot. The EMF sources of the coils E_{s1} to E_{s4} are supplied from the flux-flow variations inside the coils in flux-path regions E_{s4} to E_{y2}. The EMF value grows linearly within the flux-path region, as in Fig. 19.
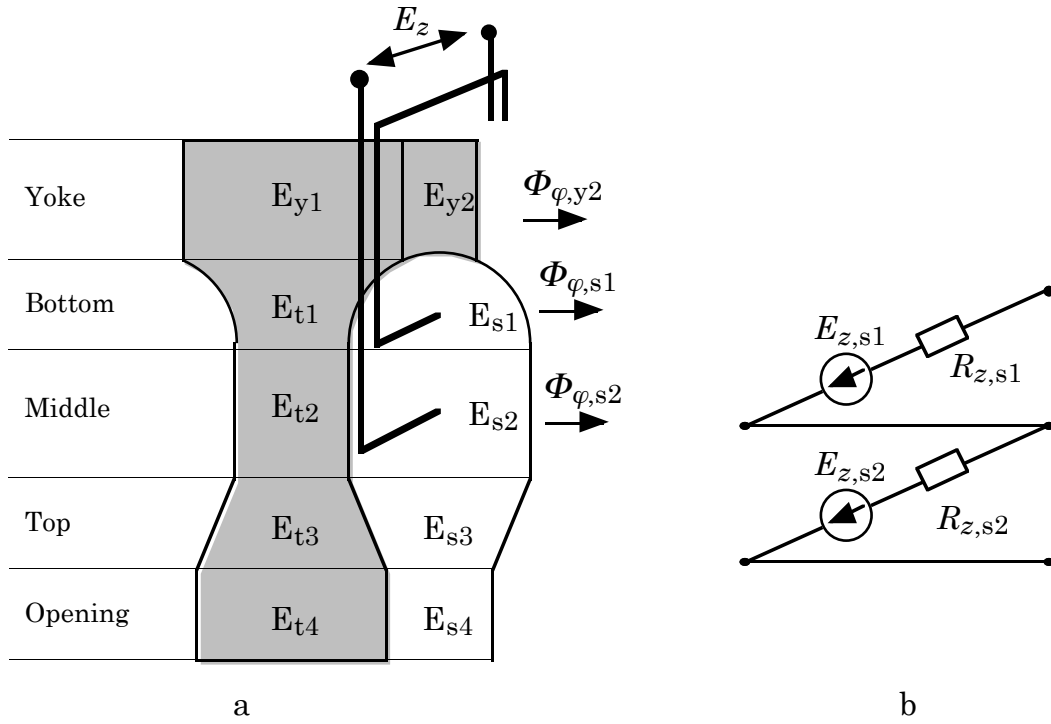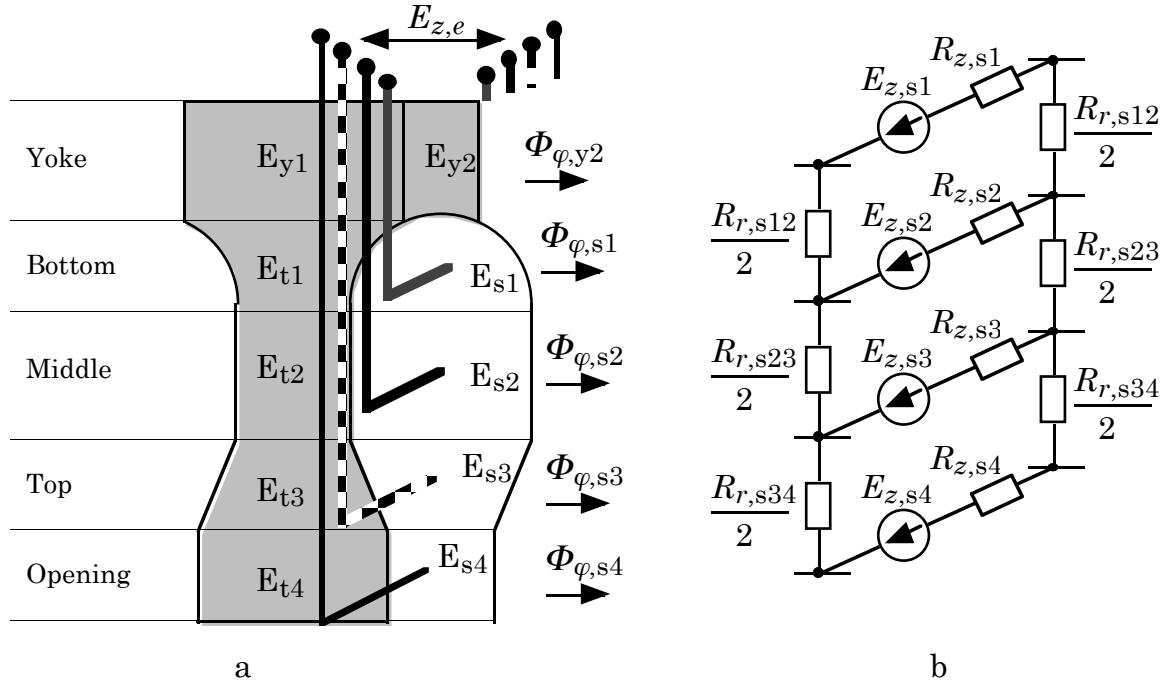
Fig. 20   Definition of the electromotive forces for a cage winding.
a) The equivalent open coils of the slot regions E_{s1} to E_{s4} are wound around the yoke.
Their connection is made in the electric model.
b) The electric model of the bar connecting the electric elements of the slot-region coils.

The electric model between the elementary bars is in Fig. 20b. The EMF sources $E_{z,e}$ are the EMF sources of the equivalent coils E_{s1} to E_{s4}. The bar resistance $R_{z,e}$ and the radial and circumferential end-ring resistances $R_{r,e}$ and $R_{\varphi,e}$ have to be defined from the dimensions of the slot regions and the end-rings.

The EMF source of an equivalent coil E_e is

$$E_{z,e} = \frac{1}{2}\left(\frac{\mathrm{d}\Phi_{\varphi,e}}{\mathrm{d}t}\right) + \sum_{i=1}^{e-1}\left(\frac{\mathrm{d}\Phi_{\varphi,i}}{\mathrm{d}t}\right) \tag{11}$$

where the summation goes from the flux of the yoke region to the neighbouring region corresponding to the target electric element E_e.

2.6 Conclusion

In this chapter, rules for the construction and the components of the universal reluctance network have been specified. The basic elements of the network, the reluctance element and the electric element, were introduced.

The machine cross-section was divided to slot pitch sectors, and the sectors to layers. Every layer was divided to flux-path regions according to the slot dimensions. The reluctance model for the slot pitch was constructed using the reluctance and electric elements representing the flux-path regions. The slot-pitch model is the basic unit to build the reluctance model of the stator, rotor, and air gap. The number of the slot-pitch models included in the modelling depends on the magnetic and electric symmetry of the stator and rotor windings and cores. Alternative versions of the air-gap model were presented.

The reluctance models of stator, rotor and air gap form the model of the machine. The electric elements form the electric models of the windings. Together, the reluctance model sand the electric models are the reluctance network of the electrical machine. The MMF sources of the reluctance model and the EMF sources of the electric model provide the energy transfer between the models.

In the next chapter, the equations connected to the reluctance network will be introduced and the methods to solve the properties of the reluctance network will be presented.

3   SYSTEM EQUATIONS

The aim of this chapter is to specify the equations to solve the properties of the universal reluctance network, the system equations. The specification demands to define the specifications of the magnetic energy and flux density of the reluctance element, and the air-gap torque connected to the reluctance model. The flux density and air-gap torque specifications are based on the magnetic energy of the reluctance element.

The system equations of the universal reluctance network are related to the electric models of the windings and the reluctance model of the flux-path regions. The voltage equations of the stator winding are related to the electric supply connected to the electric model of the distributed winding. The voltage equation of the current loop in the rotor winding is connected to the electric model of the cage winding. The flux-balance equation is related to the magnetic scalar potential of the node in the reluctance element. The equations of the magnetic energy, iron losses, flux density, and air-gap torque are connected to the flux-path region.

3.1   Voltage equations

This section presents the voltage equations for the electric model. The equations are presented for a distributed winding and for a cage winding.

The voltage equation of a phase in the distributed winding is constructed as a current loop between the supply of the electric network and the winding, as in Fig. 21. In
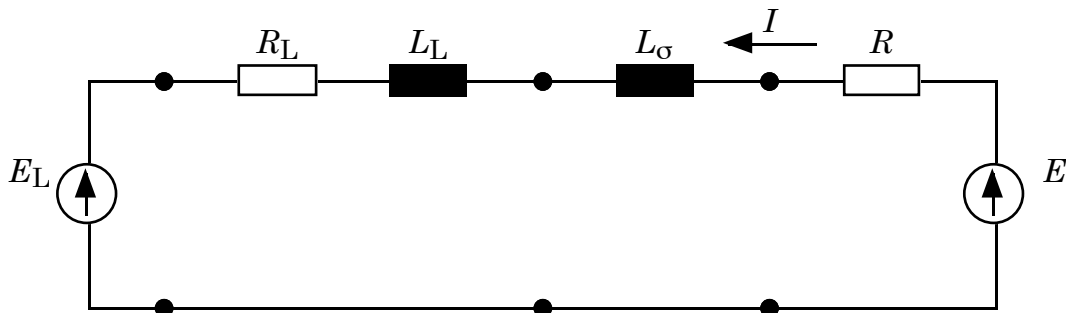
Fig. 21   The current loop for the voltage equation of a phase in a distributed winding. A principle presentation of the current loop. The components of the supply line have an index L. The inductance L_σ is the leakage inductance of the end-winding. The components E and R without any index are from the electric model of the winding.

Fig. 21, the presentation of the current loop is a principle one and used only to introduce the method. The voltage equation of the current loop is

$$\left(R_{\mathrm{L}} + R\right)I + \frac{\mathrm{d}}{\mathrm{d}t}\left[\left(L_{\mathrm{L}} + L_{\sigma}\right)I\right] + E - E_{\mathrm{L}} = 0 \tag{12}$$

where

E_{L} is the EMF of the supply,
R_{L} is the resistance of the supply line,
L_{L} is the inductance of the supply line,
L_{σ} is the leakage inductance of the end-winding,
E is the EMF of the electric model of the phase,
I is the current of the electric model of the phase, and
R is the resistance of the electric model of the phase.

In the analysis, the winding connection has to be taken into account. Because of the non-linear properties of the magnetic model, all the phase currents have an influence to each other. The single-phase current circuit has to be replaced by a three-phase one as presented in Fig. 22. The example is constructed for a wye-connected electric network and a delta-connected winding as will be used in a cage induction motor analysed in Chapter 9.
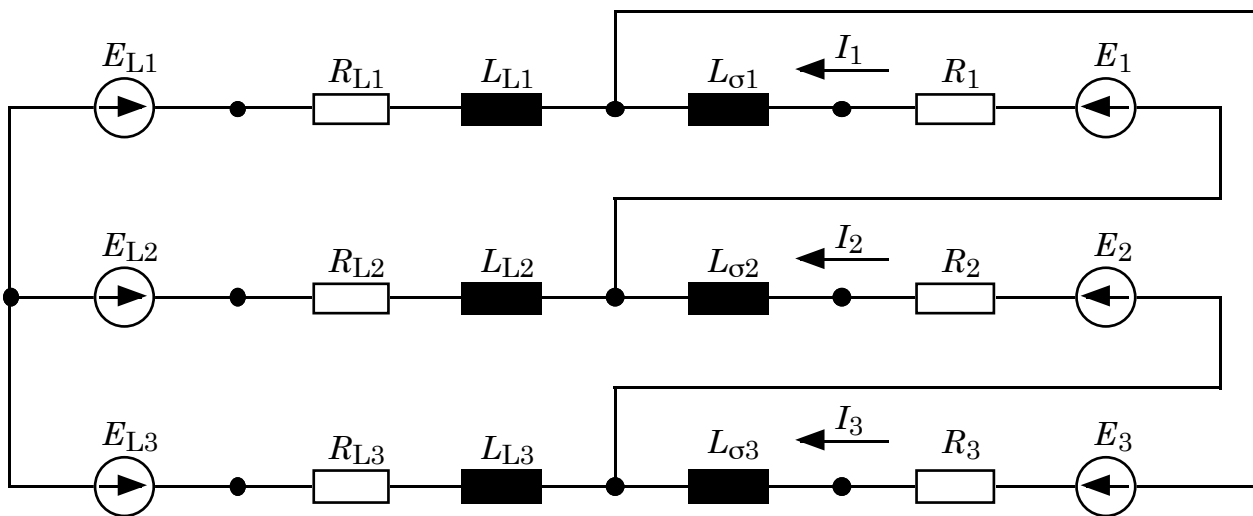
Fig. 22   The current loops for the voltage equation of a distributed winding. The components of the supply line have an index L. The inductance L_{σ} is the leakage inductance of the end-winding. The components E and R only with an index of phase are from the electric model of the winding. The supply line has a wye connection and the winding has a delta connection.

The voltage equations of the electric model of cage winding are constructed for the circumferential and radial current loops between neighbouring electric elements. The circumferential loop between the elements E_0 and E_3 has a current $I_{\varphi 0}$, as in Fig. 23. The radial loop between the elements E_0 and E_4 has a current I_{r0}. The voltage equations of the current loops are

$$
\begin{cases}
R_{z0}\Big(I_{\varphi 0} - I_{\varphi 1} + I_{r2} - I_{r0}\Big) + R_{z3}\Big(I_{\varphi 0} - I_{r5} - I_{\varphi 3} + I_{r3}\Big) \\
\quad + \Big(R_{\varphi 0} + R_{\varphi 3}\Big)I_{\varphi 0} - E_{z0} + E_{z3} = 0 \\
R_{z0}\Big(I_{r0} + I_{\varphi 1} - I_{r2} - I_{\varphi 0}\Big) + R_{z4}\Big(I_{r0} - I_{\varphi 6} + I_{\varphi 4} - I_{r4}\Big) \\
\quad + \Big(R_{r0} + R_{r4}\Big)I_{r0} + E_{z0} - E_{z4} = 0
\end{cases}
\tag{13}
$$
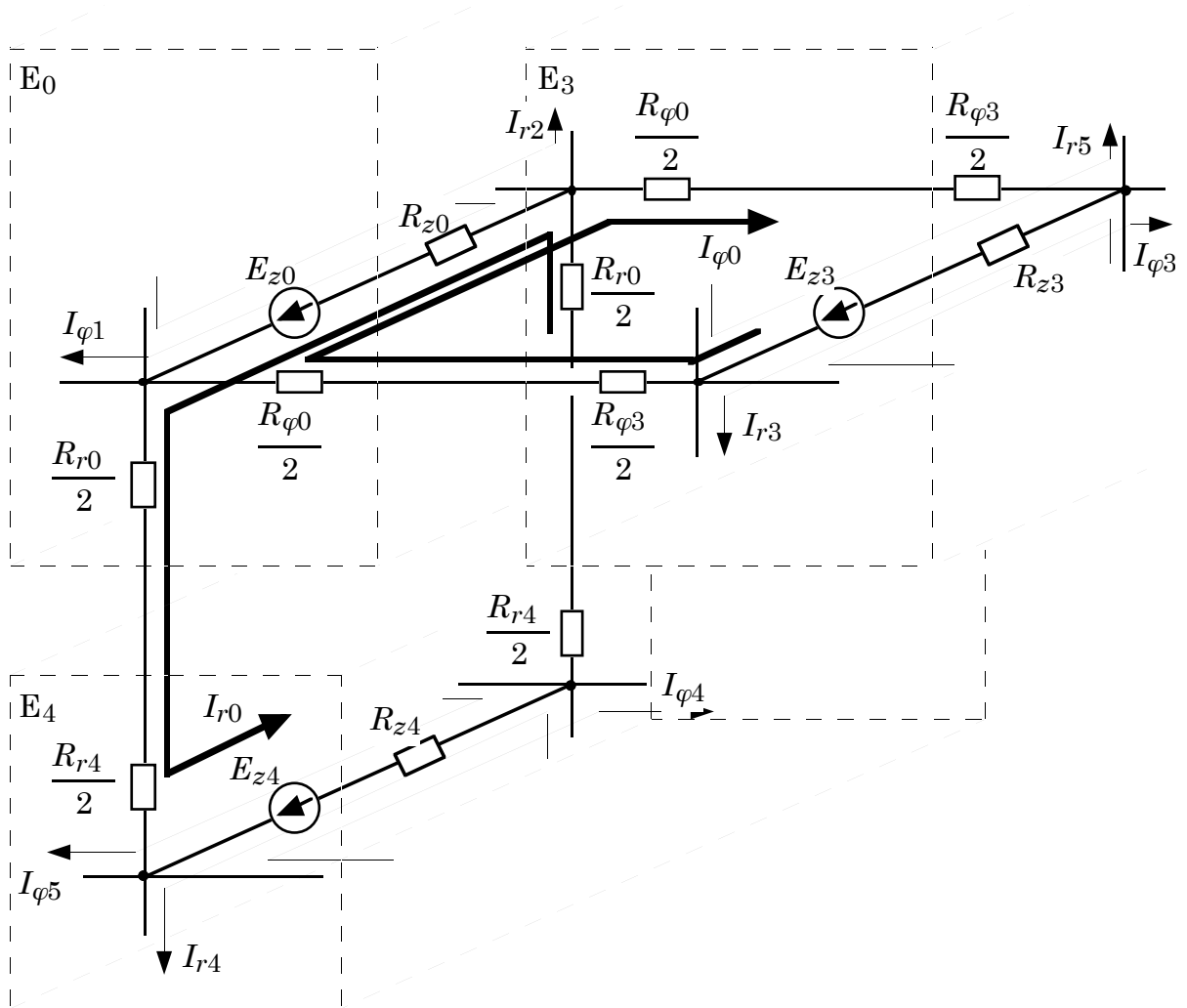
Fig. 23   The loop currents for the voltage equations of the element E_0.
The voltage equations are constructed for the circumferential loop current $I_{\varphi 0}$ between the electric elements E_0 and E_3, and for the radial loop current I_{r0} between the electric elements E_0 and E_4.

In the equations, the quantities are

E_{zi} the EMF source in the axial branch of the electric element E_i,

I_{ri}, $I_{\varphi i}$ the radial and circumferential loop currents connected to the electric element E_i, and

R_{zi}, R_{ri}, $R_{\varphi i}$ the resistances of the axial, radial and circumferential branches in the electric element E_i.

The bar current I_{z0} in the flux-path region of the element E_0 is defined by

$$I_{z0} = I_{r0} - I_{\varphi 0} + I_{\varphi 1} - I_{r2} \tag{14}$$

3.2 Flux-balance equation

This section presents the flux-balance equation for the centre and border nodes of the reluctance model.

The flux-balance equation defines the magnetic scalar potential of the node in the reluctance element. The basic equation is constructed for the node potential V_{m0} of the element E_0 in connection with the node potentials V_{mi} of the neighbouring elements E_i, as in Fig. 24. The flux-balance equation of the element E_0 is

$$\begin{aligned}
&\Lambda_{\text{left}}\Big[V_{m0} - V_{m1} + 0.5\big(F_{m\varphi 0} + F_{m\varphi 1}\big)\Big] \\
&+ \Lambda_{\text{right}}\Big[V_{m0} - V_{m3} - 0.5\big(F_{m\varphi 0} + F_{m\varphi 3}\big)\Big] \\
&+ \Lambda_{\text{up}}\Big[V_{m0} - V_{m2} + 0.5\big(F_{mr0} + F_{mr2}\big)\Big] \\
&+ \Lambda_{\text{down}}\Big[V_{m0} - V_{m4} - 0.5\big(F_{mr0} + F_{mr4}\big)\Big] = 0
\end{aligned} \tag{15}$$

where the permeances are

$$\begin{cases}
\Lambda_{\text{left}} = \dfrac{2}{R_{m\varphi 0} + R_{m\varphi 1}} \\[2mm]
\Lambda_{\text{right}} = \dfrac{2}{R_{m\varphi 0} + R_{m\varphi 3}} \\[2mm]
\Lambda_{\text{up}} = \dfrac{2}{R_{mr0} + R_{mr2}} \\[2mm]
\Lambda_{\text{down}} = \dfrac{2}{R_{mr0} + R_{mr4}}
\end{cases} \tag{16}$$
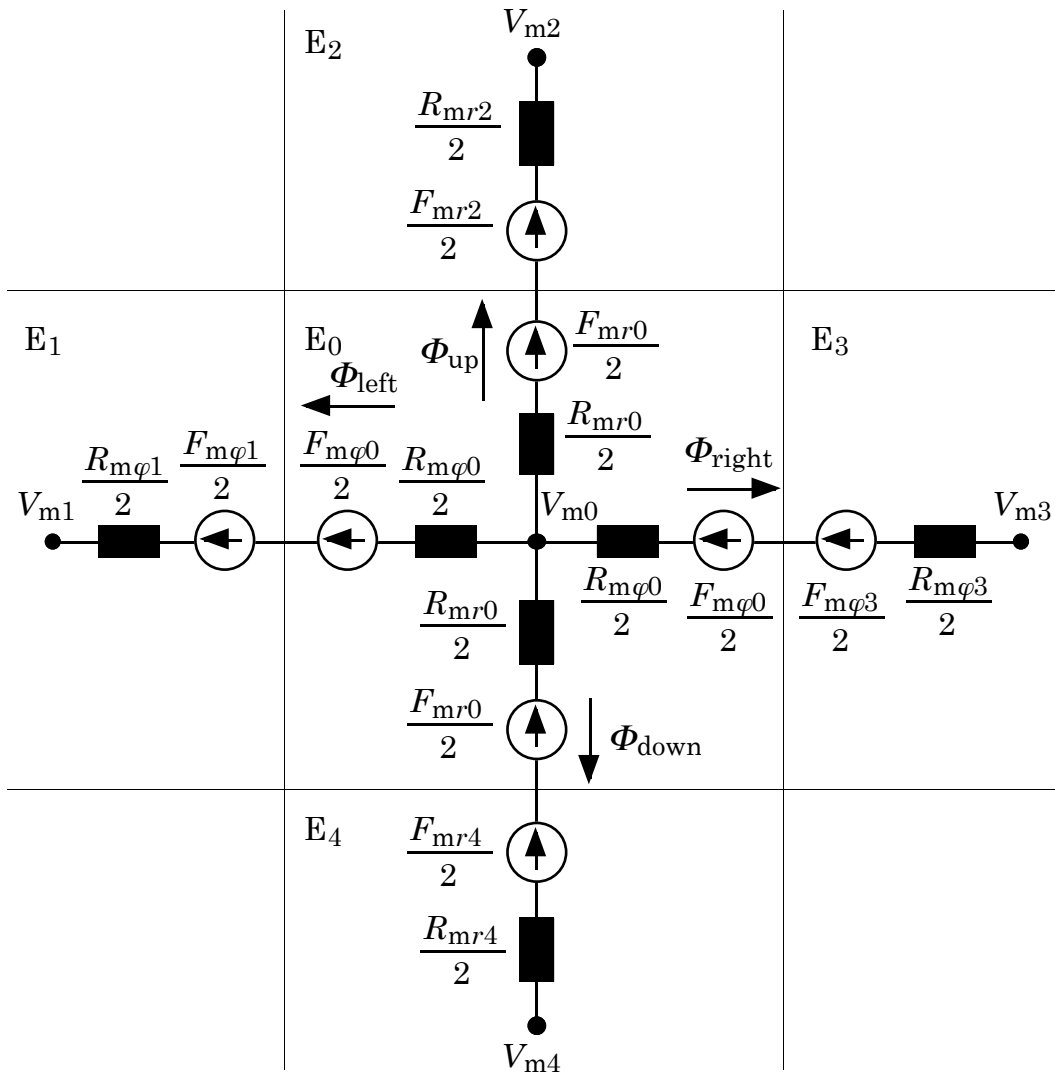
Fig. 24 The magnetic equivalent circuit of the flux-path regions for the flux-balance equation to the magnetic scalar potential V_{m0} of the node in reluctance element E_0. The target element E_0 and the neighbouring elements E_1 to E_4.

In the equations the quantities are

$F_{m\varphi i}$, F_{mri}	the circumferential and radial MMF sources of the element E_i and
$R_{m\varphi i}$, R_{mri}	the reluctances of the circumferential and radial branches in the element E_i.

A border node is used to connect two or more reluctance elements either in core region or at the border of air gap. In the core region, the border node has one branch to both the neighbouring elements. At the air-gap border, the air-gap model may have parallel branches connected to a border node. The border node means the same boundary
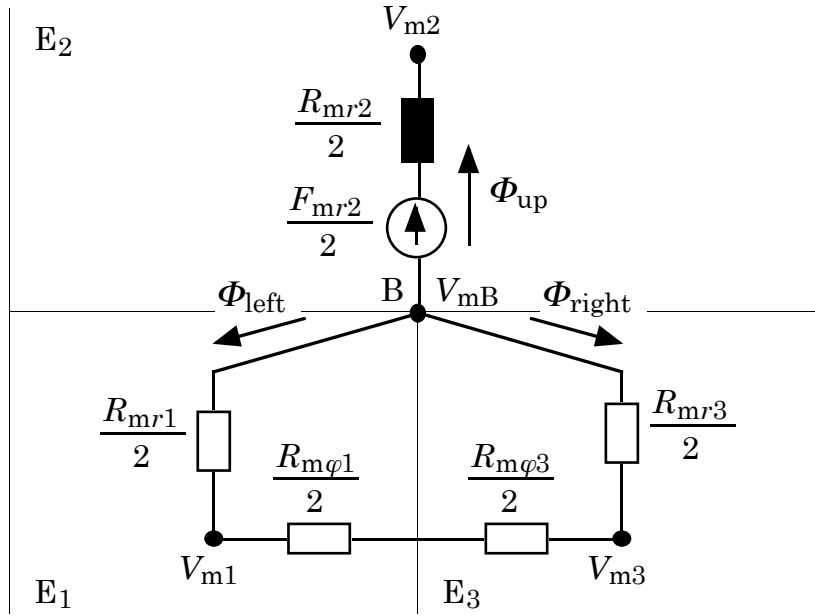
Fig. 25   The magnetic equivalent circuit of the flux-path regions for the flux-balance equation to the magnetic scalar potential V_{mB} of the border node B.
The target border node B and the connected elements: E_2 of core region, and E_1 and E_3 of air-gap region.

potential of the neighbouring elements. The balance equation is constructed for the magnetic scalar potential $V_{m,B}$ of border node B in connection with the magnetic scalar potentials of the core element E_2 and the air-gap elements E_1 and E_3, as in Fig. 25. The balance equation for the magnetic potential of node B is

$$\frac{2\left(V_{m,B} - V_{m2} + 0.5\,F_{mr2}\right)}{R_{mr2}} + \frac{2\left(V_{m,B} - V_{m1}\right)}{R_{mr1}} + \frac{2\left(V_{m,B} - V_{m3}\right)}{R_{mr3}} = 0 \qquad (17)$$

3.3   Magnetic energy

This section presents the definition of the magnetic energy stored in a flux-path region E_e. In the universal reluctance model, the magnetic energy will be used as a basis to define the flux density of the reluctance element, the torque affecting between the stator and rotor.

The magnetic energy W_{me} of a flux-path region E_e is a function of the flux density. The magnetic energy stored in the volume V_e of the flux-path region is defined at flux density B_e
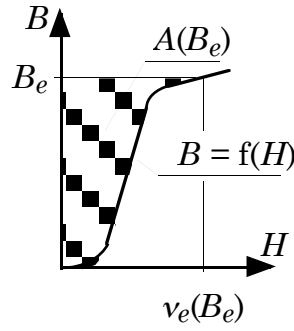
Fig. 26   Definition of the magnetic energy at a flux density B_e.
The magnetic energy stored in a volume V_e is defined using the area $A(B_e)$ between the
magnetic characteristic $B = f(H)$ of the material and the B-axis.

$$W_{m,e} = V_e A(B_e) = V_e \left[\int_{B=0}^{B=B_e} v_e(B) B \, dB \right] \tag{18}$$

where $A(B_e)$ is the area between the B-axis and the magnetic characteristic $B = f(H)$ of the material, as in Fig. 26.

When the reluctivity of the flux-path region is constant, the stored magnetic energy at flux density B_e is

$$W_{m,e} = \frac{1}{2} v_e V_e B_e^2 \tag{19}$$

3.4   Flux density

This section presents the specification of the flux density used in the universal reluctance network. The specification is based on the energy equivalence between the flux-path region and the reluctance element.

In the reluctance model, a flux-path region has a constant flux-density value B in the entire volume. To present the flux-density equation for the region E_0 in Fig. 24, a rectangular reference region is used, as in Fig. 5a. The flux components of the equivalent reluctance element E_0 are specified in Fig. 24. The magnetic energy W_{m0} of the region E_0 with a constant permeability v_0, as in Eq. (19) may be written

$$W_{m0} = W_{m\varphi 0} + W_{mr0}$$

$$= \frac{1}{4} R_{m\varphi 0} \Phi^2_{\text{left}} + \frac{1}{4} R_{m\varphi 0} \Phi^2_{\text{right}} \qquad (20)$$

$$+ \frac{1}{4} R_{mr0} \Phi^2_{\text{up}} + \frac{1}{4} R_{mr0} \Phi^2_{\text{down}}$$

Using the dimensions of Fig. 5a to the region E_0, the equation (20) can be written in the form

$$W_{m0} = \frac{1}{4} \nu_0 \frac{w_0}{h_0 l_0} \left(\Phi^2_{\text{left}} + \Phi^2_{\text{right}} \right) + \frac{1}{4} \nu_0 \frac{h_0}{w_0 l_0} \left(\Phi^2_{\text{up}} + \Phi^2_{\text{down}} \right) \qquad (21)$$

After rewriting, the magnetic energy stored in the reluctance element takes the form

$$W_{m0} = \frac{1}{2} \nu_0 V_0 \frac{\Phi^2_{\text{left}} + \Phi^2_{\text{right}}}{2 h_0^2 l_0^2} + \frac{1}{2} \nu_0 V_0 \frac{\Phi^2_{\text{up}} + \Phi^2_{\text{down}}}{2 w_0^2 l_0^2} \qquad (22)$$

Comparison of energy equation (22) with energy equation (19) gives the equivalence in a general form for flux density B_e

$$B_e = \sqrt{B^2_{\varphi,e} + B^2_{r,e}} = \sqrt{\frac{\Phi^2_{\text{left}} + \Phi^2_{\text{right}}}{2 A^2_{\varphi,e}} + \frac{\Phi^2_{\text{up}} + \Phi^2_{\text{down}}}{2 A^2_{r,e}}} \qquad (23)$$

where

$B_{\varphi,e}$ is the circumferential flux-density component of the flux-path region,

$B_{r,e}$ the radial flux-density component of the flux-path region,

$A_{\varphi,e}$ the cross-section of the flux-path region perpendicular to the circumferential flux, and

$A_{r,e}$ the cross-section of the flux-path region perpendicular to the radial flux.

3.5 Iron losses

This section defines the equations of the iron losses. Conventional equations using the sinusoidal flux-density variation will be presented, and the discrete equations for the instantaneous value of the losses will be defined.

In the time-stepping analysis, a discrete approximation of iron losses is necessary to solve the losses occurring during the time step. The approximation formulae are presented in this section. The definition of the formulae is based on the same assumption of the origin of the loss component as in conventional loss equations, (Richter 1951, see Eq. 211). The approximation formulae are set to give the same average loss-values over one period as the conventional loss equations on sinusoidal flux variation.

3.5.1 Conventional equations of iron losses

The average iron losses $P_{\mathrm{fe},e}$ of an element E_e are defined by the conventional loss equations. The assumption of the definition is a sinusoidal flux-density variation at a constant frequency. The iron losses are the sum of the hysteresis losses $P_{\mathrm{h},e}$ and the eddy-current losses $P_{\mathrm{r},e}$

$$\left\{ \begin{array}{l} P_{\mathrm{h},e} = m_{\mathrm{fe},e}\ \varepsilon_{\mathrm{h}}(f_\varepsilon,\, b_\varepsilon)\dfrac{f_e}{f_\varepsilon}\left[\dfrac{\hat{b}_e}{\hat{b}_\varepsilon}\right]^2 = p_{\mathrm{h},e}\, f_e\, \hat{b}_e^{\,2} \\[3em] P_{\mathrm{r},e} = m_{\mathrm{fe},e}\ \varepsilon_{\mathrm{r}}(f_\varepsilon,\, b_\varepsilon)\left[\dfrac{f_e}{f_\varepsilon}\dfrac{\hat{b}_e}{\hat{b}_\varepsilon}\right]^2 = p_{\mathrm{r},e}\, f_e^{\,2}\, \hat{b}_e^{\,2} \end{array} \right. \tag{24}$$

where the variables of the flux-path region are

$m_{\mathrm{fe},e}$ the weight,
f_e the frequency of flux-density variation,
b_e the flux density,
$p_{\mathrm{h},e}$ the constant factor for the hysteresis loss and
$p_{\mathrm{r},e}$ the constant factor for the eddy-current loss,

and the material definitions

ε_h the hysteresis loss factor of the material,

ε_r the eddy-current loss factor of the material,

f_ε the frequency of flux-density variation and

b_ε the flux density of the loss-factor definitions.

3.5.2 Discrete hysteresis losses

The definition of the discrete approximation is based on the hypothesis that the origin of the hysteresis losses is the energy bound to the hysteresis loop, and that the losses may be defined by the area of the hysteresis loop multiplied by the frequency with which the flux density cuts the loop and by the mass of the element, (Richter 1951, pp. 150-152). In this section, the discrete approximation formula will be presented.

The discrete approximation formula is based on the area of the hysteresis loop in the real *BH*-characteristic of the material and the sinusoidal variation of the flux density. The area of the hysteresis loop may be divided into regions of time steps $A_{BH}^{(k)}$, as in Fig. 27. The region is defined between the boundaries of the *BH*-characteristics without hysteresis (used in analysis) and with hysteresis, and the horizontal lines of
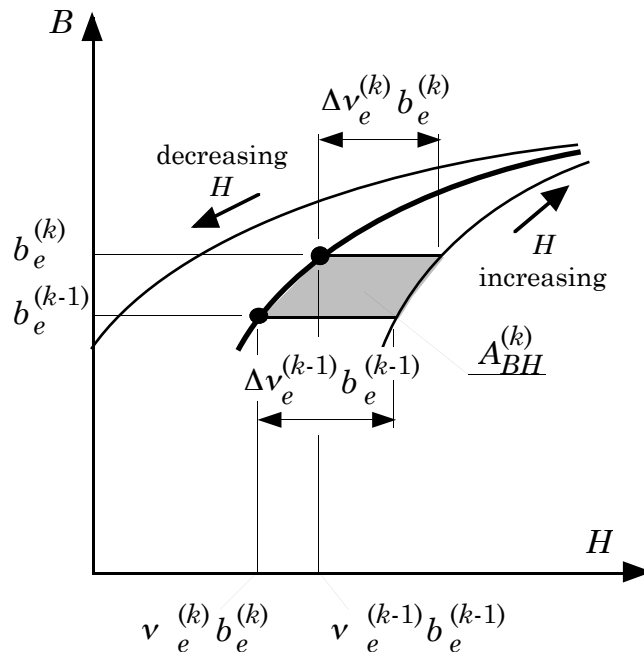
Fig. 27 Approximation of hysteresis losses in time-stepping method.
The area of a trapezium replaces the magnetic energy difference between the BH-characteristic used in analysis and the hysteresis loop curve. The energy defines a hysteresis-loss component between two calculation steps k-1 and k.

flux-density values $b^{(k)}$ and $b^{(k-1)}$ of two time steps. In Fig 27, the assumption is that the value of $b^{(k)}$ is greater than the value of $b^{(k-1)}$, and the magnetisation follows the lower side of the hysteresis loop. The region $A_{BH}^{(k)}$ may be replaced with a trapezium of height $h_{BH}^{(k)}$ and width $w_{BH}^{(k)}$ and $w_{BH}^{(k-1)}$

$$A_{BH,e}^{(k)} = \frac{h_{BH,e}^{(k)}}{2}\left(w_{BH,e}^{(k)} + w_{BH,e}^{(k-1)} \right) \tag{25}$$

where

$$\begin{cases} h_{BH,e}^{(k)} = \left| b_e^{(k)} - b_e^{(k-1)} \right| \\ w_{BH,e}^{(k)} = \left| \Delta v_e^{(k)} b_e^{(k)} \right| \\ w_{BH,e}^{(k-1)} = \left| \Delta v_e^{(k-1)} b_e^{(k-1)} \right| \end{cases} \tag{26}$$

In the equations, $\Delta v_e^{(k)} b_e^{(k)}$ is the difference between the field strengths of the *BH*-characteristics with and without the hysteresis loop at the flux density $b_e^{(k)}$. The area of the trapezium may be rewritten by replacing the field strength differences of the two time steps using an average reluctivity value $\Delta v_{ave,e}^{(k)}$

$$A_{BH,e}^{(k)} = \frac{\Delta v_{ave,e}^{(k)}}{2}\left(\left| b_e^{(k)} \right| + \left| b_e^{(k-1)} \right| \right) \left| b_e^{(k)} - b_e^{(k-1)} \right| \tag{27}$$

Comparing the sum area of the time-step trapezium areas with the conventional hysteresis-loss equation, the formula for the discrete hysteresis-loss increment at time step k can be constructed as an equation

$$\Delta P_{h,e}^{(k)} = p_{h,e}\frac{f}{4}\left(\left| b_e^{(k)} \right| + \left| b_e^{(k-1)} \right| \right) \left| b_e^{(k)} - b_e^{(k-1)} \right| \tag{28}$$

The equation bases on the sinusoidal flux-density variation at a fundamental frequency f. Using of Eq. (28) instead of the original equation, Eq. (24a), gives an approximation for the hysteresis losses at every time step. Using of Eqs. (24a) or (28) for a non-sinusoidal flux-density variation, the error made depends on the size of the harmonics of flux-density variation in comparison to the fundamental.

3.5.3 Discrete eddy-current losses

The definition of the discrete approximation is based on the origin of the eddy currents caused in the material by the flux-density variation. In this section, the discrete approximation formula will be presented.

The discrete approximation formula for the eddy-current losses is based on the square of the flux-density derivative which is replaced by the difference of flux densities $b^{(k)}$ and $b^{(k-1)}$ divided by the length of the time step Δt

$$\left(f \times B_e\right)^2 \propto \frac{1}{N} \sum_{k=1}^{N} \left(\frac{\Delta b_e^{(k)}}{\Delta t}\right)^2 = \frac{1}{N} \sum_{k=1}^{N} \left(\frac{b_e^{(k)} - b_e^{(k-1)}}{\Delta t}\right)^2 \tag{29}$$

where N is the number of time steps in the period.

The formula for the discrete eddy-current loss increment at time step k may be written as an equation

$$\Delta P_{r,e}^{(k)} = p_{r,e} \frac{2}{N} \left(\frac{b_e^{(k)} - b_e^{(k-1)}}{\Delta t}\right)^2 \tag{30}$$

3.6 Air-gap torque

This section presents the specification of the air-gap torque in the universal reluctance network. The air-gap torque T_δ will be specified from the circumferential variation in the magnetic energy of the air gap.

The air-gap torque is the sum of the elementary torques affecting the air-gap regions. The elementary torque of a flux-path region is calculated from the change in the magnetic energy $W_{m,e}$ of the region e to the circumferential direction. In this study, the rotor is locked and the differences of the quantities are replaced with derivatives

$$T_{\delta,e} = r_e F_e = -\frac{\partial W_{m,e}}{\partial \alpha} \tag{31}$$

where

r_e is the radius to the mass centre of the flux-path region,

F_e the force component caused by the energy change, and

α the angular width variable for the region.

The magnetic energy for a reluctance element was presented in Section 3.4

$$
\begin{aligned}
W_{\mathrm{m},e} &= W_{\mathrm{m}\varphi,e} + W_{\mathrm{m}r,e} \\
&= \frac{1}{4} R_{\mathrm{m}\varphi,e} \Phi^2_{\mathrm{left}} + \frac{1}{4} R_{\mathrm{m}\varphi,e} \Phi^2_{\mathrm{right}} \\
&\quad + \frac{1}{4} R_{\mathrm{m}r,e} \Phi^2_{\mathrm{up}} + \frac{1}{4} R_{\mathrm{m}r,e} \Phi^2_{\mathrm{down}}
\end{aligned}
\tag{20}
$$

The components of the magnetic energy create equivalent components for the elementary torque affecting the element to the circumferential direction

$$
T_{\delta,e} = T_{\delta\varphi,e} + T_{\delta r,e} = -\frac{\partial W_{\mathrm{m}\varphi,e}}{\partial \alpha} - \frac{\partial W_{\mathrm{m}r,e}}{\partial \alpha}
\tag{32}
$$

Using the definition of the elements in Fig. 24, the circumferential magnetic energy component of the element E_0, $W_{\mathrm{m}\varphi 0}$, is

$$
\begin{aligned}
W_{\mathrm{m}\varphi 0} &= \frac{1}{4} R_{\mathrm{m}\varphi 0} \Phi^2_{\mathrm{left}} + \frac{1}{4} R_{\mathrm{m}\varphi 0} \Phi^2_{\mathrm{right}} \\
&= R_{\mathrm{m}\varphi 0} \left[\left(\frac{V_{\mathrm{m}0} - V_{\mathrm{m}1}}{R_{\mathrm{m}\varphi 0} + R_{\mathrm{m}\varphi 1}} \right)^2 + \left(\frac{V_{\mathrm{m}0} - V_{\mathrm{m}3}}{R_{\mathrm{m}\varphi 0} + R_{\mathrm{m}\varphi 3}} \right)^2 \right]
\end{aligned}
\tag{33}
$$

The layer of the reluctance element E_0 has the main dimensions of axial length l_0 and of outer and inner radii r_{out} and r_{in}. The reluctance elements of the layer have the circumferential reluctance $R_{\mathrm{m}\varphi,e}$

$$
R_{\mathrm{m}\varphi,e} = \alpha_e \frac{\nu_0}{l_0 \ln\left(\dfrac{r_{\mathrm{out}}}{r_{\mathrm{in}}} \right)} = \alpha_e R_{\mathrm{m}\varphi}
\tag{34}
$$

where the constant reluctance $R_{\mathrm{m}\varphi}$ is independent of the change in the angular width α_e of the flux-path region.

Using the circumferential reluctance of Eq. (34), the equation for the magnetic energy $W_{m\varphi 0}$ takes the form

$$W_{m\varphi 0} = \frac{\alpha_0}{R_{m\varphi}}\left[\left(\frac{V_{m0} - V_{m1}}{\alpha_0 + \alpha_1}\right)^2 + \left(\frac{V_{m0} - V_{m3}}{\alpha_0 + \alpha_3}\right)^2\right] \tag{35}$$

The torque component $T_{\delta\varphi 0}$ from the change of the energy $W_{m\varphi 0}$ is

$$\begin{aligned} T_{\delta\varphi 0} &= -\frac{\partial W_{m\varphi 0}}{\partial \alpha} \\ &= -\frac{1}{R_{m\varphi}}\frac{\partial}{\partial \alpha}\left\{\alpha_0\left[\left(\frac{V_{m0} - V_{m1}}{\alpha_0 + \alpha_1}\right)^2 + \left(\frac{V_{m0} - V_{m3}}{\alpha_0 + \alpha_3}\right)^2\right]\right\} \end{aligned} \tag{36}$$

and after derivation of the angular width variable

$$\begin{aligned} T_{\delta\varphi 0} = &-\frac{1}{R_{m\varphi}}\left[\left(\frac{V_{m0} - V_{m1}}{\alpha_0 + \alpha_1}\right)^2 + \left(\frac{V_{m0} - V_{m3}}{\alpha_0 + \alpha_3}\right)^2\right]\frac{\partial \alpha_0}{\partial \alpha} \\ &+ \frac{2\alpha_0}{R_{m\varphi}}\frac{V_{m0} - V_{m1}}{\left(\alpha_0 + \alpha_1\right)^3}\left(\frac{\partial \alpha_0}{\partial \alpha} + \frac{\partial \alpha_1}{\partial \alpha}\right) \\ &+ \frac{2\alpha_0}{R_{m\varphi}}\frac{V_{m0} - V_{m3}}{\left(\alpha_0 + \alpha_3\right)^3}\left(\frac{\partial \alpha_0}{\partial \alpha} + \frac{\partial \alpha_3}{\partial \alpha}\right) \end{aligned} \tag{37}$$

The change in angular width α_0 is always inverse to the changes in angular widths α_1 and α_3. The equation for the elementary component $T_{\delta\varphi 0}$ is

$$\begin{aligned} T_{\delta\varphi 0} &= -\frac{1}{R_{m\varphi}}\left[\left(\frac{V_{m0} - V_{m1}}{\alpha_0 + \alpha_1}\right)^2 + \left(\frac{V_{m0} - V_{m3}}{\alpha_0 + \alpha_3}\right)^2\right]\frac{\partial \alpha_0}{\partial \alpha} \\ &= -\frac{1}{\alpha_0}W_{m\varphi 0}\frac{\partial \alpha_0}{\partial \alpha} \end{aligned} \tag{38}$$

Using the definition of the elements in Fig. 24, the radial magnetic energy component of the element E_0, W_{mr0}, is

$$W_{\mathrm{m}r0} = \frac{1}{4} R_{\mathrm{m}r0} \Phi_{\mathrm{up}}^2 + \frac{1}{4} R_{\mathrm{m}r0} \Phi_{\mathrm{down}}^2$$

$$= R_{\mathrm{m}r0} \left[\left(\frac{V_{\mathrm{m}0} - V_{\mathrm{m}2}}{R_{\mathrm{m}r0} + R_{\mathrm{m}r2}} \right)^2 + \left(\frac{V_{\mathrm{m}0} - V_{\mathrm{m}4}}{R_{\mathrm{m}r0} + R_{\mathrm{m}r4}} \right)^2 \right] \tag{39}$$

The layers of the air gap have the main dimensions of axial length l_e and of outer and inner radii $r_{\mathrm{out},e}$ and $r_{\mathrm{in},e}$. The reluctance elements in the same sector as the reluctance element E_0 have the radial reluctance $R_{\mathrm{m}r,e}$

$$R_{\mathrm{m}r,e} = \frac{1}{\alpha_0} \frac{\nu_e}{l_e} \ln\left(\frac{r_{\mathrm{out},e}}{r_{\mathrm{in},e}} \right) = \frac{1}{\alpha_0} R_{\mathrm{m},e} \tag{40}$$

where the reluctance $R_{\mathrm{m},e}$ is independent of the change in angular width α_0.

Using the radial reluctances of the equation (40), the equation for the magnetic energy $W_{\mathrm{m}r0}$ takes the form

$$W_{\mathrm{m}r0} = R_{\mathrm{m}0} \left[\left(\frac{V_{\mathrm{m}0} - V_{\mathrm{m}2}}{R_{\mathrm{m}0} + R_{\mathrm{m}2}} \right)^2 + \left(\frac{V_{\mathrm{m}0} - V_{\mathrm{m}4}}{R_{\mathrm{m}0} + R_{\mathrm{m}4}} \right)^2 \right] \alpha_0 \tag{41}$$

The torque component $T_{\delta r0}$ from the change in energy $W_{\mathrm{m}r0}$ is

$$T_{\delta r0} = -\frac{\partial W_{\mathrm{m}r0}}{\partial \alpha}$$

$$= -R_{\mathrm{m}0} \left[\left(\frac{V_{\mathrm{m}0} - V_{\mathrm{m}2}}{R_{\mathrm{m}0} + R_{\mathrm{m}2}} \right)^2 + \left(\frac{V_{\mathrm{m}0} - V_{\mathrm{m}4}}{R_{\mathrm{m}0} + R_{\mathrm{m}4}} \right)^2 \right] \frac{\partial \alpha_0}{\partial \alpha} \tag{42}$$

$$= -\frac{1}{\alpha_0} W_{\mathrm{m}r0} \frac{\partial \alpha_0}{\partial \alpha}$$

The total elementary torque $T_{\delta 0}$ for the reluctance element E_0 is

$$T_{\delta 0} = -\frac{1}{\alpha_0} W_{\mathrm{m}\varphi 0} \frac{\partial \alpha_0}{\partial \alpha} - \frac{1}{\alpha_0} W_{\mathrm{m}r0} \frac{\partial \alpha_0}{\partial \alpha}$$

$$= -\frac{1}{\alpha_0} W_{\mathrm{m}0} \frac{\partial \alpha_0}{\partial \alpha} \tag{43}$$

The equation is in a general form

$$T_{\delta,e} = -\frac{\partial W_{\mathrm{m},e}}{\partial \alpha} = -\frac{1}{\alpha_e} W_{\mathrm{m},e} \frac{\partial \alpha_e}{\partial \alpha} \tag{44}$$

The air-gap torque T_δ is the resulting torque of all the flux-path regions in the air gap

$$T_\delta = \sum_e T_{\delta,e} = -\sum_e \left(\frac{1}{\alpha_e} W_{\mathrm{m},e} \frac{\partial \alpha_e}{\partial \alpha} \right) \tag{45}$$

The summation in the equation is over the entire air-gap volume.

When the rotor is rotating, a discrete circumferential air-gap torque $T_\delta^{(k)}$ is calculated replacing the derivative of the magnetic energy with the difference of energy values on time steps

$$
\begin{aligned}
T_\delta^{(k)} &= \sum_e \left[T_{\delta,e}^{(k)} \right] = \sum_e \left[-\frac{\Delta W_{\mathrm{m},e}}{\Delta \alpha} \right]^{(k)} \\
&= \frac{-1}{\alpha_{\mathrm{R}}^{(k)} - \alpha_{\mathrm{R}}^{(k-1)}} \sum_e \left[W_{\mathrm{m},e}^{(k)} - W_{\mathrm{m},e}^{(k-1)} \right]
\end{aligned}
\tag{46}
$$

where α_{R} is the angle variable for the rotor position.

When the rotor is at a standstill, the discrete circumferential air-gap torque $T_\delta^{(k)}$ is calculated from the change between the time steps in the magnetic energy stored in the air gap

$$T_\delta^{(k)} = \sum_e T_{\delta,e}^{(k)} = -\sum_e \left[\frac{1}{\alpha_e} \left(W_{\mathrm{m},e}^{(k)} - W_{\mathrm{m},e}^{(k-1)} \right) \frac{\partial \alpha_e}{\partial \alpha} \right] \tag{47}$$

3.7 Conclusion

In this chapter, the system equations of the universal reluctance network were specified. The system equations of the universal reluctance network were related to the electric model of the windings and the reluctance model of the flux-path regions.

For the stator winding, the voltage equation was presented connecting the electric model of the distributed winding to the electric supply network. For the rotor winding, the voltage equations were presented connecting the electric elements of the cage winding.

For the reluctance model, the flux-balance equations were presented to the magnetic scalar potential of the centre and border nodes in the reluctance element. The magnetic energy stored in the reluctance element was defined. The specifications of the flux density and air-gap torque were introduced basing on the magnetic energy of the reluctance element. Furthermore, the equations of the iron losses were presented using the conventional loss equations on sinusoidal flux variation. Finally, the discrete equations for the iron-loss components were defined from the conventional equations.

The specifications of the reluctance will be introduced in more details in the next chapter. The system equations will be collected to a matrix equation to solve using matrix calculations in Chapter 6.

4 MATERIAL PROPERTIES

In this chapter, the magnetic properties of the universal reluctance network are introduced. The magnetic properties included in this chapter are the magnetic axial length of the flux-paths and the approximation of the material reluctivity used in the present study. Two special reluctivity specifications for the sinusoidal (phasor) magnetic quantities will be introduced.

There will be an introduction to the influence of flux-path geometry to field-strength definition. Three exceptions to the reluctivity definition of the universal reluctance network will be presented:

- the reluctivity definition of a tooth region when the region has a significant cross-sectional change,
- the reluctivity definition of a yoke region when the circumferential length of the yoke has a significant cross-sectional change as a function of core radius, and
- the reluctivity definition of the slot opening.

4.1 Magnetic length of the air gap

This section introduces the axial length of the reluctance model of the air gap.

In the reluctance model, the axial length of the air gap l_δ is defined by using the traditional equations (Richter 1951, see Eqs. 243, 245)

$$\begin{cases} l_\delta = l_S + 2\delta & \text{when } l_S = l_R \\ l_\delta = 0.5\left(l_S + l_R\right) & \text{when } l_S \neq l_R \end{cases} \tag{48}$$

where

l_S is the axial length of the stator,
l_R the axial length of the rotor, and
δ the radial length of the air gap.

4.2 Magnetic length of the core

This section defines the axial length of the reluctance models of the stator and rotor.

The stator and rotor cores consist of iron sheets covered with a non-magnetic insulation material. The flux in the core flows both in the iron and in the insulation of the sheets. The quantity of flux flowing in the insulation depends on the saturation of the iron. Furthermore, the core may have radial ventilation ducts, which can be created by collecting the sheets into small sheet packages and by leaving radial channels between the packages when setting them into the frame. The radial ventilation ducts function as a parallel path for the flux. The quantity of flux flowing in the ducts depends on the saturation of the iron in the packages.

The axial length of the core l consists of the thickness of the sheet packages and the axial length of the ventilation ducts

$$l = \left(n_v + 1 \right) l_{pc} + n_v l_v \tag{49}$$

where

l_{pc} is the thickness of a sheet package,
n_v the number of the ventilation ducts, and
l_v the axial length of a ventilation duct.

The thickness of the sheet package includes the thickness of the sheet insulation. The axial length of the core has three components, the length of the iron l_{fe}, the length of the insulation, and the length of the ventilation ducts

$$l = l_{fe} + \left(1 - \eta_{fe} \right)\left(n_v + 1 \right) l_{pc} + n_v l_v \tag{50}$$

where the length of the iron l_{fe} is

$$l_{fe} = \eta_{fe} \left(n_v + 1 \right) l_{pc} \tag{51}$$

In the equations, η_{fe} is the fill factor for the iron sheets.

In the reluctance model, the different properties of the axial length are represented as three parallel flux-branches, as in Fig. 28.

l_{fe}

$\mathrm{n_v}l_{\mathrm{v}}$

$(1 - \eta_{\mathrm{fe}})(l - \mathrm{n_v}l_{\mathrm{v}})$
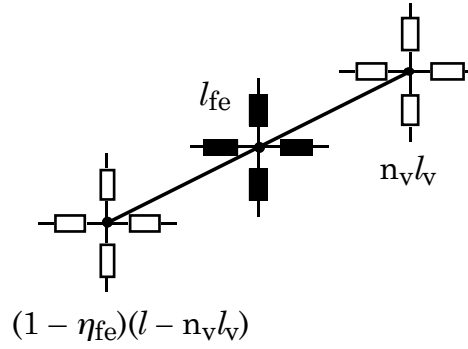
Fig. 28   The axial reluctance model for a flux-path region.
The model takes into account the sheet insulation, the iron, and the radial ventilation
ducts.

4.3   Reluctivity

This section concentrates on the definition of the reluctivity v in the flux-path regions. The reluctivity function of the universal reluctance network will be specified for time-stepping and sinusoidal analysis. A discussion about the variable cross-section of a flux-path region introduces a method to use a larger element with an element dependent reluctivity specification. The section is divided into subsections: reluctivity function, reluctivity with phasor quantities, reluctivity of tooth, reluctivity of yoke, and reluctivity of slot opening.

In this section, the abbreviations r_{m} for reluctance factor and λ for permeance factor are used for the dimension ratios of the flux-path region. The abbreviations are defined by the quantitative equation for the reluctance

$$R_{\mathrm{m},e} = v_e \frac{l_\Phi}{A_\Phi} = v_e r_{\mathrm{m}} \tag{52}$$

and by the quantitative equation for the permeance

$$\Lambda_e = \frac{1}{v_e} \frac{A_\Phi}{l_\Phi} = \frac{1}{v_e} \lambda \tag{53}$$

In the equations

l_Φ is the length of the flux-path region throughout the flux flow and

A_Φ the area of the region perpendicular to the flux flow.

4.3.1 Reluctivity approximation

This section defines the function of the reluctivity used in the universal reluctance network.

In the universal reluctance network, the reluctivity is defined using the total flux density, Eq. (23). The definition of flux density does not assume anything about the radial and circumferential cross-sections. Only the rectangular reference region has been used in the derivation. To define a correct value for the reluctivity of a flux-path region with a variable cross-section, the region should be divided into smaller regions to keep the change of cross-section small and model them using the average cross-section of a region division in its flux-density definition.

The *BH*-characteristic of iron, without hysteresis, gives the reluctivity value

$$v_e(B_e) = \frac{H(B_e)}{B_e} \tag{54}$$

In the analysis, the *BH*-characteristic of the core region is presented as a polynomial function in proportion to the flux density squared

$$v_e(B_e) = \sum_{i=0}^{3} \left[a_i \left(B_e^2 \right)^i \right] \tag{55}$$

with the constants a_i. The values for the polynomial constants are defined by a curve fitting as a common reluctivity to the parallel flux paths of Fig. 28. The middle path has the *BH*-characteristic of iron, Eq. 54, and the side paths have the linear *BH*-characteristic of air.

The definition of reluctivity of the core region assumes that the flux density has a constant value in the flux-path region. The radial and circumferential cross-sections of the flux path region are constant or average cross-sections will be used.

4.3.2 Effective reluctivity

The assumption of a sinusoidal time variation for the current, flux, flux density, and voltage is a solution to reduce calculation time. The assumption is valid for steady-state operation of the motor. The effective reluctivity defined by (Luomi et al. 1986) takes into account the time-sinusoidal nature of the flux distribution. The effective

reluctivity will be used with complex phasors. The effective reluctivity is assumed to be a function of the amplitude of the complex phasor $\vec{b}$ of the flux density and constant in time.

In the approximation of a sinusoidal time variation, the current, flux, flux density, and voltage are assumed to be equal to the amplitude of their fundamental time variation, i.e. they have the form

$$x = \hat{x} \cos(\omega\, t + \varphi) \tag{56}$$

where

$\quad x \qquad$ is the current, flux, flux density, and voltage,

$\quad \hat{x} \qquad$ the amplitude of the fundamental,

$\quad \omega \qquad$ the angular frequency of the fundamental, and

$\quad \varphi \qquad$ the phase shift of the fundamental.

The current, flux, flux density, and voltage can be presented using a complex phasor, i.e. they take the form

$$\vec{x} = \hat{x}\, e^{j\varphi} \tag{57}$$

where j is the imaginary unit $j = \sqrt{-1}$.

The reluctance network may be analysed using the complex phasors. As a result, the flux and current may be presented at any point of time t from the equation

$$\begin{cases} \Phi(t) = \mathrm{Re}\left\{ \vec{\Phi}\, e^{j\omega t} \right\} \\ i(t) = \mathrm{Re}\left\{ \vec{i}\, e^{j\omega t} \right\} \end{cases} \tag{58}$$

where Re{ } represents an operator taking the real part of a complex number.

Two kinds of effective reluctivities are possible:

   – For a sinusoidal voltage source, the analysis has an approximation of a time-sinusoidal flux density using an effective reluctivity

$$v_{\text{eff}} = \frac{1}{T} \int_{t=0}^{T} \left[\frac{h(t)}{\hat{b} \cos(\omega t)} \mathrm{d}t \right] \qquad (59)$$

where

$\hat{b}$ is the amplitude of the sinusoidal flux-density wave form,

T the time of period of the fundamental of the flux-density variation, and

$h(t)$ the instantaneous value of the magnetic field strength.

– For a sinusoidal current source, the analysis has an approximation of a time-sinusoidal magnetic field strength using an effective reluctivity

$$v_{\text{eff}} = \frac{\hat{h}}{\dfrac{2}{T} \int_{t=0}^{T} \left[b(t) \cos(\omega t) \mathrm{d}t \right]} \qquad (60)$$

where

$\hat{h}$ is the amplitude of the sinusoidal magnetic field strength wave form,

T the time of period of the fundamental of the variation of the magnetic field strength, and

$b(t)$ the instantaneous value of the flux density.

4.3.3   Reluctivity of a tooth

The magnetic potential drop in a tooth is approximated traditionally using Simpson's rule from the field strengths at various distances along the tooth height (Richter 1951, see Eq. 269). In this study, the approximation is replaced by dividing the flux-path region of the tooth into radial divisions. In the analysis of the reluctance network, the region is treated as a single element with its own reluctivity function.

In the universal reluctance network, the definition of reluctivity assumes that the radial and circumferential cross-sections of the flux path region are constant or almost constant. To model a tooth with a variable circumferential width, the tooth has to be divided into smaller regions. This means a fine mesh. To reduce the number of elements in the network, this study specifies a new way to construct the reluctivity of

the tooth. This will be achieved by dividing the flux-path region into divisions according to the assumed main direction of flux.

The use of the assumed flux direction does not accord with the theme of the universal reluctance network. Its advantage, however, is a more precise analysis of flux in electrical machine with fewer elements. For the theme of the universal reluctance network, there is an alternative to adjusting the flux-direction in the analysis. First, the analysis defines the flux flow and then runs again using this information to select the appropriate reluctivity function.

The assumption made in the approximation is that the main direction of the flux flow is the direction of the radial height of the tooth, as in Fig. 29. The reluctivities in the divisions of the flux-path region are determined for a radial flux Φ_r flowing through the region. The sum of the magnetic potential drops over the divisions defines the magnetic potential drop for the region. The flux density B_e of the region is defined from the flux Φ_r and from the average cross-section $A_{\Phi,\text{ave}}$ of the divisions.

The resulting reluctivity of the tooth, for the flux density B_e, is

$$v_e(B_e) = \frac{\sum\limits_{i=1}^{n}\left(v_i(B_i)\,r_{\mathrm{m}r,i}\right)}{\sum\limits_{i=1}^{n} r_{\mathrm{m}r,i}} \tag{61}$$

where
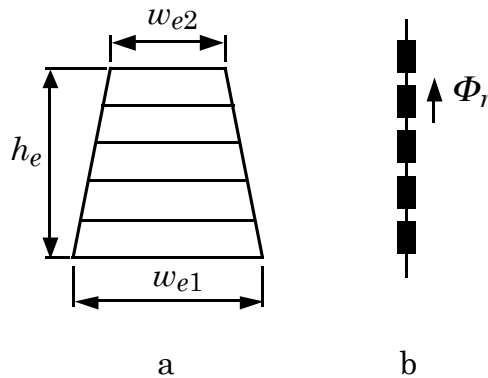
Fig. 29 *The reluctivity definition in a tooth uses the radial flux component.*
a) The divisions in a tooth region to define the reluctivity function of the tooth.
b) The reluctance model of the tooth for the main direction of the flux flow.

n is the number of the divisions,

ν_i the reluctivity of the division i according to Eq. (54),

B_i the flux density of the division i, and

$r_{\mathrm{m}r,i}$ the reluctance factor of the division i.

The resulting reluctivity function of the tooth, in accordance with Eq. (55), is constructed from the results of Eq. (61) at different flux-density values. The constants a_i of the polynomial are defined by a curve fitting with the calculated reluctivity values.

The resulting radial and circumferential reluctances of the tooth are

$$\begin{cases} R_{\mathrm{m}r,e} = \nu_e \sum_{i=1}^{n} r_{\mathrm{m}r,i} \\ R_{\mathrm{m}\varphi,e} = \dfrac{\nu_e}{\sum_{i=1}^{n} \lambda_{\varphi,i}} \end{cases} \tag{62}$$

where

ν_e is the reluctivity defined from Eq. (61), and

$\lambda_{\varphi,i}$ the permeance factor of the circumferential branch in the division i.

4.3.4 Reluctivity of yoke

The circumferential flux in the yoke does not have a uniform distribution over the entire yoke cross-section. Traditionally, the real distribution is determined using empirical functions (Richter 1951, pp. 161-167). In the reluctance network used in this study, the uneven flux distribution is approximated by dividing the flux-path region in the yoke into parallel regions in a circumferential direction. In the analysis of the network, the region is treated as a single element with its own reluctivity function.

In the universal reluctance network, the definition of reluctivity assumes an even flux distribution in the flux path region. To model a yoke with an uneven flux distribution, the yoke has to be divided into smaller regions to get an almost even distribution of flux flow in the region. This means a fine mesh. To reduce the number of elements in the network, this study uses a special way to construct the reluctivity function of the yoke. This will be achieved by dividing the flux-path region into divisions according to the assumed main direction of flux, circumferential along the yoke. The use of the

predefined flux direction does not accord with the theme of the universal reluctance network. For the theme of the universal reluctance network, there is no remarkable error in practice for the model of the yoke. Most portion of the flux in the yoke flows in circumferential direction. The advantage, however, is a more precise analysis of the flux flow with fewer elements.

In the approximation, the reluctivities in the divisions of the flux-path region are determined for a circumferential flux Φ_φ flowing through the yoke, as in Fig. 30. The magnetic potential drop of the parallel divisions defines how the flux is branched. The flux density B_e of the yoke is defined from the flux Φ_φ and from the cross-section A_Φ of the yoke.

The resulting reluctivity of the yoke, for the flux density B_e, is

$$\nu_e(B_e) = \frac{\displaystyle\sum_{i=1}^{n} \lambda_{\varphi,i}}{\displaystyle\sum_{i=1}^{n} \frac{\lambda_{\varphi,i}}{\nu_i(B_i)}} \tag{63}$$

where

$\quad$ n $\qquad$ is the number of the divisions,
$\quad$ ν_i $\qquad$ the reluctivity of the division i according to Eq. (54),
$\quad$ B_i $\qquad$ the flux density of the division i, and
$\quad$ $\lambda_{\varphi,i}$ $\qquad$ the permeance factor of the division i.
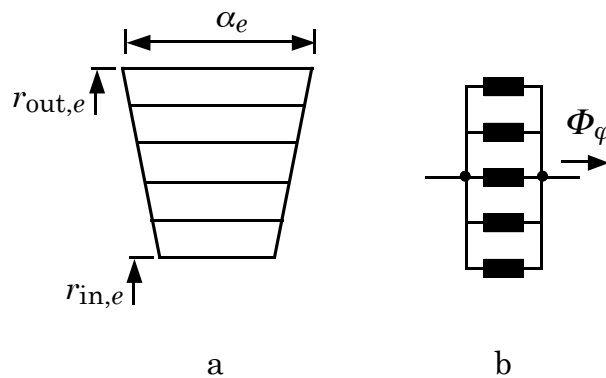
Fig. 30 *The reluctivity definition in the yoke using the circumferential flux.*
a) The divisions in a yoke region to define the reluctivity function of the yoke.
b) The reluctance model of the yoke for the main direction of the flux flow.

The resulting reluctivity function of the yoke, in accordance with Eq. (55), is constructed from the results of Eq. (63) at different flux-density values using a curve fitting.

The resulting radial and circumferential reluctances of the yoke are

$$
\begin{cases}
R_{\mathrm{m}r,e} = \nu_e \displaystyle\sum_{i=1}^{n} r_{\mathrm{m}r,i} \\[2em]
R_{\mathrm{m}\varphi,e} = \dfrac{\nu_e}{\displaystyle\sum_{i=1}^{n} \lambda_{\varphi,i}}
\end{cases}
\tag{64}
$$

where

ν_e is the reluctivity defined from Eq. (63), and

$r_{\mathrm{m}r,i}$ the reluctance factor of the radial branch in the division i.

4.3.5 Reluctivity of the slot opening

The magnetic potential drop in the tooth tip was considered in (Akbaba & Fakhro 1987, Savelainen 1980). They used a variable fictitious slot opening to model the saturation of the tooth tip when the circumferential flux flows across the slot opening. In the present study, this theory is adapted within the reluctance network. The approximation of the variable fictitious slot opening is made by using a semi-saturated flux-path region in the slot opening. In the analysis of the reluctance network, the flux-path region is treated as a single element with its own reluctivity function.

In the study as an exception to the universal reluctance network, the definition of a slot-opening region bases on the circumferential main direction of the flux flow. The slot-opening region consists of three subdivisions: the real slot opening (either of iron or air) in the middle and two elements of iron at the sides separated from the tooth tips of the neighbouring teeth, as in Fig. 31. The circumferential dimension of the side elements is half the width of the slot opening. The axial and radial dimensions, and the material are of the tooth tips.

The reluctivity function of the slot-opening region E_0 is determined for a circumferential flux Φ_φ flowing through the region, as in Fig. 31. The sum of the magnetic potential drops over the three subdivisions defines the magnetic potential
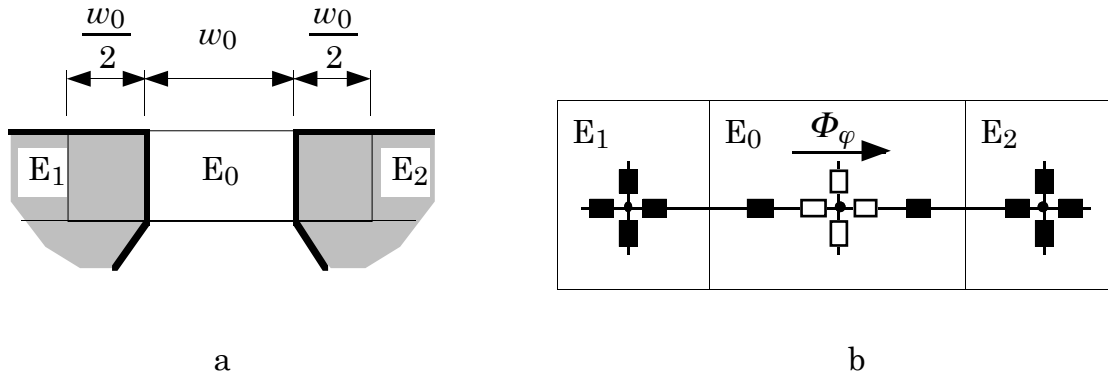
Fig. 31 The reluctivity definition of the slot-opening region uses a saturable model.
a) The enlargement of the slot-opening region includes a portion of the neighbouring tooth tips E_1 and E_2 to the slot-opening region E_0.
b) The saturable reluctance element E_0 of the slot-opening region connected to the reluctance elements of teeth, E_1 and E_2.

drop for the region. The flux density B_0 of the region is defined from the flux Φ_φ and from the circumferential cross-section $A_{\varphi 0}$ of the slot opening.

The resulting reluctivity v_{equi} of the slot-opening region, for the flux density B_0, is

$$v_{\text{equi}}(B_0) = 0.5\, v_1(B_1)\frac{A_{\varphi 0}}{A_{\varphi 1}} + v_0(B_0) + 0.5\, v_2(B_2)\frac{A_{\varphi 0}}{A_{\varphi 2}} \tag{65}$$

where the subscripts for the reluctivities and the circumferential cross-sections are according to Fig. 31.

The resulting reluctivity function of the slot opening, in accordance with Eq. (55), is constructed using a curve fitted to the results of Eq. (65) at different flux-density values.

The resulting radial and circumferential reluctances of the slot opening are

$$\begin{cases} R_{\text{m}r0} = v_{\text{equi}} r_{\text{m}r0} \\ R_{\text{m}\varphi 0} = v_{\text{equi}} r_{\text{m}\varphi 0} \end{cases} \tag{66}$$

where

v_{equi} is the resulting reluctivity of the slot opening defined from Eq. (65),

$r_{\mathrm{m}r0}$ the radial permeance factor of the slot opening region E_0 and

$r_{\mathrm{m}\varphi0}$ the circumferential permeance factor of the slot opening region E_0.

4.4   Conclusion

In this chapter, the magnetic properties of the universal reluctance network were introduced. The chapter specified the axial length of the flux paths. The reluctivity function was specified using the material *BH*-characteristic of the flux-path region. The reluctivity functions for the sinusoidal (phasor) magnetic quantities were introduced.

The methods used to determine the influence of the flux-path geometry were developed. Three exceptions to the reluctivity definition of the universal reluctance network were specified for the regions of tooth, yoke, and slot opening. The method was to use a main direction of the flux flow through the region, divide the region according to the flux flow, and define the resulting reluctivity function:

- The variable width of the tooth region was taken into account by defining the resulting reluctivity using the serial reluctance of the tooth-region divisions.
- The uneven flux distribution of the yoke region was taken into account by defining the resulting reluctivity using the parallel reluctance of the yoke-region divisions.
- The saturated tooth tip on the slot opening was taken into account by defining the resulting reluctivity using the serial reluctance of the tooth tips and the slot opening.

The definitions in this chapter will be used in the reluctance network definitions for the machines in Chapter 9. In the next chapter, a new component will be presented to combine the electric element to the reluctance element of a flux-path region in the reluctance model.

5 MODELLING OF EDDY-CURRENT LOSSES

A magnetic capacitance C_m is presented in the reluctance model in (Oberretl 1963) and in the simulation model using electric components in (Roberts 1960 and 1962) to take the resistive losses into the magnetic model. The main analysis target has been the eddy-current losses rising in the conductors.

The aim of this chapter is to specify a magnetic capacitance for the universal reluctance network and the rules for the placement of the capacitance. The simple form of the equations in the presentations of Oberretl and Roberts based on the square form of the flux-path regions. In order to use the same technique in the universal reluctance network, the flux equation must be reformulated. The formula for the magnetic capacitance will be developed, and the flux equation of the reluctance element node will be reformed to include the flux component of the capacitive branch.

5.1 Eddy-current losses of a flux-path region

In this section, the interconnection of a reluctance element and an electric element as a model of eddy currents in a flux-path region will be presented.

According to Section 2.5, a flux-path region with a conductor (or a conducting material) may be modelled as a combination of a reluctance element with an MMF source and an electric element having only the axial branch, as in Fig. 13. The eddy currents induced in the conductor may be modelled by short-circuiting the axial branch of the electric element. The resistance of the axial branch depends on the resistivity of the flux-path region.

For a circumferential flux flow Φ_φ, the flux-path region E_0 may be represented in the reluctance model as a combination of a reluctance element with an MMF source $F_{m\varphi 0}$ and an electric element with a short-circuited axial branch, as in Fig. 32. The reluctance model represents the magnetic energy distribution of the flux-path region. The electric model represents the electric energy distribution of the flux-path region.

In the reluctance element, the product of the magnetic voltage drop ΔV_{m0} over the circumferential total reluctance $R_{m\varphi 0}$ and the flux Φ_φ, going through the reluctance is twice the magnetic energy W_{m0} stored in the flux-path region

$$\Delta V_{m0}\Phi_\varphi = R_{m\varphi 0}\Phi_\varphi^2 = 2W_{m0} \tag{67}$$
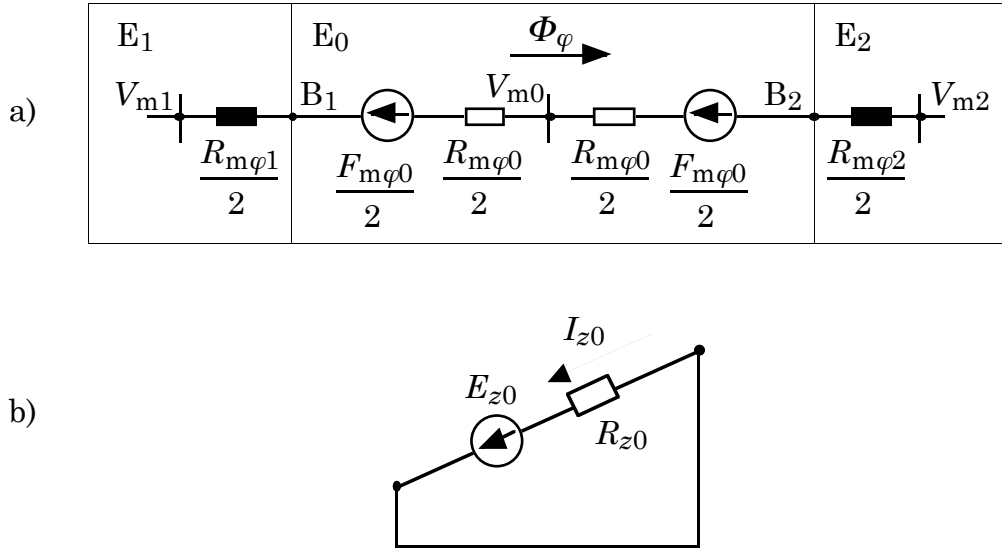
Fig. 32 The circumferential branch of the reluctance model for eddy currents.
a) The reluctance element E_0 of a conductor for the circumferential flux flow.
b) The electric model of the short-circuited conductor modelling the eddy currents.

The product of the magnetic voltage drop over the MMF source, $F_{m\varphi0}$, and the flux Φ_φ, represents double of the magnetic energy dissipation caused by the eddy currents

$$F_{m0}\Phi_{\varphi0} = 2\Delta W_{m0} \tag{68}$$

This portion of magnetic energy, ΔW_{m0}, is changed to heat energy.

In the electric element, the product of the electric voltage drop ΔV_0 over the axial resistance R_{z0} and the current I_{z0} going through the resistance is the electric power ΔP_0 dissipated as heat. The equivalent heat energy ΔW_{e0} at a time interval Δt is

$$\Delta W_{e0} = \Delta P_0\Delta t = \Delta V_0 I_{z0}\,\Delta t = R_{z0}I_{z0}^2\,\Delta t \tag{69}$$

The product of the value of EMF source E_{z0} and the current I_{z0} represent the electric power P_0 supplied from the magnetic field. The equivalent energy W_{e0} at the time interval Δt is

$$W_{e0} = P_0\Delta t = E_{z0}I_{z0}\,\Delta t \tag{70}$$

The connection of the magnetic and electric elements is the pair of equations

$$\begin{cases} F_{m0} = -I_{z0} \\ E_{z0} = -\dfrac{d\Phi_\varphi}{dt} \end{cases} \tag{71}$$

A small change of flux $\Delta\Phi_\varphi$, from a value Φ_φ to the value $\Phi_\varphi + \Delta\Phi_\varphi$, in a small time interval Δt induces an EMF to the electric model. The supplied energy in the electric model is

$$W_{e0} = P_0\Delta t = E_{z0}I_{z0}\,\Delta t = \frac{\Delta\Phi_\varphi}{\Delta t}I_{z0}\,\Delta t = \Delta\Phi_\varphi I_{z0} = \Delta\Phi_\varphi F_{m0} = 2\,\Delta W_{m0} \tag{72}$$

The dissipated magnetic energy, caused by the eddy currents, is opposite to the change caused by the supplied magnetic energy. When the supplied magnetic energy increases, the dissipated magnetic energy is taken from the supplied magnetic energy. When the supplied magnetic energy decreases, the dissipated magnetic energy is taken from the stored magnetic energy of the flux-path region. When modelling the flux flow in the reluctance model, the energy dissipation caused by the eddy currents is capacitive to the magnetic energy of the flux-path region.

In the next section, a capacitance will be added to the reluctance element presented in Chapter 2. The magnetic capacitance will be used as an equivalent for the eddy-current losses.

5.2 Magnetic capacitance

In this section, the theory for using a capacitance as a resistive-loss component will be presented. The new equation of flux flow between the neighbouring regions will be developed. Moreover, the placement of the capacitance in the reluctance element will be specified. The purpose of the discussion is to simplify the reluctance model and replace the electric element by using the capacitance when the electric model connected to the flux-path is a EMF source loaded by a resistance.

The circumferential flux Φ_φ flows through the flux-path region E_0, and induces the EMF source E_{z0} of the electric element, as in Fig. 32

$$E_{z0} = -\frac{d\Phi_\varphi}{dt} = -\frac{1}{R_{m\varphi}}\frac{d\left(V_{m1} - V_{m2} - F_{m\varphi0}\right)}{dt} \tag{73}$$

where the circumferential reluctance $R_{m\varphi}$ is the total reluctance between the nodes of reluctance elements E_1 and E_2

$$R_{m\varphi} = 0.5\,R_{m\varphi 1} + R_{m\varphi 0} + 0.5\,R_{m\varphi 2} \tag{74}$$

The equation (73) can be rewritten by using the magnetic potentials at the boundary nodes B_1 and B_2 of the region E_0

$$E_{z0} = -\frac{d\Phi_\varphi}{dt} = -\frac{1}{R_{m\varphi 0}}\frac{d\left(V_{m,B1} - V_{m,B2} - F_{m\varphi 0}\right)}{dt} \tag{75}$$

where the value of E_{z0} is independent of the model outside region E_0.

The layout of the reluctance element E_0 may be changed by moving the component $F_{m\varphi 0}$ outside the boundary nodes and dividing it to both sides of the reluctance element E_0, as in Fig. 33. Equation (75) changes to

$$E_{z0} = -\frac{d\Phi_\varphi}{dt} = -\frac{1}{R_{m\varphi 0}}\frac{d\left(V^{*}_{m,B1} - V^{*}_{m,B2}\right)}{dt} \tag{76}$$
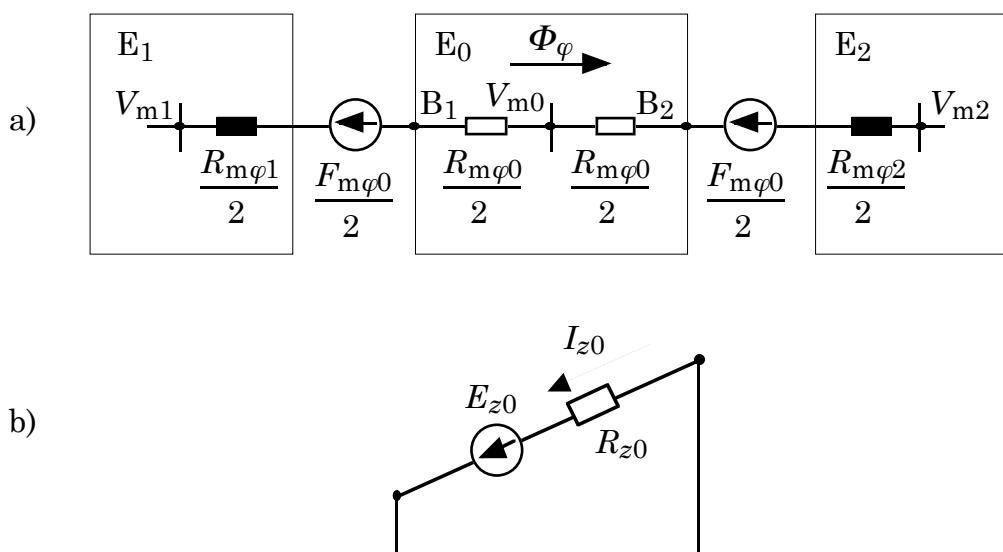
Fig. 33   An alternative layout of the reluctance element E_0 on the circumferential branch for the layout in Fig. 32.
a)   The reluctance element E_0 of a conductor for the circumferential flux flow.
b)   The electric model of the short-circuited conductor modelling the eddy currents.

The asterisk indicates that the values of these potentials are changed because of the new definition of reluctance element as represented in Fig. 32.

The axial current I_{z0} flowing in the electric element is

$$I_{z0} = \frac{E_{z0}}{R_{z0}} = -\frac{1}{R_{z0}\,R_{m\varphi0}}\frac{d\left(V^*_{m,B1} - V^*_{m,B2}\right)}{dt} \tag{77}$$

Using Eq. (77) for the MMF source $F_{m\varphi0}$, equal to $-I_{z0}$, in the equation of the circumferential flux, the asterisk will be omitted from the quantities because the potential values belong to the new element layout that will be used in the analysis.

The equation of the circumferential flux Φ_φ is

$$\begin{aligned}
\Phi_\varphi &= \frac{V_{m,B1} - V_{m,B2}}{R_{m\varphi0}} - \frac{F_{m0}}{R_{m\varphi0}} \\
&= \frac{V_{m,B1} - V_{m,B2}}{R_{m\varphi0}} + \frac{1}{R_{z0}\,R^2_{m\varphi0}}\frac{d\left(V_{m,B1} - V_{m,B2}\right)}{dt}
\end{aligned} \tag{78}$$

The equation is a capacitive equation for determining magnetic potentials.

Using a definition for a magnetic capacitance $C_{m\varphi0}$

$$C_{m\varphi0} = \frac{1}{R_{z0}\,R^2_{m\varphi0}} \tag{79}$$

the equation of the circumferential flux Φ_φ, Eq. (78), may be rewritten in a form

$$\Phi_\varphi = \frac{V_{m,B1} - V_{m,B2}}{R_{m\varphi0}} + C_{m\varphi0}\frac{d\left(V_{m,B1} - V_{m,B2}\right)}{dt} \tag{80}$$

The equation represents a circumferential flux Φ_φ flowing in a reluctance model for the circumferential branch presented in Fig. 34 where the MMF source $F_{m\varphi0}$ and the electric element with the EMF source E_{z0} loaded by the resistance R_{z0} is replaced by a capacitance $C_{m\varphi0}$ connected to the border nodes B_1 and B_2 of the reluctance element E_0.
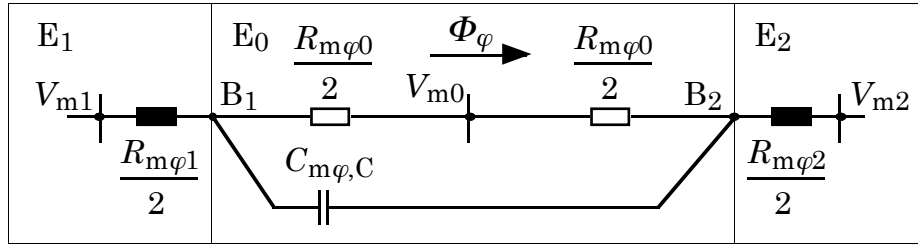
Fig. 34 The capacitive reluctance model of the reluctance element E_0 for the circumferential flux taking into account the eddy currents in the element.

For the radial branch of the reluctance element E_0, a radial flux Φ_r flowing through the region can be defined using the potentials of the border nodes, as in Fig. 35

$$\Phi_r = \frac{V_{m,B3} - V_{m,B4}}{R_{mr0}} + \frac{1}{R_{z0}\,R_{mr0}^2}\frac{d\left(V_{m,B4} - V_{m,B3}\right)}{dt} \tag{81}$$

a

b
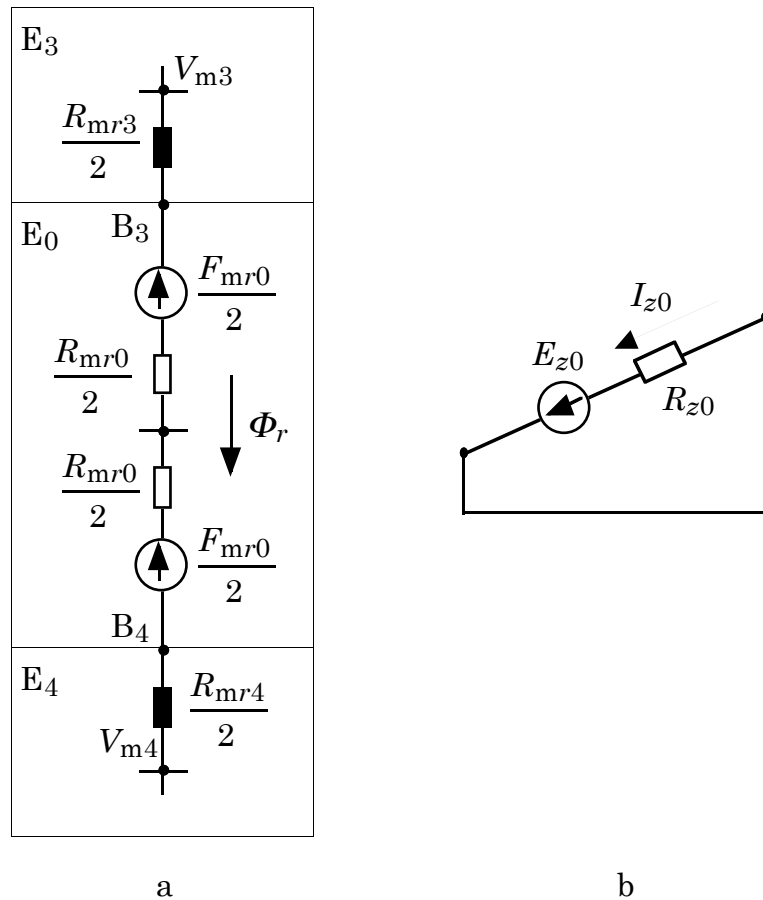
Fig. 35 An alternative layout of the reluctance element E_0 on the radial branch.
a) The reluctance element E_0 of a conductor for the radial flux flow.
b) The electric model of the short-circuited conductor modelling the eddy currents.

The equation is a capacitive equation for determining magnetic potentials. Using a definition for a magnetic capacitance C_{mr0}

$$C_{mr0} = \frac{1}{R_{z0}\, R_{mr0}^2} \tag{82}$$

the equation may be rewritten in a form

$$\Phi_r = \frac{V_{m,B3} - V_{m,B4}}{R_{mr0}} + C_{mr0} \frac{d\left(V_{m,B4} - V_{m,B3}\right)}{dt} \tag{83}$$

The capacitive two-dimensional reluctance model is presented in Fig. 36. The flux-balance equation for the node potential V_{m0} of reluctance element E_0 is

$$
\begin{aligned}
2\frac{V_{m0} - V_{m,B1}}{R_{m\varphi0}} + 2\,C_{m\varphi0} \frac{d\left(V_{m0} - V_{m,B1}\right)}{dt} \\
+ 2\frac{V_{m0} - V_{m,B2}}{R_{m\varphi0}} + 2\,C_{m\varphi0} \frac{d\left(V_{m0} - V_{m,B2}\right)}{dt} \\
+ 2\frac{V_{m0} - V_{m,B3}}{R_{mr0}} + 2\,C_{mr0} \frac{d\left(V_{m0} - V_{m,B3}\right)}{dt} \\
+ 2\frac{V_{m0} - V_{m,B4}}{R_{mr0}} + 2\,C_{mr0} \frac{d\left(V_{m0} - V_{m,B4}\right)}{dt} = 0
\end{aligned}
\tag{84}
$$
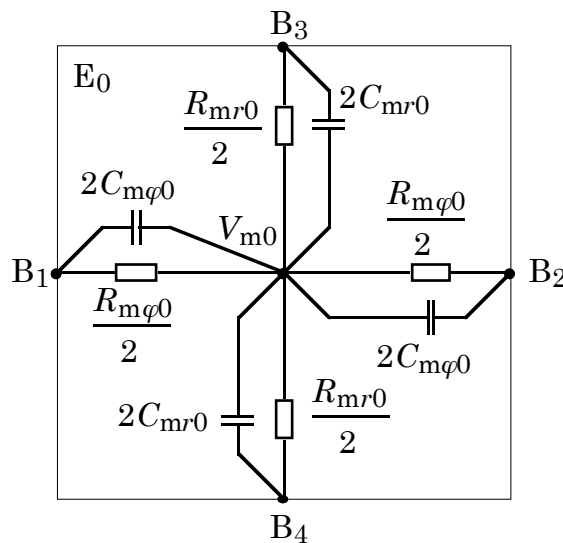
Fig. 36   *A two-dimensional capacitive reluctance model of element E_0.*

In the construction of the reluctance network, account must be taken of the following rules:

- When modelling the eddy currents of the conducting region, the magnetic capacitances must be present in both the main directions, the circumferential and the radial direction, as in Fig. 36. Otherwise, the modelling does not take into account both of the flux components.
- When modelling the currents induced in a coil wound around the region, only the main direction perpendicular to the coil cross-section needs the magnetic capacitances, as in Fig. 37.
- The MMF sources, caused by currents flowing in the other reluctance elements, cannot be included in the capacitance model. These must be distributed among the main branches of the capacitive reluctance element as presented in the previous chapters, as in Fig. 38.

a   b   c
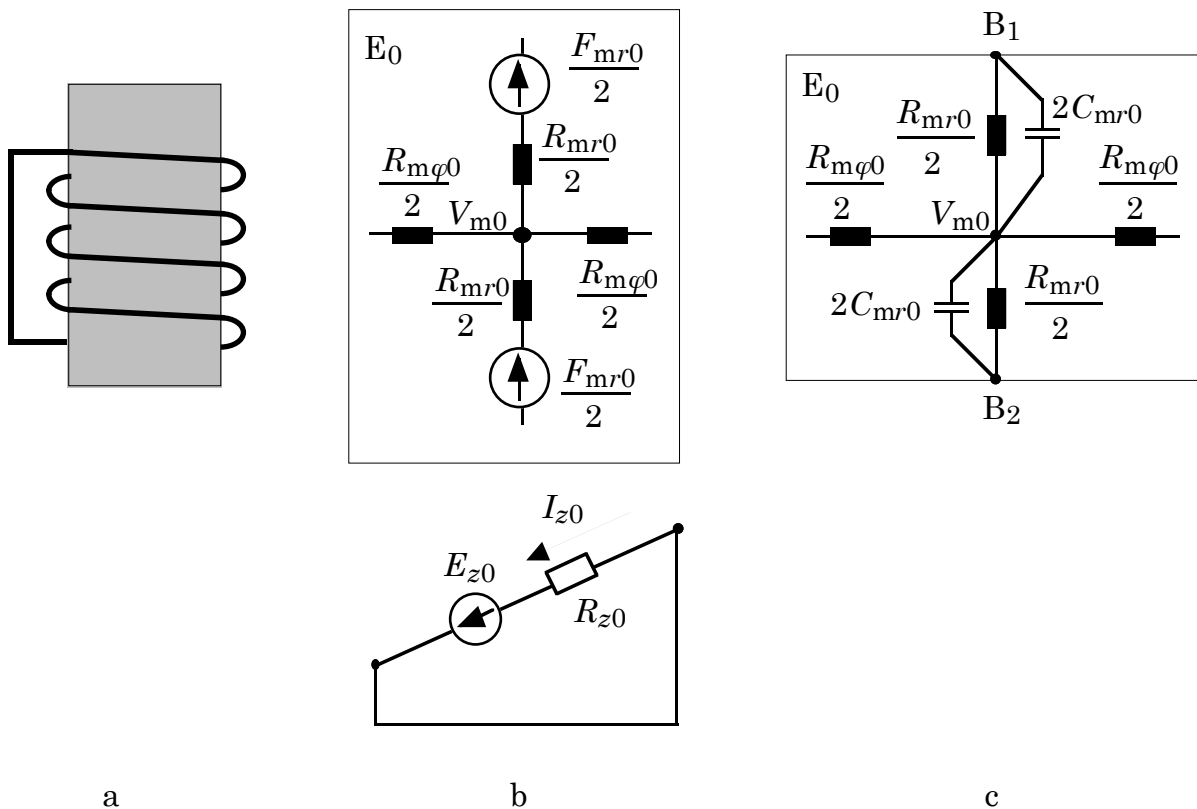
Fig. 37   Alternative layouts of the reluctance element E_0 of a short-circuited coil.
a) A concentric, short-circuited coil wound around the flux-path region.
b) The reluctance element E_0 of the flux-path region and the electric element modelling the coil.
c) The capacitive reluctance element E_0 replacing the separate reluctance and electric elements.
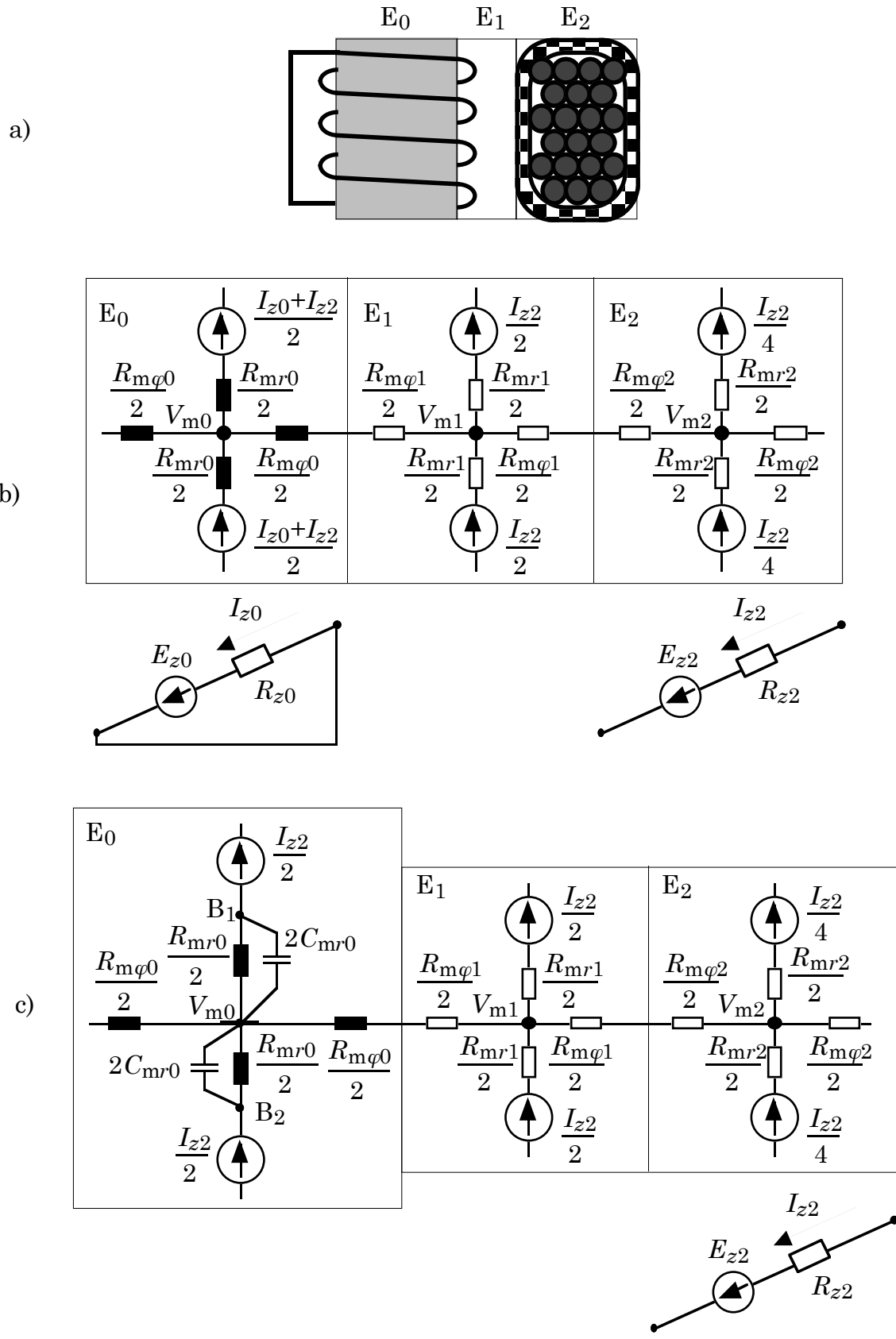
Fig. 38 *Alternative layouts of the reluctance element E_0 of a short-circuited coil.*
a) A concentric, short-circuited coil and a multi-wire coil.
b) The reluctance and electric models of the flux-path regions.
c) Using the capacitive reluctance element E_0 for a short-circuited coil.

5.3 Eddy-current losses in iron

In this section, the magnetic capacitance will be demonstrated, when used to estimate the eddy-current losses in the core region.

The eddy currents caused by the flux variation in the iron may be defined in the reluctance network as with the eddy currents in the conductor. For a massive iron or for an iron-sheet package, the equivalent of the conductor region is possible. The solution of capacitance directs at least one part of the iron losses into the correct positions. The hysteresis losses of the material remain unsolved when using this model because of the different origin discussed in Chapter 3.

The conventional equation for eddy-current losses of the flux-path region e was presented in Eq. (24)

$$P_{\mathrm{r},e} = p_{\mathrm{r},e}\, f_e^2\, \hat{b}_e^2 \tag{85}$$

The eddy-current losses may be modelled as the losses dissipated in an equivalent bar current in the flux-path region. The loss equation, Eq. (85), is modified to form an equivalent equation with the resistance $R_{P\mathrm{fe},e}$ and the induced EMF source $E_{P\mathrm{fe},e}$ causing the same power loss for the flux-path region e. The eddy-current losses are given by

$$P_{\mathrm{r},e} = p_{\mathrm{r},e} \frac{1}{A_{\Phi,e}^2} \left(\frac{\mathrm{d}\Phi_e}{\mathrm{d}t} \right)^2 = \frac{E_{P\mathrm{fe},e}^2}{R_{P\mathrm{fe},e}} \tag{86}$$

where $A_{\Phi,e}$ is the area of the flux-path region perpendicular to the flux Φ_e.

The equivalent bar resistances $R_{P\mathrm{fe},\varphi,e}$ and $R_{P\mathrm{fe},r,e}$ for the circumferential and radial branches in the flux-path region e are

$$\begin{cases} R_{P\mathrm{fe},\varphi,e} = \dfrac{A_{\varphi,e}^2}{p_{\mathrm{r},e}} \\[2em] R_{P\mathrm{fe},r,e} = \dfrac{A_{r,e}^2}{p_{\mathrm{r},e}} \end{cases} \tag{87}$$

Using the equivalent resistances and the reluctances of the flux-path region, it is possible to construct a capacitive reluctance element, where the definition of magnetic capacitances $C_{m\varphi,\text{fe},e}$ and $C_{mr,\text{fe},e}$ is equivalent to the magnetic capacitances $C_{m\varphi}$ and C_{mr} in Eqs. (79) and (82)

$$
\begin{cases}
C_{m\varphi,\text{fe},e} = \dfrac{1}{R_{P\text{fe},\varphi,e}\, R_{m\varphi,e}^2} \\[4mm]
C_{mr,\text{fe},e} = \dfrac{1}{R_{P\text{fe},r,e}\, R_{mr,e}^2}
\end{cases}
\tag{88}
$$

In the construction of the reluctance network, account must be taken of the rule:

> When modelling the eddy-current losses, magnetic capacitances must be present for both of the main directions, the circumferential and the radial direction. Otherwise, the model does not take into account both of the flux-density components.

5.4 Conclusion

In this chapter, the magnetic capacitance for the universal reluctance network was specified. The magnetic capacitance was used as an equivalent for the eddy-current losses. The formula for the magnetic capacitance was developed, and the flux equation of the reluctance element node was reformed. In addition, the capacitance was included in the reluctance element of the universal reluctance network replacing the separate electric element of the flux-path region. The magnetic capacitance was additionally defined for the eddy-current losses in the core.

In the construction of the universal reluctance network, the following rules must be taken into account:

- When modelling the eddy -currents of the conducting region, the magnetic capacitances must be present for both of the main directions, the circumferential and the radial direction. Otherwise, the modelling does not take into account both of the flux components.
- When modelling the currents induced in a coil wound around the region, only one main direction perpendicular to the coil cross-section receives the magnetic capacitances.

- The MMF sources, caused by currents flowing in the other reluctance elements, cannot be included in the capacitance model. These must be distributed among the main branches of the capacitive reluctance element as presented in the previous chapters.
- When modelling the eddy-current losses in iron, the magnetic capacitances must be on both the main directions, the circumferential and the radial direction. Otherwise, the model does not take into account both of the flux-density components.

6 SOLUTION ALGORITHM

The aim of this chapter is to collect the system equations for time-stepping and sinusoidal analysis and solve them simultaneously using a matrix equation.

In this chapter, an introduction is included to the analysis of the reluctance model (MEC) in comparison with the finite element method (FEM). There will be a discussion about differences in what appear to be identical system equations.

6.1 Equations of the universal reluctance network

This section introduces the time-dependent and sinusoidal-approximation system equations used in the universal reluctance model. The system equations of the reluctance network consist of the equations of the winding, flux-path regions, and motion. In this study, of the equations of motion only the air-gap torque is considered.

6.1.1 Equations of the winding

The winding equations connect the electric model to the magnetic model and to the external voltage source. The equations are the voltage, EMF, and MMF equations.

Voltage equations

For a distributed winding, the single-phase equation with an external voltage source, as in Fig. 21, is

$$\left(R_\mathrm{L} + R \right) I + \frac{\mathrm{d}}{\mathrm{d}t}\left[\left(L_\mathrm{L} + L_\sigma \right) I \right] + E - E_\mathrm{L} = 0 \tag{89}$$

where the quantities are

    R_L the line -resistance,
    R the resistance of the winding phase,
    L_L the line inductance,
    L_σ the leakage inductance of the end-winding,
    I the phase current,
    E the phase EMF induced in the winding, and
    E_L the phase EMF of the external voltage source.

For a cage winding, the voltage equations are constructed for the radial and circumferential current circuits of the electric element E_0, as in Fig. 23

$$\begin{cases} -R_{z0}I_{z0} + R_{z3}I_{z3} + \left(R_{\varphi 0} + R_{\varphi 3}\right)I_{\varphi 0} + \dfrac{\mathrm{d}}{\mathrm{d}t}\left[L_{\sigma,0,3}I_{\varphi 0}\right] - E_{z0} + E_{z3} = 0 \\[2mm] R_{z0}I_{z0} - R_{z4}I_{z4} + \left(R_{r0} + R_{r4}\right)I_{r0} + \dfrac{\mathrm{d}}{\mathrm{d}t}\left[L_{\sigma,0,4}I_{r0}\right] + E_{z0} - E_{z4} = 0 \end{cases} \tag{90}$$

where the quantities are

$R_{z,e}$ the axial resistance of the electric element e,

$R_{\varphi,e}$ the circumferential resistance of the electric element e,

$R_{r,e}$ the radial resistance of the electric element e,

$L_{\sigma,e,i}$ the leakage inductance of the end-winding between the electric elements e and i,

$I_{z,e}$ the axial current of the electric element e,

$I_{\varphi,e}$ the circumferential current of the electric element e,

$I_{r,e}$ the radial current of the electric element e, and

$E_{z,e}$ the axial EMF induced in the equivalent coil connected to the electric element e.

EMF equations

For a distributed winding, the EMF equation for the EMF E_z induced in the equivalent coil of a coil-side, as in Fig. 17, is

$$E_z - \frac{\mathrm{d}\Psi}{\mathrm{d}t} = 0 \tag{91}$$

where Ψ is the flux linkage of the coil-side.

For a cage winding, the EMF equation for the axial EMF $E_{z,e}$ induced in the equivalent coil connected to the electric element e, as in Fig. 20, is

$$E_{z,e} - \frac{\mathrm{d}\Psi_e}{\mathrm{d}t} = 0 \tag{92}$$

where Ψ_e is the flux linkage of the equivalent coil.

MMF equations

For a distributed winding, the MMF equation for the MMF difference $\Delta F_{\mathrm{m},e}$ of reluctance element e is

$$\Delta F_{\mathrm{m},e} - \frac{A_{z,e}}{A_{\mathrm{coil}}} N_{\mathrm{eff,coil}} I_{\mathrm{coil}} = 0 \tag{93}$$

where the quantities are

$A_{z,e}$ the axial current-carrying area of the element,
A_{coil} the total area of the coil in the slot,
$N_{\mathrm{eff,coil}}$ the number of effective turns of the coil, and
I_{coil} the current of the coil.

For a cage winding, the MMF equation for the MMF difference $\Delta F_{\mathrm{m},e}$ of reluctance element e is

$$\Delta F_{\mathrm{m},e} - I_{z,e} = 0 \tag{94}$$

where $I_{z,e}$ is the axial current of the element.

Sinusoidal equations

In the sinusoidal approximation, the quantities are replaced by complex phasors and the time derivative of the complex phasor by the multiplication by $j\omega$.

The equations of the distributed winding are in the sinusoidal approximation

$$\begin{cases} \left(R_{\mathrm{L}} + R\right)\vec{I} + j\omega\left(L_{\mathrm{L}} + L_{\sigma}\right)\vec{I} + \vec{E} - \vec{E}_{\mathrm{L}} = 0 \\ \vec{E}_z - j\omega\vec{\Psi} = 0 \\ \Delta\vec{F}_{\mathrm{m},e} - \dfrac{A_{z,e}}{A_{\mathrm{coil}}} N_{\mathrm{eff,coil}} \vec{I}_{\mathrm{coil}} = 0 \end{cases} \tag{95}$$

The equations of the cage winding are in the sinusoidal approximation

$$\begin{cases} -R_{z0}\vec{I}_{z0} + R_{z3}\vec{I}_{z3} + \left(R_{\varphi 0} + R_{\varphi 3}\right)\vec{I}_{\varphi 0} + j\omega L_{\sigma,0,3}\vec{I}_{\varphi 0} - \vec{E}_{z0} + \vec{E}_{z3} = 0 \\ R_{z0}\vec{I}_{z0} - R_{z4}\vec{I}_{z4} + \left(R_{r0} + R_{r4}\right)\vec{I}_{r0} + j\omega L_{\sigma,0,4}\vec{I}_{r0} + \vec{E}_{z0} - \vec{E}_{z4} = 0 \\ \vec{E}_{z,e} - j\omega\vec{\Psi}_e = 0 \\ \Delta\vec{F}_{\mathrm{m},e} - \vec{I}_{z,e} = 0 \end{cases} \tag{96}$$

6.1.2 Equations of the flux path

The flux-path equations define the flux balance on the reluctance model, the flux density of the reluctance elements, and connect the stator, rotor and air-gap models. The flux-path equations are the flux-balance equations of the magnetic potentials of the centre and border nodes, and the flux-density equations.

Flux-balance equation

For the centre node in an element E_0, as in Fig. 24, the flux-balance equation is

$$\Phi_{\mathrm{left}} + \Phi_{\mathrm{right}} + \Phi_{\mathrm{up}} + \Phi_{\mathrm{down}} = 0 \tag{97}$$

where the flux components are

- for a basic reluctance element, as in Fig. 24

$$\begin{cases} \Phi_{\mathrm{left}} = \dfrac{2}{R_{\mathrm{m}\varphi 0} + R_{\mathrm{m}\varphi 1}}\left[V_{\mathrm{m}0} - V_{\mathrm{m}1} + 0.5\left(F_{\mathrm{m}\varphi 0} + F_{\mathrm{m}\varphi 1}\right)\right] \\ \Phi_{\mathrm{right}} = \dfrac{2}{R_{\mathrm{m}\varphi 0} + R_{\mathrm{m}\varphi 3}}\left[V_{\mathrm{m}0} - V_{\mathrm{m}3} - 0.5\left(F_{\mathrm{m}\varphi 0} + F_{\mathrm{m}\varphi 3}\right)\right] \\ \Phi_{\mathrm{up}} = \dfrac{2}{R_{\mathrm{m}r0} + R_{\mathrm{m}r2}}\left[V_{\mathrm{m}0} - V_{\mathrm{m}2} + 0.5\left(F_{\mathrm{m}r0} + F_{\mathrm{m}r2}\right)\right] \\ \Phi_{\mathrm{down}} = \dfrac{2}{R_{\mathrm{m}r0} + R_{\mathrm{m}r4}}\left[V_{\mathrm{m}0} - V_{\mathrm{m}4} - 0.5\left(F_{\mathrm{m}r0} + F_{\mathrm{m}r4}\right)\right] \end{cases} \tag{98}$$

where

$R_{\mathrm{m}\varphi,e}$ is the circumferential reluctance of the element e,
$R_{\mathrm{m}r,e}$ is the radial reluctance of the element e,
$V_{\mathrm{m},e}$ is the magnetic potential of the centre node in element e,
$F_{\mathrm{m}\varphi,e}$ is the circumferential MMF source of the element e, and
$F_{\mathrm{m}r,e}$ is the radial MMF source of the element e.

- for a capacitive element, as in Fig. 36

$$
\begin{cases}
\Phi_{\text{left}} = 2\dfrac{V_{\text{m}0} - V_{\text{m,B1}}}{R_{\text{m}\varphi 0}} + 2\,C_{\text{m}\varphi 0}\dfrac{\text{d}\!\left(V_{\text{m}0} - V_{\text{m,B1}}\right)}{\text{d}t} \\[4mm]
\Phi_{\text{right}} = 2\dfrac{V_{\text{m}0} - V_{\text{m,B2}}}{R_{\text{m}\varphi 0}} + 2\,C_{\text{m}\varphi 0}\dfrac{\text{d}\!\left(V_{\text{m}0} - V_{\text{m,B2}}\right)}{\text{d}t} \\[4mm]
\Phi_{\text{up}} = 2\dfrac{V_{\text{m}0} - V_{\text{m,B3}}}{R_{\text{m}r0}} + 2\,C_{\text{m}r0}\dfrac{\text{d}\!\left(V_{\text{m}0} - V_{\text{m,B3}}\right)}{\text{d}t} \\[4mm]
\Phi_{\text{down}} = 2\dfrac{V_{\text{m}0} - V_{\text{m,B4}}}{R_{\text{m}r0}} + 2\,C_{\text{m}r0}\dfrac{\text{d}\!\left(V_{\text{m}0} - V_{\text{m,B4}}\right)}{\text{d}t}
\end{cases} \tag{99}
$$

where

$R_{\text{m}\varphi 0}$ is the circumferential reluctance of the element E_0,

$R_{\text{m}r0}$ is the radial reluctance of the element E_0,

$V_{\text{m}0}$ is the magnetic potential of the centre node in element E_0,

$V_{\text{m},i}$ is the magnetic potential of a border node i in element E_0,

$C_{\text{m}\varphi 0}$ is the circumferential magnetic capacitance of the element E_0, and

$C_{\text{m}r0}$ is the radial magnetic capacitance of the element E_0.

Flux-density equation

The flux density $\boldsymbol{B}_e$ is a vector quantity having a circumferential and radial component, $B_{\varphi,e}$ and $B_{r,e}$. Using the length of the flux-density vector, B_e, the flux density equation for a reluctance element e is

$$
B_e^2 - \frac{\Phi_{\text{left}}^2 + \Phi_{\text{right}}^2}{2\,A_{\varphi,e}^2} - \frac{\Phi_{\text{up}}^2 + \Phi_{\text{down}}^2}{2\,A_{r,e}^2} = 0 \tag{100}
$$

where

B_e is the length of the flux-density vector $B_e = \sqrt{B_{\varphi,e}^2 + B_{r,e}^2}$

Φ_i is the flux component defined in Eqs. (98) and (99),

$A_{\varphi,e}$ is the circumferential cross-section of the element, and

$A_{r,e}$ is the radial cross-section of the element.

Sinusoidal equations

In the sinusoidal approximation, the quantities are replaced by complex phasors and the time derivative of the complex phasor by the multiplication by $j\omega$.

The flux balance equation in the sinusoidal approximation is

$$\vec{\Phi}_{\text{left}} + \vec{\Phi}_{\text{right}} + \vec{\Phi}_{\text{up}} + \vec{\Phi}_{\text{down}} = 0 \tag{101}$$

where the flux components are

- for a basic reluctance element, as in Fig. 24

$$\begin{cases} \vec{\Phi}_{\text{left}} = \dfrac{2}{R_{\text{m}\varphi 0} + R_{\text{m}\varphi 1}}\left[\vec{V}_{\text{m}0} - \vec{V}_{\text{m}1} + 0.5\left(\vec{F}_{\text{m}\varphi 0} + \vec{F}_{\text{m}\varphi 1}\right)\right] \\[2mm] \vec{\Phi}_{\text{right}} = \dfrac{2}{R_{\text{m}\varphi 0} + R_{\text{m}\varphi 3}}\left[\vec{V}_{\text{m}0} - \vec{V}_{\text{m}3} - 0.5\left(\vec{F}_{\text{m}\varphi 0} + \vec{F}_{\text{m}\varphi 3}\right)\right] \\[2mm] \vec{\Phi}_{\text{up}} = \dfrac{2}{R_{\text{m}r0} + R_{\text{m}r2}}\left[\vec{V}_{\text{m}0} - \vec{V}_{\text{m}2} + 0.5\left(\vec{F}_{\text{m}r0} + \vec{F}_{\text{m}r2}\right)\right] \\[2mm] \vec{\Phi}_{\text{down}} = \dfrac{2}{R_{\text{m}r0} + R_{\text{m}r4}}\left[\vec{V}_{\text{m}0} - \vec{V}_{\text{m}4} - 0.5\left(\vec{F}_{\text{m}r0} + \vec{F}_{\text{m}r4}\right)\right] \end{cases} \tag{102}$$

- for a capacitive element, as in Fig. 36

$$\begin{cases} \vec{\Phi}_{\text{left}} = \left(\dfrac{2}{R_{\text{m}\varphi 0}} + j2\omega C_{\text{m}\varphi 0}\right)\left(\vec{V}_{\text{m}0} - \vec{V}_{\text{m,B1}}\right) \\[2mm] \vec{\Phi}_{\text{right}} = \left(\dfrac{2}{R_{\text{m}\varphi 0}} + j2\omega C_{\text{m}\varphi 0}\right)\left(V_{\text{m}0} - V_{\text{m,B2}}\right) \\[2mm] \vec{\Phi}_{\text{up}} = \left(\dfrac{2}{R_{\text{m}r0}} + j2\omega C_{\text{m}r0}\right)\left(V_{\text{m}0} - V_{\text{m,B3}}\right) \\[2mm] \vec{\Phi}_{\text{down}} = \left(\dfrac{2}{R_{\text{m}r0}} + j2\omega C_{\text{m}r0}\right)\left(\vec{V}_{\text{m}0} - \vec{V}_{\text{m,B4}}\right) \end{cases} \tag{103}$$

In the sinusoidal approximation, the flux density $\vec{B}_e$ is a vector quantity in space and a phasor quantity in time. In space, it has the circumferential and radial component, which are the phasors $\vec{B}_{\varphi,e}$ and $\vec{B}_{r,e}$. The flux density, the vector in space and the phasor in time, is

$$\boldsymbol{B}_e = \mathrm{Re}\left\{\boldsymbol{B}_e\right\} + j\mathrm{Im}\left\{\boldsymbol{B}_e\right\} = \mathrm{Re}\left\{\vec{B}_{re} + i\vec{B}_{\varphi e}\right\} + j\mathrm{Im}\left\{\vec{B}_{re} + i\vec{B}_{\varphi e}\right\} \tag{104}$$

where

Re{ }   means the operator giving the real part of the complex number,

Im{ }   means the operator giving the imaginary part of the complex number,

j means the imaginary unit $j = \sqrt{-1}$ in time, and

i means the imaginary unit $i = \sqrt{-1}$ in space.

The flux-density equations are the equations for the real and imaginary time-components of the flux density

$$\begin{cases} \left(\mathrm{Re}\left\{\boldsymbol{B}_e\right\}\right)^2 - \dfrac{\left(\mathrm{Re}\left\{\vec{\Phi}_{\mathrm{left}}\right\}\right)^2 + \left(\mathrm{Re}\left\{\vec{\Phi}_{\mathrm{right}}\right\}\right)^2}{2A_{\varphi,e}^2} - \dfrac{\left(\mathrm{Re}\left\{\vec{\Phi}_{\mathrm{up}}\right\}\right)^2 + \left(\mathrm{Re}\left\{\vec{\Phi}_{\mathrm{down}}\right\}\right)^2}{2A_{r,e}^2} = 0 \\[3em] \left(\mathrm{Im}\left\{\boldsymbol{B}_e\right\}\right)^2 - \dfrac{\left(\mathrm{Im}\left\{\vec{\Phi}_{\mathrm{left}}\right\}\right)^2 + \left(\mathrm{Im}\left\{\vec{\Phi}_{\mathrm{right}}\right\}\right)^2}{2A_{\varphi,e}^2} - \dfrac{\left(\mathrm{Im}\left\{\vec{\Phi}_{\mathrm{up}}\right\}\right)^2 + \left(\mathrm{Im}\left\{\vec{\Phi}_{\mathrm{down}}\right\}\right)^2}{2A_{r,e}^2} = 0 \end{cases}$$
$$\tag{105}$$

where the quantities $\vec{\Phi}_i$ are the flux phasors defined in Eqs. (102) and (103).

6.1.3   Equations of motion

The equations of motion connect the magnetic model to the mechanical model. In this study, only the equation of the air-gap torque is used. The summation in the torque equation collects all the movement derivatives for the magnetic energy of the air-gap elements e

$$T_\delta + \sum_e \left(\frac{W_{\mathrm{m},e}}{\alpha_e} \frac{\partial \alpha_e}{\partial \alpha}\right) = 0 \tag{106}$$

where the quantities are

T_δ the air-gap torque,

$W_{\mathrm{m},e}$ the magnetic (co-)energy of the air-gap element e,

α_e the angular width of the sector of the element e, and

α the angular width variable.

The equation in the sinusoidal approximation is identical.

6.2 Derivative of flux balance equation

In this section, the derivative of the flux-balance equation is discussed as an example of the derivatives of the system equations in the universal reluctance network. Additionally, this section introduces differences in how the reluctance model (MEC) and the finite element method (FEM) define the derivative. The discussion will show differences in what appear to be the same kind of system equations.

In the magnetic field analysis, both the analysis tools, MEC and FEM, solve definite quantities. In the FEM model, the magnetic vector potentials of nodes are solved. In the MEC model used in this study, the magnetic scalar potentials of nodes are solved. In the literature on MEC model theory, both the magnetic vector potentials and the magnetic scalar potentials are used. For example, Atkins (Atkins 1958) and Ostovic (Ostovic 1989a) use magnetic scalar potentials, Oberretl (Oberretl 1963) and Roberts (Roberts 1960, 1962) use magnetic vector potentials.

In the FEM model, the conventional element is a triangular element of either first or second order. Each element has either three (first order) or six (second order) unknown nodal potentials. In the MEC model using the magnetic scalar potentials of nodes, the elements are of different shape but of equal two-axis analogy. Each element has one unknown centre potential. To connect more than two elements through a common potential line, the border between the elements has an extra unknown potential.

In the universal reluctance model, the scalar potentials and the information about the reluctivity of the element are calculated at the same time. When the distribution of scalar potentials is solved, the reluctivity derivatives of the elements are taken into account when calculating the necessary increments to the potentials.

In the reluctance model presented in Fig. 39a or Fig. 39b, the flux-balance equation of the scalar potential V_{m0} of element E_0 may be written as

$$
\begin{aligned}
f(V_{m0}) = {} & \frac{2}{R_{m\varphi0} + R_{m\varphi1}}\left(V_{m0} - V_{m1}\right) + \frac{2}{R_{mr0} + R_{mr2}}\left(V_{m0} - V_{m2}\right) \\
& + \frac{2}{R_{m\varphi0} + R_{m\varphi3}}\left(V_{m0} - V_{m3}\right) + \frac{2}{R_{mr0} + R_{mr4}}\left(V_{m0} - V_{m4}\right) = 0
\end{aligned}
\tag{107}
$$
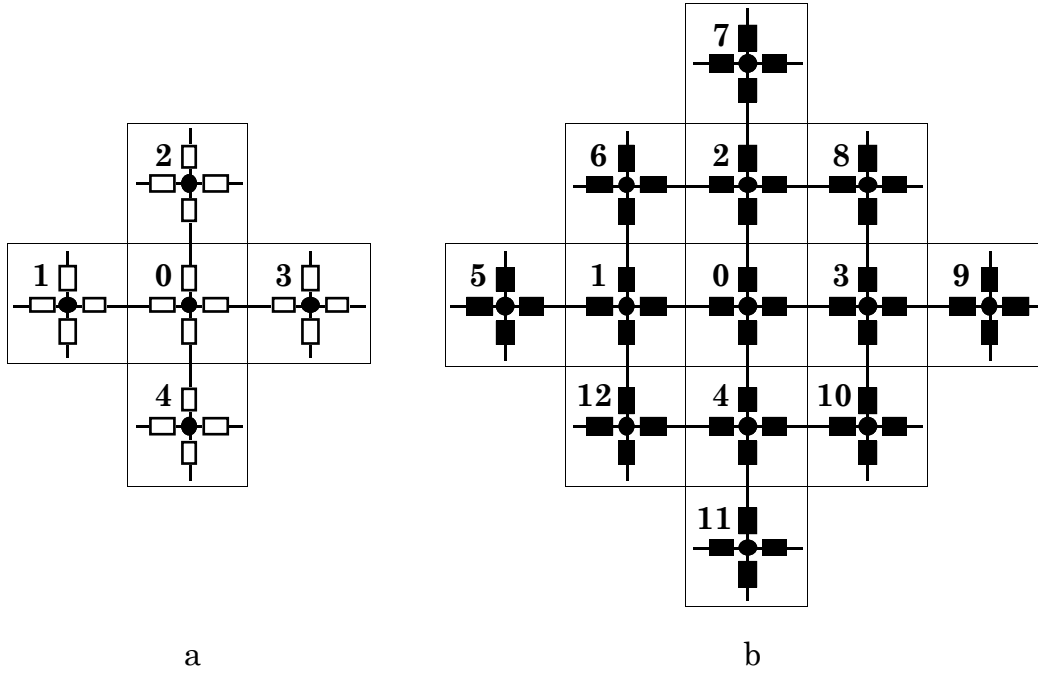
Fig. 39 The nodal potentials influencing the flux-balance equation and the derivative
formula of the nodal potential of element E_0, indexed by 0.
a) The reluctivity of the reluctance elements E_0 to E_4 is constant.
b) The reluctivity of the reluctance elements E_0 to E_4 is a function of flux density.

The reluctance models in Fig. 39 have different material properties of elements. In the
models, the circumferential and radial reluctances of the element e are

$$
\begin{cases}
R_{m\varphi,e} = \nu_e r_{m\varphi,e} \\
R_{mr,e} = \nu_e r_{mr,e}
\end{cases}
\tag{108}
$$

where the circumferential and radial reluctance factors $r_{m\varphi,e}$ and $r_{mr,e}$, defined in
Section 4.3, are independent of the material properties. In Fig. 39a, the reluctivity ν_e
is constant, and in Fig. 39b, the reluctivity ν_e is a function of flux density B_e.

For the elements of constant reluctivity in Fig. 39a, the derivative of Eq. (107) is

$$
\sum_{j=0}^{4} \left[\frac{\partial f(V_{m0})}{\partial V_{mj}} \right] =
$$

$$
\frac{2}{R_{m\varphi 0} + R_{m\varphi 1}} \left[\frac{\partial V_{m0}}{\partial V_{m0}} - \frac{\partial V_{m1}}{\partial V_{m1}} \right] + \frac{2}{R_{mr0} + R_{mr2}} \left[\frac{\partial V_{m0}}{\partial V_{m0}} - \frac{\partial V_{m2}}{\partial V_{m2}} \right]
\tag{109}
$$

$$
+ \frac{2}{R_{m\varphi 0} + R_{m\varphi 3}} \left[\frac{\partial V_{m0}}{\partial V_{m0}} - \frac{\partial V_{m3}}{\partial V_{m3}} \right] + \frac{2}{R_{mr0} + R_{mr4}} \left[\frac{\partial V_{m0}}{\partial V_{m0}} - \frac{\partial V_{m4}}{\partial V_{m4}} \right]
$$

The derivative formula, Eq. (109), has only the derivatives of the nodal potentials presented in Fig. 39a.

In the model of Fig. 39b, the reluctances in Eq. (107) are functions of flux densities of the regions E_0 to E_4. The flux densities B_0 to B_4 of the regions are functions of the nodal potential of the region and the nodal potentials of the neighbouring regions

$$
\begin{cases}
R_{m\varphi0} = \nu_0(B_0)\,r_{m\varphi0} = \nu_0(V_{m0},V_{m1},V_{m2},V_{m3},V_{m4})\,r_{m\varphi0} \\
R_{mr0} = \nu_0(B_0)\,r_{mr0} = \nu_0(V_{m0},V_{m1},V_{m2},V_{m3},V_{m4})\,r_{mr0} \\
R_{m\varphi1} = \nu_1(B_1)\,r_{m\varphi1} = \nu_1(V_{m0},V_{m1},V_{m5},V_{m6},V_{m12})\,r_{m\varphi1} \\
R_{mr2} = \nu_2(B_2)\,r_{mr2} = \nu_2(V_{m0},V_{m2},V_{m6},V_{m7},V_{m8})\,r_{mr2} \\
R_{m\varphi3} = \nu_3(B_3)\,r_{m\varphi3} = \nu_3(V_{m0},V_{m3},V_{m8},V_{m9},V_{m10})\,r_{m\varphi3} \\
R_{mr4} = \nu_4(B_4)\,r_{mr4} = \nu_4(V_{m0},V_{m4},V_{m10},V_{m11},V_{m12})\,r_{mr4}
\end{cases}
\tag{110}
$$

For the elements of variable reluctivity in Fig. 39b, the derivative of Eq. (107) is

$$
\sum_{j=0}^{12}\left[\frac{\partial f(V_{m0})}{\partial V_{mj}}\right] =
$$

$$
\frac{2}{R_{m\varphi0}+R_{m\varphi1}}\left[\frac{\partial V_{m0}}{\partial V_{m0}}-\frac{\partial V_{m1}}{\partial V_{m1}}\right] + \frac{2}{R_{mr0}+R_{mr2}}\left[\frac{\partial V_{m0}}{\partial V_{m0}}-\frac{\partial V_{m2}}{\partial V_{m2}}\right]
$$

$$
+\frac{2}{R_{m\varphi0}+R_{m\varphi3}}\left[\frac{\partial V_{m0}}{\partial V_{m0}}-\frac{\partial V_{m3}}{\partial V_{m3}}\right] + \frac{2}{R_{mr0}+R_{mr4}}\left[\frac{\partial V_{m0}}{\partial V_{m0}}-\frac{\partial V_{m4}}{\partial V_{m4}}\right]
$$

$$
-\frac{2\left(V_{m0}-V_{m1}\right)}{\left(R_{m\varphi0}+R_{m\varphi1}\right)^2}\sum_{j=0}^{12}\left[r_{m\varphi0}\frac{\partial \nu_0}{\partial B_0^2}\frac{\partial B_0^2}{\partial V_{mj}}+r_{m\varphi1}\frac{\partial \nu_1}{\partial B_1^2}\frac{\partial B_1^2}{\partial V_{mj}}\right]
$$

$$
-\frac{2\left(V_{m0}-V_{m2}\right)}{\left(R_{mr0}+R_{mr2}\right)^2}\sum_{j=0}^{12}\left[r_{mr0}\frac{\partial \nu_0}{\partial B_0^2}\frac{\partial B_0^2}{\partial V_{mj}}+r_{mr2}\frac{\partial \nu_2}{\partial B_2^2}\frac{\partial B_2^2}{\partial V_{mj}}\right]
\tag{111}
$$

$$
-\frac{2\left(V_{m0}-V_{m3}\right)}{\left(R_{m\varphi0}+R_{m\varphi3}\right)^2}\sum_{j=0}^{12}\left[r_{m\varphi0}\frac{\partial \nu_0}{\partial B_0^2}\frac{\partial B_0^2}{\partial V_{mj}}+r_{m\varphi3}\frac{\partial \nu_3}{\partial B_3^2}\frac{\partial B_3^2}{\partial V_{mj}}\right]
$$

$$
-\frac{2\left(V_{m0}-V_{m4}\right)}{\left(R_{mr0}+R_{mr4}\right)^2}\sum_{j=0}^{12}\left[r_{mr0}\frac{\partial \nu_0}{\partial B_0^2}\frac{\partial B_0^2}{\partial V_{mj}}+r_{mr4}\frac{\partial \nu_4}{\partial B_4^2}\frac{\partial B_4^2}{\partial V_{mj}}\right]
$$

All the nodal potentials having a derivative in the derivative formula, Eq. (111), are presented in Fig. 39b.

The increment ΔV_{m0} for the potential V_{m0} may be calculated from the equation

$$\Delta V_{m0} = \frac{f(V_{m0}) - \sum_{j=1}^{12}\left[\frac{\partial f(V_{m0})}{\partial V_{mj}} \Delta V_{mj}\right]}{\frac{\partial f(V_{m0})}{\partial V_{m0}}} \tag{112}$$

In the FEM model, the vector potentials are calculated separately from the reluctivity of the element. When the distribution of the vector potentials is solved, the reluctivity of the elements is checked. If necessary, the vector potentials are solved using the new reluctivity values. The vector potentials connected to the derivative formula of the FEM model are presented in Fig. 40a for the first-order and in Fig. 40b for the second order element independent of the material of the elements.

The differences between the MEC and FEM models are:

- The MEC model has a large number of unknowns connected to an equation. The calculation speed in matrix form is slow because the matrix of the derivatives of equations approximates to the full matrix.
- The FEM model has a small number of unknowns connected to an equation. The calculation speed in matrix form is fast because the matrix of the derivatives of equations is a sparse matrix and the elements are concentrated around the

a   b
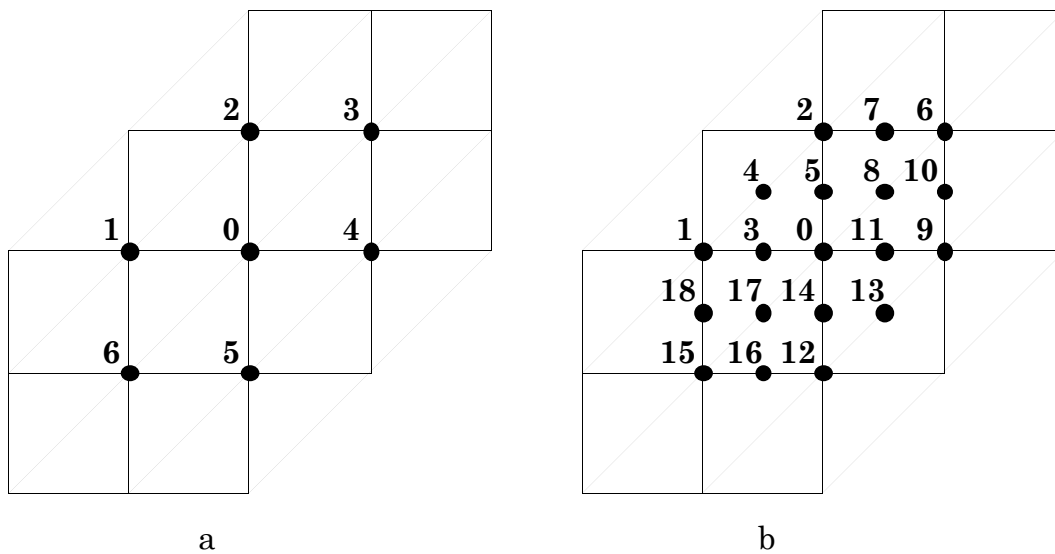
Fig. 40   The nodal vector potentials influencing the energy equations and the derivative formula of the nodal potential A_{z0} in FEM models.
a) A first-order FEM model and b) a second-order FEM model.

diagonal of the matrix.

The total calculation speed depends on the sparsity of the derivative matrix and the number of iterations required to obtain a result. The method used in the FEM model, to take into account only a portion of the variables that are influencing the equation balance, converges more slowly than the method used in the MEC model. The common effect of the sparsity and the number of derivatives depends on the MEC model construction:

- When the MEC model has only one layer in the yoke and one element or at least one sector of elements in a tooth, the number of derivatives of equations is the smallest one to take into account the properties of iron. The sparsity of the derivative matrix is almost the same as in the FEM model. The iteration speed and the convergence are fast.
- When the MEC model has many layers in the yoke and many sectors of elements in a tooth, the number of rows like Eq. (111) increases in the derivative matrix. The derivative matrix changes from a sparse structure to almost a full matrix. The advantage of the MEC model in iteration speed disappears. The situation between the speed of methods used in the MEC and FEM models is reversed.

6.3 Matrix equation

This section introduces the procedure to solve the system equations in the universal reluctance network.

The equations of the reluctance network can be written as a matrix equation

$$\mathbf{AX} - \mathbf{F} = \mathbf{0} \tag{113}$$

where the quantities are

$\mathbf{A}$ the time-dependent square-matrix,
$\mathbf{X}$ the vector of the unknowns, and
$\mathbf{F}$ the time-dependent vector of the sources.

The indexing in the following matrices and vectors results in the group of equations:

- index = 1   the group of equations of the stator winding and stator flux-paths,
- index = 2   the group of equations of the air-gap flux-paths,

- index = 3   the group of equations of the rotor winding and rotor flux-paths, and

- index = 4   the group of equations of the air-gap torque.

The square-matrix $\mathbf{A}$ is

$$\mathbf{A} = \begin{bmatrix} \mathbf{A}_1 & \mathbf{0} & \mathbf{0} & \mathbf{0} \\ \mathbf{0} & \mathbf{A}_2 & \mathbf{0} & \mathbf{0} \\ \mathbf{0} & \mathbf{0} & \mathbf{A}_3 & \mathbf{0} \\ \mathbf{0} & \mathbf{0} & \mathbf{0} & \mathbf{A}_4 \end{bmatrix} \tag{114}$$

where $\mathbf{0}$ indicates that all the elements of the region are zeroes.

The vectors $\mathbf{X}$ and $\mathbf{F}$ are

$$\mathbf{X} = \begin{bmatrix} \mathbf{X}_1, \mathbf{X}_2, \mathbf{X}_3, \mathbf{X}_4 \end{bmatrix}^{\mathrm{T}} \tag{115}$$

$$\mathbf{F} = \begin{bmatrix} \mathbf{F}_1, \mathbf{F}_2, \mathbf{F}_3, \mathbf{F}_4 \end{bmatrix}^{\mathrm{T}} \tag{116}$$

For the numerical solution, the equation is transformed into a discrete form

$$\mathbf{M}^{(k)}\mathbf{X}^{(k)} + \mathbf{F}^{(k)} = \mathbf{R}^{(k)} \tag{117}$$

where

     k is the time-stepping index of the analysis,
     $\mathbf{M}^{(k)}$ the discrete coefficient matrix,
     $\mathbf{X}^{(k)}$ the discrete vector $\mathbf{X}$,
     $\mathbf{F}^{(k)}$ the discrete vector $\mathbf{F}$, and
     $\mathbf{R}^{(k)}$ the residual vector at time step k.

The discretisation of the equations is done using the Crank-Nicholson method, whereby the time derivative of the variable x at time step k is replaced by the values of the variable x at time steps k and k-1 according to the trapezoidal rule

$$\frac{1}{2}\left(\frac{\mathrm{d}x^{(k)}}{\mathrm{d}t} + \frac{\mathrm{d}x^{(k-1)}}{\mathrm{d}t} \right) = \frac{x^{(k)} - x^{(k-1)}}{\Delta t} \tag{118}$$

The discrete matrix $\mathbf{M}^{(k)}$ and the discrete vectors $\mathbf{X}^{(k)}$, $\mathbf{F}^{(k)}$, and $\mathbf{R}^{(k)}$ are

$$\mathbf{M}^{(k)} = \begin{bmatrix} \mathbf{M}_1^{(k)} & \mathbf{0} & \mathbf{0} & \mathbf{0} \\ \mathbf{0} & \mathbf{M}_2^{(k)} & \mathbf{0} & \mathbf{0} \\ \mathbf{0} & \mathbf{0} & \mathbf{M}_3^{(k)} & \mathbf{0} \\ \mathbf{0} & \mathbf{0} & \mathbf{0} & \mathbf{M}_4^{(k)} \end{bmatrix} \tag{119}$$

$$\mathbf{X}^{(k)} = \left[\mathbf{X}_1^{(k)}, \mathbf{X}_2^{(k)}, \mathbf{X}_3^{(k)}, \mathbf{X}_4^{(k)} \right]^{\mathrm{T}} \tag{120}$$

$$\mathbf{F}^{(k)} = \left[\mathbf{F}_1^{(k)}, \mathbf{F}_2^{(k)}, \mathbf{F}_3^{(k)}, \mathbf{F}_4^{(k)} \right]^{\mathrm{T}} \tag{121}$$

$$\mathbf{R}^{(k)} = \left[\mathbf{R}_1^{(k)}, \mathbf{R}_2^{(k)}, \mathbf{R}_3^{(k)}, \mathbf{R}_4^{(k)} \right]^{\mathrm{T}} \tag{122}$$

The matrix equation Eq. (117) is solved by iteration. The value of the variable vector $\mathbf{X}^{(k)}$, at time step k is iterated until the residual vector $\mathbf{R}^{(k)}$ is acceptably small. The value of the variable vector for the next iteration step $i+1$ is calculated from the equation group

$$\begin{cases} \mathbf{X}_{(i+1)}^{(k)} = \mathbf{X}_{(i)}^{(k)} - \Delta\mathbf{X} \\ \mathbf{D}_{(i)}^{(k)} \Delta\mathbf{X} - \mathbf{R}_{(i)}^{(k)} = \mathbf{0} \end{cases} \tag{123}$$

where

$\quad i \qquad$ is the iteration step at time step k,

$\quad \Delta\mathbf{X} \qquad$ the difference vector,

$\quad \mathbf{R}_{(i)}^{(k)} \qquad$ the residual vector $\mathbf{R}^{(k)}$ and

$\quad \mathbf{D}_{(i)}^{(k)} \qquad$ the derivative of the matrix $\mathbf{M}^{(k)}$ at the iteration step i.

An element of the matrix $\mathbf{D}_{(i)}^{(k)}$ is

$$\mathbf{D}_{(i)}^{(k)}\big[a,b\big] = \mathbf{M}_{(i)}^{(k)}\big[a,b\big] + \sum_{m=1}^{n}\left\{\mathbf{X}_{(i)}^{(k)}\big[m\big] \cdot \frac{\partial \mathbf{M}_{(i)}^{(k)}\big[a,m\big]}{\partial \mathbf{X}\big[b\big]}\right\} \tag{124}$$

where a is a row, b a column, and n the number of columns in the matrix $\mathbf{M}^{(k)}$.

6.4 Conclusion

In this chapter, the system equations for time-stepping and sinusoidal-approximation analysis were collected, and the method for matrix calculation was introduced. The reluctance model (MEC) and the finite element method (FEM) were compared according to how they solve the iterative calculation process.

While the system equations were of the same type, there were differences in the methods. A discussion was presented about the sparsity of the matrix and the iteration speed. The method used in FEM model solves first the nodal potentials and then the reluctivity of elements. The method used in the MEC model of this study solves the nodal potentials and the reluctivity of elements together. It was noted that the method of FEM model converges more slowly than the method of MEC model as long as the MEC model uses fewer parallel elements with variable reluctivity.

7 SINGLE-PHASE EQUIVALENT CIRCUIT

This chapter introduces a single-phase equivalent circuit for the cage-induction machine. The components of the model will be specified using results of the analysis of the reluctance network.

7.1 Reference slot-pitch model

In the analysis using the reluctance network, the electric model of the stator winding is connected to a sinusoidal voltage supply. The rotor is at stand-still and the air-gap model in the reluctance network is constant. The analysis uses the time-stepping method for a steady state analysis and divides the period of the fundamental voltage harmonic into calculation time-steps. The method solves the flux and current distribution on the reluctance model at every time step. The distribution gives the magnetic energy and the loss energy in the reluctance elements.

To form the components of a single-phase equivalent circuit, a reference slot-pitch will be constructed, as in Fig. 29. The reference slot-pitch represents the effect of all the slot pitches of the machine cross-section. The energy of the model is the energy of all the flux-path regions on the machine cross-section and calculated over one period of the supply frequency. In the reference slot-pitch, the energy of flux-path region is the
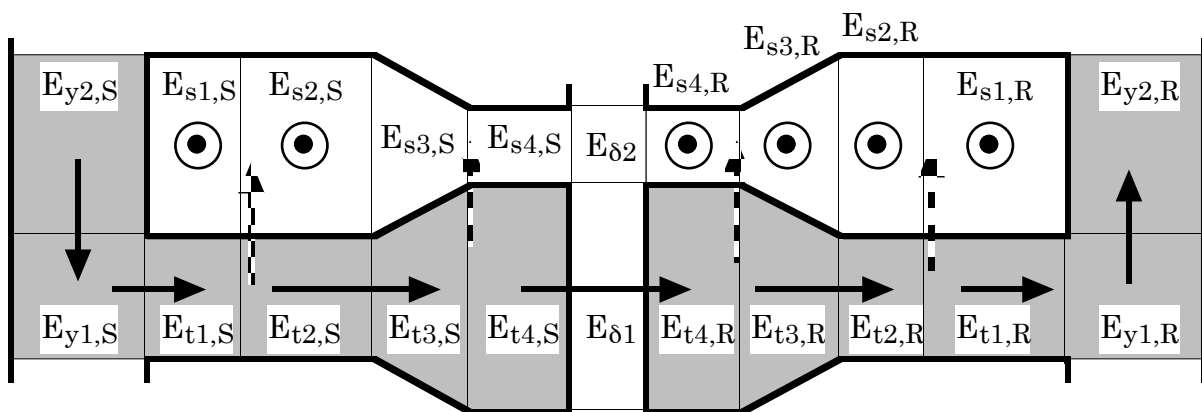
Fig. 41   The reference slot-pitch of the cage-induction motor.
The assumed flux flow is shown by arrows, the dashed arrow means a leakage flux component and the black arrow a main flux component. The index y in the name of a region means the yoke, s the slot, and t the tooth. The stator regions are with an index S, the air-gap regions with an index δ and the rotor regions with an index R.

sum of energy from the reluctance elements of the flux-path regions on the machine cross-section having the same position in its own slot-pitch sector.

The property of a reluctance element is based on the radial and circumferential flux components presented as arrows in the reference slot-pitch, as in Fig. 41. In the reference slot-pitch, the energy components are collected according to the radial and circumferential components of energy.

7.2 Basis of construction

In this study, a single-phase equivalent circuit used for a double-cage motor will be constructed. The single-phase equivalent circuit consists of resistances and reactances, as in Fig. 42. The resistances represent the average losses in the windings and in the core. The reactances are the equivalents of the magnetic energy in the stator, in the air gap, and in the rotor. The definition of the resistances and reactances is based on the average energy distribution in the machine over one period of the supply frequency. An extension of iron loss resistances parallel to all reactances will be used, as in (Perho 1993). The chosen equivalent circuit models the leakage-flux paths, iron losses, and the current distribution in the rotor cage with more details than the standard single-phase equivalent circuit.

In the single-phase equivalent circuit, the definition of a component bases on the main or leakage flux paths:
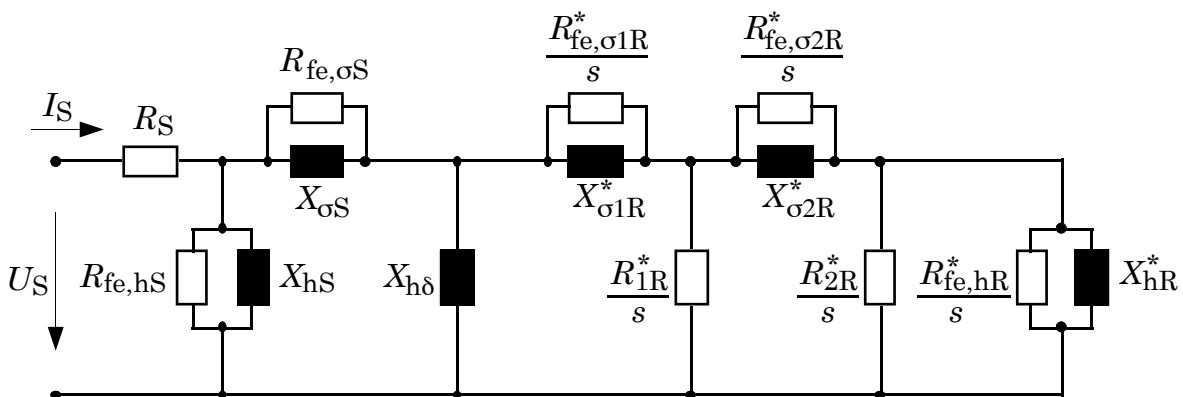
Fig. 42   The single-phase equivalent circuit of the cage-induction motor (Perho 1993). The components of the main flux path have an index h and the components of the leakage flux path an index σ. s is the slip of the rotor. The asterisk indicates that the quantity is referred to the stator.

- In the yoke region, the path of the main flux and the path of the leakage flux join. In the equivalent circuit, the component represents the energy of the joined flux path region. In the reference slot-pitch, the energy in an element of yoke is calculated as a sum of both the circumferential and radial flux flow.
- In the tooth region, the path of the main flux and the path of the leakage flux deviate. In the equivalent circuit, there have to be two components to represent both the main-flux energy and the leakage-flux energy of the region. In the reference slot-pitch, the energy in an element of tooth is calculated as a sum for the circumferential flux flow corresponding the effect of leakage flux and for the radial flux flow corresponding the effect of main flux.
- In the slot region, only the leakage flux flows on the region. In the equivalent circuit, the component represents the energy of the flux path region. In the reference slot-pitch, the energy in an element of slot is calculated as a sum of both the circumferential and radial flux flow.

The single-phase equivalent circuit may have as many branches as there are elements in the reference slot-pitch. To reduce the size of the equivalent circuit, the energy of elements will be combined. The main aspect is to combine the energy according to the flux flow. The energy of slot and the energy of leakage flux of tooth will be combined to a common leakage reactance, as $X_{\sigma S}$ includes the energy of the reluctance elements $E_{s1,S}$ to $E_{s4,S}$ and the circumferential-flux energy of the reluctance elements $E_{t1,S}$ to $E_{t4,S}$. The energy of yoke and the energy of main flux of tooth will be combined to a common main reactance, as X_{hS} includes the energy of the reluctance elements $E_{y1,S}$ and $E_{y2,S}$ and the radial-flux energy of the reluctance elements $E_{t1,S}$ to $E_{t4,S}$.

7.3 Equivalent resistance for winding losses

This section defines the equivalent resistance of the cage-winding in the rotor. The resistance is the equivalent of the heat energy produced in the winding.

A conductor in one reluctance element E_i dissipates a heat energy $\Delta W_{e,i}$. The heat energy associated with a time step k is

$$\Delta W_{e,i}^{(k)} = \frac{\Delta t}{2} R_i \left(i_i^{(k)} \right)^2 \tag{125}$$

where the quantities are

Δt the length of the time step,

R_i the resistance of the branch of the electric element of E_i, and

i_i the current of the branch of the electric element of E_i.

The heat energy $W_{e,i}$ dissipated in the element E_i over one cycle of the fundamental frequency is

$$W_{e,i} = \sum_{k=1}^{N} \Delta W_{e,i}^{(k)} = \frac{\Delta t}{2} R_i \left[\sum_{k=1}^{N} \left(i_i^{(k)} \right)^2 \right] \tag{126}$$

where N is the number of time steps in the cycle.

In the cage winding, the electric element associated to the reluctance element E_i consists of the axial branch (the bar) and the radial and circumferential branches (the end ring segment of the rotor cage), as in Fig. 14. The heat energy $W_{e,i}$ dissipated in the element E_i includes the heat energies in the bar and in the end-ring segments connected to the bar. The heat energy $W_{e,i}$ is

$$
\begin{aligned}
W_{e,i} &= \sum_{k=1}^{N} \left(\Delta W_{ez,i}^{(k)} + \Delta W_{e\varphi,i}^{(k)} + \Delta W_{er,i}^{(k)} \right) \\
&= \frac{\Delta t}{2} \left\{ R_{z,i} \left[\sum_{k=1}^{N} \left(i_{z,i}^{(k)} \right)^2 \right] + R_{\varphi,i} \left[\sum_{k=1}^{N} \left(i_{\varphi,i}^{(k)} \right)^2 \right] + R_{r,i} \left[\sum_{k=1}^{N} \left(i_{r,i}^{(k)} \right)^2 \right] \right\}
\end{aligned}
\tag{127}
$$

where

$R_{z,i}$ is the resistance of the axial branch,

$i_{z,i}$ is the current of the axial branch,

$R_{\varphi,i}$ is the resistance of the circumferential branch,

$i_{\varphi,i}$ is the current of the circumferential branch,

$R_{r,i}$ is the resistance of the radial branch, and

$i_{r,i}$ is the current of the radial branch,

In the reference slot-pitch, a reluctance element E_j has the same place as the reluctance element E_i in its slot-pitch sector. The reluctance element E_j collects the heat energy of all the reluctance elements E_i having the same position

$$W_{\mathrm{e},j} = \sum_{q=1}^{Q} \left[W_{\mathrm{e},i} \right]_q \tag{128}$$

where Q is the number of slots.

Every reluctance element E_j of the reference slot-pitch may have its own resistance R_j in the single-phase equivalent circuit. The resistance is based on the heat energy dissipated in the conductor of the element and divided to one phase of the stator (supply) winding

$$W_{\mathrm{e},j} = \sum_{q=1}^{Q} \left[W_{\mathrm{e},i} \right]_q = m\, R_j\, I_j^2\, T \tag{129}$$

where

m is the number of phases in the stator winding,

I_j is the rms-value of the sinusoidal current flowing through the resistance R_j, and

T is the length of the period of the supply frequency.

To define the resistance for the stator winding in the equivalent circuit, as R_{S} in Fig 42, the heat energy dissipated in the stator winding is the sum of the energies of the wound slot regions of the reference slot-pitch, as $\mathrm{E}_{\mathrm{s1,R}}$ and $\mathrm{E}_{\mathrm{s2,S}}$ in Fig. 41. The resistance R_{S} is

$$R_{\mathrm{S}} = \frac{W_{\mathrm{e,Es1S}} + W_{\mathrm{e,Es2S}}}{m\, I_{\mathrm{S}}^2\, T} \tag{130}$$

where I_{S} is the rms-value of the sinusoidal current in the equivalent circuit flowing through the resistance R_{S}.

To use two equivalent resistances for the rotor winding in the equivalent circuit, as R_{1R} and R_{2R} in Fig. 42, the heat energy dissipated in the rotor winding have to be divided according to the energies of the regions of the reference slot-pitch, as $\mathrm{E}_{\mathrm{s1,R}}$ to $\mathrm{E}_{\mathrm{s4,R}}$ in Fig. 41. One solution is to combine the heat energy in regions $\mathrm{E}_{\mathrm{s3,R}}$ and $\mathrm{E}_{\mathrm{s4,R}}$ near the air gap to the resistance R_{1R} and the heat energy in regions $\mathrm{E}_{\mathrm{s1,R}}$ and $\mathrm{E}_{\mathrm{s2,R}}$ to the resistance R_{2R}. The resistances R_{1R} and R_{2R} are

$$\begin{cases} R_{1R}^{*} = \dfrac{W_{e,Es3R} + W_{e,Es4R}}{m\,I_{1R}^{2}\,T} \\[2em] R_{2R}^{*} = \dfrac{W_{e,Es1R} + W_{e,Es2R}}{m\,I_{2R}^{2}\,T} \end{cases} \tag{131}$$

where I_{1R} and I_{2R} are the rms-values of the sinusoidal currents in the equivalent circuit flowing through the resistances R_{1R} and R_{2R}. The asterisk in the quantities indicates that the quantity is referred to the stator.

7.4 Equivalent resistance for iron losses

This section defines the equivalent resistance of the iron losses in the core. The resistance is the equivalent of the heat energy. The position, in which the resistance component is substituted in the single-phase equivalent circuit, depends on the reluctance element of the reference slot-pitch where the heat energy is collected. The position of the element and the direction of the flux flow define the resistance component.

The flux density of the reluctance element has a circumferential and radial component. The assumption made in this analysis is that a flux-path region can belong to both the main-flux and leakage-flux paths. The steady-state flux-density distribution is defined in every time step for both of the flux-density components. The flux-density time-variation in every reluctance element is replaced with Fourier-series. The iron losses are defined as a sum of the losses of the harmonics.

The iron losses $P_{fe,i}$ of a reluctance element E_i may be written as components caused by the circumferential and radial component of the flux density B_i

$$P_{fe,i} = P_{fe}(B_{\varphi,i}) + P_{fe}(B_{r,i}) \tag{132}$$

In the tooth region, the flux paths of the main and leakage fluxes deviate. In the reference slot-pitch, the radial flux-component flows on the main-flux path. The iron losses of the flux component belong to the main-flux path. In the reference slot-pitch, the circumferential flux-component flows on the leakage-flux path. The iron losses of the circumferential flux-density belong to the leakage-flux path.

In the yoke region, the flux paths of the main and leakage fluxes join. Both of the iron-loss components belong to the energy of the joined flux path. In the reference slot-pitch, the circumferential flux is the main source of the iron losses in the yoke. The radial loss component $P_{\text{fe}}(B_{\varphi,i})$ takes into account the iron losses from the flux going to the tooth area.

The iron-loss energy $W_{\text{b},i}$ of the reluctance element E_i has the energy components $W_{\text{b}r,i}$ and $W_{\text{b}\varphi,i}$ associated with the iron losses of the radial and circumferential flux components in the period of the supply frequency

$$
\begin{cases}
W_{\text{b}r,i} = T P_{\text{fe}}(B_{r,i}) \\
W_{\text{b}\varphi,i} = T P_{\text{fe}}(B_{\varphi,i})
\end{cases}
\tag{133}
$$

where T is the length of the period of the fundamental harmonic of supply voltage.

In the reference slot-pitch, a reluctance element E_j has the same place as the reluctance element E_i in its slot-pitch sector. The reluctance element E_j collects the iron-loss energy of all the reluctance elements E_i having the same position

$$
\begin{cases}
W_{\text{b}r,j} = \displaystyle\sum_{q=1}^{Q} \left[W_{\text{b}r,i} \right]_q \\
W_{\text{b}\varphi,j} = \displaystyle\sum_{q=1}^{Q} \left[W_{\text{b}\varphi,i} \right]_q
\end{cases}
\tag{134}
$$

Every reluctance element E_j of the reference slot-pitch may have its own resistances $R_{\text{fe},j}$ in the single-phase equivalent circuit. The energy dissipated in the equivalent resistance is equal to the heat energy $W_{\text{b},j}$, either the radial or circumferential component, divided to one phase of the stator winding

$$
W_{\text{b},j} = \sum_{q=1}^{Q} \left[W_{\text{b},i} \right]_q = \frac{m U_j^2 T}{R_{\text{fe},j}}
\tag{135}
$$

where U_j is the rms-value of the sinusoidal voltage over the resistance $R_{\text{fe},j}$.

The modelling of iron losses in a tooth region of the reference slot-pitch, e.g. the element $\text{E}_{\text{t1,S}}$ in Fig. 41, needs two resistance components in the equivalent circuit

$$
\begin{cases}
R_{\text{fe},\sigma,\text{Et1S}} = \dfrac{mU^2_{\sigma,\text{Et1S}}\, T}{W_{\text{b}\varphi,\text{Et1S}}} \\[3em]
R_{\text{fe},\text{h},\text{Et1S}} = \dfrac{mU^2_{\text{h},\text{Et1S}}\, T}{W_{\text{b}r,\text{Et1S}}}
\end{cases}
\tag{136}
$$

where $U_{\sigma,\text{Et1S}}$ and $U_{\text{h},\text{Et1S}}$ are the rms-values of the sinusoidal voltages in the equivalent circuit over the resistances $R_{\text{fe},\sigma,\text{Et1S}}$ and $R_{\text{fe},\text{h},\text{Et1S}}$.

In the equivalent circuit of Fig. 42, the resistance $R_{\text{fe},\sigma,\text{Et1S}}$ is combined in the resistance $R_{\text{fe},\sigma\text{S}}$ modelling the iron losses of stator caused by the leakage-flux components. The resistance $R_{\text{fe},\text{h},\text{Et1S}}$ is included in the resistance $R_{\text{fe},\text{hS}}$ modelling the iron losses of stator caused by the main-flux components.

The iron-loss resistances in the equivalent circuit, Fig. 42, are defined using the iron-loss energy of the regions in the reference slot-pitch, Fig. 41,

- for the iron losses in the stator

$$
\begin{cases}
R_{\text{fe},\sigma\text{S}} = \dfrac{mU^2_{\sigma\text{S}}\, T}{W_{\text{b},\sigma\text{S}}} \\[3em]
R_{\text{fe},\text{hS}} = \dfrac{mU^2_{\text{hS}}\, T}{W_{\text{b},\text{hS}}}
\end{cases}
\tag{137}
$$

- for the iron losses in the rotor

$$
\begin{cases}
R^{*}_{\text{fe},\sigma 1\text{R}} = \dfrac{mU^2_{\sigma 1\text{R}}\, T}{W_{\text{b},\sigma 1\text{R}}} \\[2.5em]
R^{*}_{\text{fe},\sigma 2\text{R}} = \dfrac{mU^2_{\sigma 2\text{R}}\, T}{W_{\text{b},\sigma 2\text{R}}} \\[2.5em]
R^{*}_{\text{fe},\text{hR}} = \dfrac{mU^2_{\text{hR}}\, T}{W_{\text{b},\text{hR}}}
\end{cases}
\tag{138}
$$

In the equations, $U_{\sigma i}$ and $U_{\text{h}i}$ are the rms-values of the sinusoidal voltages in the equivalent circuit over the resistances $R_{\text{fe},\sigma i}$ and $R_{\text{fe},\text{h}i}$ and the iron-loss energies are

$$
\begin{cases}
W_{\mathrm{b},\sigma\mathrm{S}} = W_{\mathrm{b}\varphi,\mathrm{Et1S}} + W_{\mathrm{b}\varphi,\mathrm{Et2S}} + W_{\mathrm{b}\varphi,\mathrm{Et3S}} + W_{\mathrm{b}\varphi,\mathrm{Et4S}} \\[4pt]
W_{\mathrm{b},\mathrm{hS}} = W_{\mathrm{b},\mathrm{Ey1S}} + W_{\mathrm{b},\mathrm{Ey2S}} \\[2pt]
\qquad\quad + W_{\mathrm{b}r,\mathrm{Et1S}} + W_{\mathrm{b}r,\mathrm{Et2S}} + W_{\mathrm{b}r,\mathrm{Et3S}} + W_{\mathrm{b}r,\mathrm{Et4S}} \\[4pt]
W_{\mathrm{b},\sigma1\mathrm{R}} = W_{\mathrm{b}\varphi,\mathrm{Et3R}} + W_{\mathrm{b}\varphi,\mathrm{Et4R}} \\[4pt]
W_{\mathrm{b},\sigma2\mathrm{R}} = W_{\mathrm{b}\varphi,\mathrm{Et1R}} + W_{\mathrm{b}\varphi,\mathrm{Et2R}} \\[4pt]
W_{\mathrm{b},\mathrm{hR}} = W_{\mathrm{b},\mathrm{Ey1R}} + W_{\mathrm{b},\mathrm{Ey2R}} \\[2pt]
\qquad\quad + W_{\mathrm{b}r,\mathrm{Et1R}} + W_{\mathrm{b}r,\mathrm{Et2R}} + W_{\mathrm{b}r,\mathrm{Et3R}} + W_{\mathrm{b}r,\mathrm{Et4R}}
\end{cases}
\tag{139}
$$

7.5 Equivalent reactance

This section defines the equivalent reactance of the magnetic energy. The position, in which the reactance component is substituted in the single-phase equivalent circuit, depends on the reluctance element of the reference slot-pitch where the magnetic energy is collected. The position of the element and the direction of the flux flow define the reactance component.

The magnetic energy calculation is based on the flux-density value, Section 3.3. In the analysis using the reluctance network, the flux density and the magnetic energy of a reluctance element E_i are calculated at every time step. The magnetic energy $\Delta W_{\mathrm{m},i}$ of the element E_i is for the flux-density value b_i at time step k

$$
\Delta W_{\mathrm{m},i}^{(k)} = V_i \int\limits_{b=0}^{b=b_i^{(k)}} \left[v(b)\, b\, \mathrm{d}b \right]
\tag{140}
$$

The magnetic energy $\Delta W_{\mathrm{m},i}$ of the element E_i may be divided to the magnetic energy components $\Delta W_{\mathrm{m}r,i}$ and $\Delta W_{\mathrm{m}\varphi,i}$ according to the radial and circumferential flux-density components $b_{r,i}$ and $b_{\varphi,i}$ of the element at the time step k

$$
\begin{cases}
\Delta W_{\mathrm{m}r,i}^{(k)} = \left[\dfrac{b_{r,i}^{(k)}}{b_i^{(k)}} \right]^2 \Delta W_{\mathrm{m},i}^{(k)} \\[20pt]
\Delta W_{\mathrm{m}\varphi,i}^{(k)} = \left[\dfrac{b_{\varphi,i}^{(k)}}{b_i^{(k)}} \right]^2 \Delta W_{\mathrm{m},i}^{(k)}
\end{cases}
\tag{141}
$$

The magnetic energy W_m over one period is the average of the energy values ΔW_m during the period. The components $W_{mr,i}$ and $W_{m\varphi,i}$ in the element E_i are

$$
\begin{cases}
W_{mr,i} = \dfrac{1}{N} \sum_{k=1}^{N} \Delta W_{mr,i}^{(k)} \\[3mm]
W_{m\varphi,i} = \dfrac{1}{N} \sum_{k=1}^{N} \Delta W_{m\varphi,i}^{(k)}
\end{cases}
\tag{142}
$$

In the reference slot-pitch, a reluctance element E_j has the same place as the reluctance element E_i in its slot-pitch sector. The reluctance element E_j collects the magnetic energy of all the reluctance elements E_i having the same position

$$
\begin{cases}
W_{mr,j} = \sum_{q=1}^{Q} \left[W_{mr,i} \right]_q \\[3mm]
W_{m\varphi,j} = \sum_{q=1}^{Q} \left[W_{m\varphi,i} \right]_q
\end{cases}
\tag{143}
$$

Every reluctance element E_j of the reference slot-pitch may have its own reactances X_j in the single-phase equivalent circuit. The energy dissipated in the equivalent reactance is equal to the magnetic energy $W_{m,j}$, either the radial or circumferential component, divided to one phase of the stator winding

$$
W_{m,j} = \sum_{q=1}^{Q} \left[W_{m,i} \right]_q = \frac{m U_j^2 T}{X_j}
\tag{144}
$$

where U_j is the rms-value of the sinusoidal voltage over the reactances X_j.

The modelling of magnetic energy in a tooth region of the reference slot-pitch, e.g. the element $E_{t1,S}$ in Fig. 41, needs two reactance components

$$
\begin{cases}
X_{\sigma,Et1S} = \dfrac{m U_{\sigma,Et1S}^2 T}{W_{m\varphi,Et1S}} \\[4mm]
X_{h,Et1S} = \dfrac{m U_{h,Et1S}^2 T}{W_{mr,Et1S}}
\end{cases}
\tag{145}
$$

where $U_{\sigma,\mathrm{Et1S}}$ and $U_{\mathrm{h,Et1S}}$ are the rms-value of the sinusoidal voltages in the equivalent circuit over the reactances $X_{\sigma,\mathrm{Et1S}}$ and $X_{\mathrm{h,Et1S}}$

In the equivalent circuit of Fig. 42, the reactance $X_{\sigma,\mathrm{Et1S}}$ is combined in the reactance $X_{\sigma\mathrm{S}}$ modelling the magnetic energy of stator caused by the leakage-flux components. The reactance $X_{\mathrm{h,Et1S}}$ is included in the reactance X_{hS} modelling the magnetic energy of stator caused by the main-flux components. When defining the analogue for both the iron-loss and magnetic energy of the same flux path, the equivalent resistance and reactance are parallel components, as $R_{\mathrm{fe},\sigma,\mathrm{Et1S}}$ and $X_{\sigma,\mathrm{Et1S}}$, and $R_{\mathrm{fe,h,Et1S}}$ and $X_{\mathrm{h,Et1S}}$. In the equivalent circuit in Fig. 42, the parallel components are $R_{\mathrm{fe},\sigma\mathrm{S}}$ and $X_{\sigma\mathrm{S}}$, and $R_{\mathrm{fe,hS}}$ and X_{hS}.

The reactances in the equivalent circuit, Fig. 42, are defined using the magnetic energy of the elements in the reference slot-pitch, Fig. 41,

- for the magnetic energy in the stator

$$
\begin{cases}
X_{\sigma\mathrm{S}} = \dfrac{mU_{\sigma\mathrm{S}}^2\, T}{W_{\mathrm{m},\sigma\mathrm{S}}} \\[4mm]
X_{\mathrm{hS}} = \dfrac{mU_{\mathrm{hS}}^2\, T}{W_{\mathrm{m,hS}}}
\end{cases}
\tag{146}
$$

- for the magnetic energy in the air gap

$$
X_{\mathrm{h}\delta} = \frac{mU_{\mathrm{h}\delta}^2\, T}{W_{\mathrm{m,E}\delta 1} + W_{\mathrm{m,E}\delta 2}}
\tag{147}
$$

- for the magnetic energy in the rotor

$$
\begin{cases}
X_{\sigma 1\mathrm{R}}^{*} = \dfrac{mU_{\sigma 1\mathrm{R}}^2\, T}{W_{\mathrm{m},\sigma 1\mathrm{R}}} \\[4mm]
X_{\sigma 2\mathrm{R}}^{*} = \dfrac{mU_{\sigma 2\mathrm{R}}^2\, T}{W_{\mathrm{m},\sigma 2\mathrm{R}}} \\[4mm]
X_{\mathrm{hR}}^{*} = \dfrac{mU_{\mathrm{hR}}^2\, T}{W_{\mathrm{m,hR}}}
\end{cases}
\tag{148}
$$

In the equations, $U_{\sigma i}$ and $U_{\mathrm{h}i}$ are the rms-values of the sinusoidal voltages in the equivalent circuit over the reactances $X_{\sigma i}$ and $X_{\mathrm{h}i}$, and the magnetic energies are

$$
\begin{cases}
W_{\mathrm{m},\sigma\mathrm{S}} = W_{\mathrm{m,Es1S}} + W_{\mathrm{m,Es2S}} + W_{\mathrm{m,Es3S}} + W_{\mathrm{m,Es4S}} \\
\qquad + W_{\mathrm{m}\varphi,\mathrm{Et1S}} + W_{\mathrm{m}\varphi,\mathrm{Et2S}} + W_{\mathrm{m}\varphi,\mathrm{Et3S}} + W_{\mathrm{m}\varphi,\mathrm{Et4S}} \\
W_{\mathrm{m},\mathrm{hS}} = W_{\mathrm{m,Ey1S}} + W_{\mathrm{m,Ey2S}} \\
\qquad + W_{\mathrm{m}r,\mathrm{Et1S}} + W_{\mathrm{m}r,\mathrm{Et2S}} + W_{\mathrm{m}r,\mathrm{Et3S}} + W_{\mathrm{m}r,\mathrm{Et4S}} \\
W_{\mathrm{m},\sigma 1\mathrm{R}} = W_{\mathrm{m,Es3R}} + W_{\mathrm{m,Es4R}} + W_{\mathrm{m}\varphi,\mathrm{Et3R}} + W_{\mathrm{m}\varphi,\mathrm{Et4R}} \\
W_{\mathrm{m},\sigma 2\mathrm{R}} = W_{\mathrm{m,Es1R}} + W_{\mathrm{m,Es2R}} + W_{\mathrm{m}\varphi,\mathrm{Et1R}} + W_{\mathrm{m}\varphi,\mathrm{Et2R}} \\
W_{\mathrm{m},\mathrm{hR}} = W_{\mathrm{m,Ey1R}} + W_{\mathrm{m,Ey2R}} \\
\qquad + W_{\mathrm{m}r,\mathrm{Et1R}} + W_{\mathrm{m}r,\mathrm{Et2R}} + W_{\mathrm{m}r,\mathrm{Et3R}} + W_{\mathrm{m}r,\mathrm{Et4R}}
\end{cases}
\tag{149}
$$

7.6 Conclusion

This chapter has presented the reference slot-pitch model for the energy distribution in the machine cross-section and the single-phase equivalent circuit of the cage-induction machine. The single-phase equivalent circuit with two branches for the losses of the rotor winding was used. All stator and rotor reactances in the equivalent circuit have the parallel iron-loss resistance. The chosen equivalent circuit models the leakage-flux paths, iron losses, and the current distribution in the rotor cage with more details than the standard single-phase equivalent circuit. The resistances represent the average losses in the windings and in the core. The reactances are the equivalents of the magnetic energy in the stator, in the air gap, and in the rotor. The definition of the resistances and reactances based on the average energy distribution in the machine over one period of the supply frequency.

The energy distribution was specified using the time-stepping analysis of the reluctance network. The heat energy dissipated in the rotor winding was calculated from the resistive losses in the electric elements of the winding model. The iron losses were calculated using the Fourier-series of the flux-density variation in the reluctance elements. The magnetic energy distribution was calculated from the magnetic energy stored in the reluctance elements.

The energy distribution of the whole reluctance model was collected in the reference slot-pitch. Every flux-path region of the reference slot-pitch includes the energy components of the flux-path regions having the same place in their slot-pitch sector as the flux-path region of the reference slot-pitch.

The components of the single-phase equivalent circuit were specified using the energy components of the reference slot-pitch. The position in which an equivalent circuit component was substituted in the single-phase equivalent circuit was dependent on the flux-path region in the reference slot-pitch where the energy was collected. Every region may have its own resistance and reactance components in the single-phase equivalent circuit. The energy dissipated in the equivalent-circuit component is equal to the energy component of the flux-path region in the reference model divided to one phase of the stator winding.

To reduce the size of the equivalent circuit, the energy components of the elements were combined according to the flux flow. The energy of the slots and the energy of leakage flux of the teeth were collected to the common leakage reactance and resistance components. The energy of the yoke and the energy of main flux of the teeth were collected to the common main reactance and resistance components.

In Chapter 9, the equivalent single-phase equivalent circuits, with a layout according to this chapter, will be defined and used for a cage induction motor with a single-cage and for a cage induction motor with a double-cage rotor. The energy components of the reluctance network will be combined to form a common resistance or reactance components in the equivalent circuit. The rules of combination will be different depending on the rotor type.

8   COMPUTER PROGRAM

In this chapter, a computer program package will be introduced. The program package is developed in this study to use in the analysis of the universal reluctance network. The package defines the components of the reluctance network for the machine, according to Chapter 2. It solves the equations presented in Chapter 6. The values for the variables are iterated according to Chapter 6.

The chapter will introduce the input data files, the general flow of the program, and the output file alternatives.

8.1   Input data of program

The input data of the program package is read from three input files. The definitions of the stator and rotor of the machine have their own input files. The third file includes the operating instructions and instructions for the output. The input data files of the stator and rotor consist of the core, slotting, winding and supply definitions.

The core definitions of the stator and rotor are

  - outer diameter of core,
  - inner diameter of core,
  - axial length of core,
  - axial iron length (optional),
  - axial width of a ventilation duct,
  - number of slots,
  - number of poles, and
  - number of ventilation ducts.

The layout of the slot specifies the dimensions of the slot-pitch sector. The layout of the tooth is defined by the program. The sector dimensions use the reference regions as a basis. The sector starts from the middle of the air gap. The first dimension region is the segment from the air gap. The next dimension regions are from the layout of the slot. The slot is divided to a collection of reference regions. The last dimension region is the segment from the yoke.

The slotting definitions are

- number of dimension regions used in the slot-pitch sector (radial division of the slot dimensions),
- number of region blocks (connected regions), and
- list of connected regions included in each region block.

Definitions of regions are
- form of region (segment/rectangle/trapezium/circle),
- height of region,
- width of region,
- radius of region,
- number of radial divisions in region,
- circumferential divisions in the tooth section,
- circumferential divisions in the slot section,
- reluctivity code of the tooth section,
- reluctivity code of the slot section,
- fill factor of the tooth section,
- fill factor of the slot section,
- resistivity code of bar in the slot section, and
- resistivity code of end-ring in the slot section.

Flags for the region
- slot section uses partly the reluctivity of tooth section (yes/no) and
- slot section includes conductor (yes/no).

The winding definitions of the stator and rotor are

- winding type (single layer/double layer/cage),
- number of phases,
- number of neutrals,
- number of parallel branches of winding,
- width of coil in slot pitches,
- number of turns in coil,
- axial length of half a coil, cage bar,
- outer diameter of end-ring (cage winding),
- inner diameter of end-ring (cage winding), and
- axial width of end-ring (cage winding).

The line definitions are

- winding connection (star/star and neutral/delta),
- supply connection (star/star and neutral/delta),
- impedance connected in series with the winding EMF,
- impedance connected in series with the supply EMF,
- source type (current source/voltage source),
- wave form of source (sinusoidal/rectangle/constant),
- rms-value of source voltage or source current,
- frequency of source voltage or source current, and
- phase-shift of source voltage or source current at zero time.

The input file of operating instructions controls the program flow. The instructions define the target of the program, the size of the reluctance network, and the initial state of the calculation. The program saves all the results in output files at different moments of the analysis. The operating instructions control which results should be saved. The alternatives are the initial state before the time analysis, during the time-stepping process for each time step, and after the process for the last time step.

The operating instructions are

- machine type (cage induction machine/-),
- method of analyse (steady-state/from zero-state),
- operation target (short circuit/open circuit/fixed speed/process dependent),
- operation (motor/generator),
- number of time steps in period,
- number of periods,
- model size (full machine/pole/pole pair),
- air-gap model (only radial reluctances/one radial division/two radial divisions/all radial divisions specified by slot-pitch sector data),
- slip (optional),
- direction of rotation, and
- rotational angle at zero-time.

  Flags for the output
- the initial state (yes/no)
- all time steps (yes/no)
- the last step (yes/no)

8.2 Procedure of program

The program package consists of C-language programs described in the simplified flow chart in Fig. 43. The program defines the flux-path regions of the slot-pitch sector of the stator and rotor from the input data. Using the flux-path regions as units, the reluctance model of the stator, rotor and air-gap will be constructed according to Chapter 2. The materials of the elements are defined by the reluctivity curves of the program package and by the flux-path region combinations, as in Chapter 4.

In the time-stepping analysis, the quantities of the reluctance network are first defined using sinusoidal approximation for the quantities, Chapter 6. The calculation is iterative. When the iteration is converged, the results are used as initial values of the quantities at the first time-step in the time-stepping analysis. At each time step k, the calculation is iterative.

For a magnetic potential V, current i, and flux density b at a time step k , the criteria of convergence for the itereations step i are

$$
\frac{\left|\Delta V^{(k)}_{(i)}\right|}{\left|V^{(k)}_{(i)}\right|} < 10^{-6}, \quad \frac{\left|\Delta i^{(k)}_{(i)}\right|}{\left|i^{(k)}_{(i)}\right|} < 10^{-6}, \quad \frac{\left|\Delta b^{(k)}_{(i)}\right|}{\left|b^{(k)}_{(i)}\right|} < 10^{-4} \tag{150}
$$

Both in the iteration of the sinusoidal approximation and in the time-step iteration, the program gives an alarm if the iteration needs more than five iteration turns. The program stops when the number of iteration turns exceeds ten.

8.3 Output of program

The results of the reluctance network analysis are saved in the output files. The file can include all chosen results or only one group of the chosen results. The layout of the file in the first case is a chart of results where the results are collected as groups. In the second case, the results are presented as rows and sorted by the time-step order, the stator, rotor and air-gap results in their own files. The results for the initial state and for the last time step are saved as a chart of results. The results for the time-stepping are saved to their own files. The layout of the files is compatible with Microsoft Excel or an equivalent program.
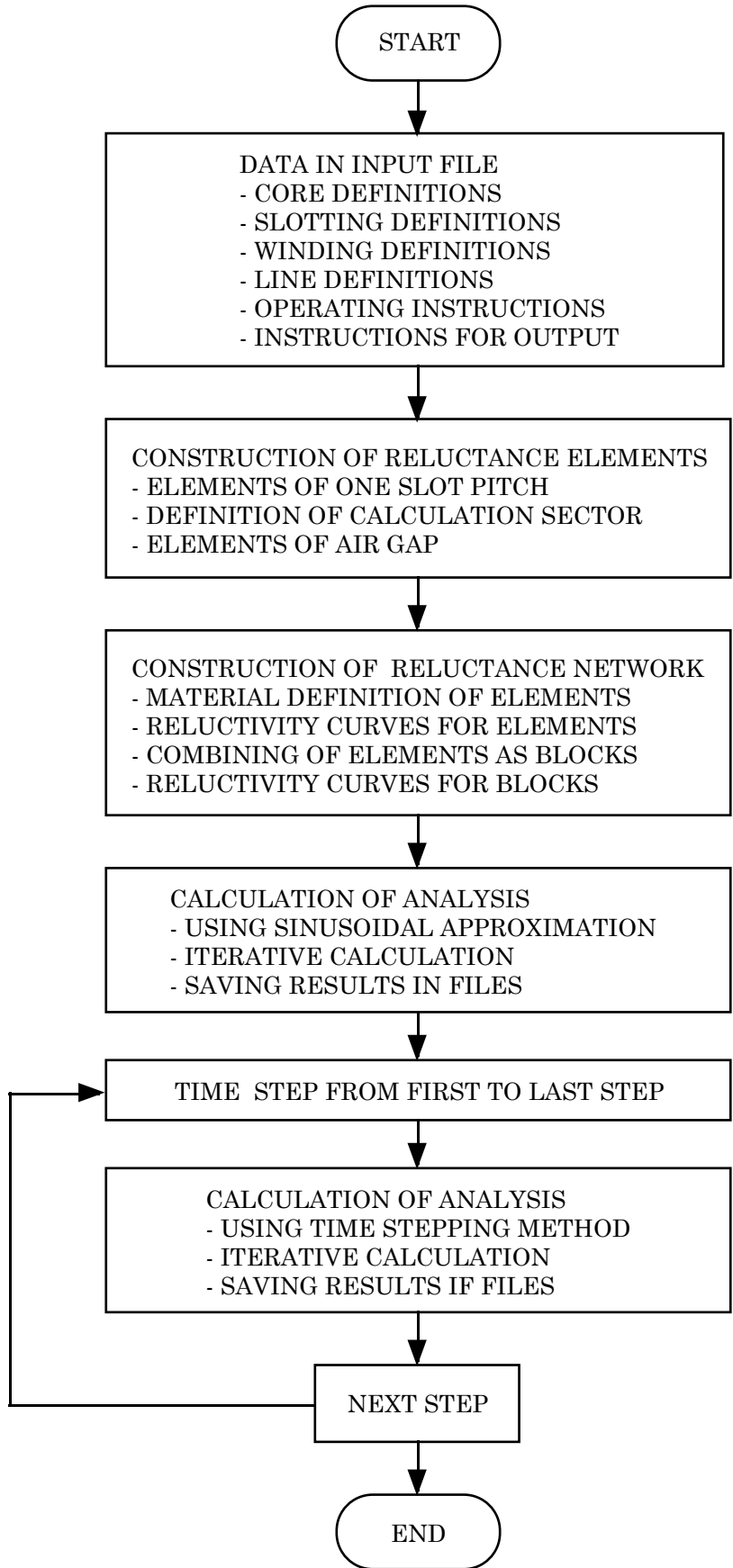
START

DATA IN INPUT FILE
- CORE DEFINITIONS
- SLOTTING DEFINITIONS
- WINDING DEFINITIONS
- LINE DEFINITIONS
- OPERATING INSTRUCTIONS
- INSTRUCTIONS FOR OUTPUT

CONSTRUCTION OF RELUCTANCE ELEMENTS
- ELEMENTS OF ONE SLOT PITCH
- DEFINITION OF CALCULATION SECTOR
- ELEMENTS OF AIR GAP

CONSTRUCTION OF RELUCTANCE NETWORK
- MATERIAL DEFINITION OF ELEMENTS
- RELUCTIVITY CURVES FOR ELEMENTS
- COMBINING OF ELEMENTS AS BLOCKS
- RELUCTIVITY CURVES FOR BLOCKS

CALCULATION OF ANALYSIS
- USING SINUSOIDAL APPROXIMATION
- ITERATIVE CALCULATION
- SAVING RESULTS IN FILES

TIME STEP FROM FIRST TO LAST STEP

CALCULATION OF ANALYSIS
- USING TIME STEPPING METHOD
- ITERATIVE CALCULATION
- SAVING RESULTS IF FILES

NEXT STEP

END

Fig. 43   Flow chart of the program package.

The optional files or data groups, in which the results are saved, are

as a chart form
- the input data
- the winding construction,
- the flux-path regions, and
- the potential nodes of reluctance models.

as a chart or row form the values in the reluctance models
- node potentials and MMF sources,
- circumferential and radial flux components,
- flux density and its circumferential and radial components,
- magnetic energy and its circumferential and radial components,
- hysteresis and eddy-current losses,
- currents of circumferential and radial loops in electric elements,
- axial, circumferential and radial currents in electric elements,
- EMF sources in electric elements,
- voltages, phase EMF sources and phase currents in distributed winding,
- voltages, phase EMF sources and phase currents in source,
- electric energy and current losses in winding elements, and
- air-gap torque.

8.4 Conclusion

In this chapter, the developed computer program package of a universal reluctance network was introduced. The program package will be used in the analysis of the next chapter.

The input data was saved in three input files. The details of the stator and rotor construction were in the stator and rotor files. The operating instructions were in the third file. The operation of the program was discussed shortly. The program followed the methods presented in the previous chapters to construct the reluctance network and to solve the system equations. The output of the program was saved in the files and controlled by the user. According to operating instructions, the results for the initial state, for the last time step, and for the time-stepping were saved to their own files. The list of the optional output files was given.

9 ANALYSIS RESULTS

In this chapter, two cage induction motors, 15 kW and 37 kW, will be analysed using a reluctance network. The computer program package of the universal reluctance network will be used in the analysis. The components of the single-phase equivalent circuits will be defined. The saturation of the starting reactance and the leakage reactances of the stator and rotor will be presented. The computed starting torque and stator current of the motors will be compared with the measured results.

9.1 Per-unit values

In the analysis, the supply voltage is sinusoidal. The amplitude of the voltage is varied to study the saturation of the components in the single-phase equivalent circuit, as in Fig. 42. The components of the equivalent circuit will be defined from the analysis at different voltages. The quantities calculated from the reluctance network will be represented as per-unit values in the comparison with the measured values.

The per-unit values r for a resistive component and x for a reactive component are defined with respect to the base impedance Z_N of the motor

$$Z_N = \frac{U_N}{I_N} \tag{151}$$

where U_N and I_N are the rated rms-values of the line-to-neutral voltage and the line current.

The definition of the per-unit value r for a resistance R is

$$r = \frac{R}{Z_N} \tag{152}$$

The definition of the per-unit value x for a reactance X is

$$x = \frac{X}{Z_N} \tag{153}$$

9.2 Analysed motors

This section introduces the two cage induction motors analysed as a demonstration of the reluctance network, a 15 kW single-cage and a 37 kW double-cage motor. The section describes the method used in the reluctance model construction for the core cross-section.

Both of the motors have unskewed rotors. The data relating to the motors are presented in Table 1, the layout of the slots in Fig. 44, and the slot dimensions defining the flux-path regions in Table 2.

The flux-path regions of the motors are defined using the slot-pitch sectors in the stator and rotor as presented in Chapter 2. The reluctivities of the tooth and yoke regions are defined taking into account the assumed main direction of flux according to Section 4.3. The air-gap reluctance model is a single-layer model as presented in Fig. 12c.

The layout of the slot specifies the dimensions of the flux-path regions in the slot

Table 1. Cage induction motors.

|	15 kW	37 kW
Output	15 kW	37 kW
Voltage	380 V	380 V
Current	30 A	73 A
Frequency	50 Hz	50 Hz
Synchronous speed	1500 rpm	1500 rpm
Connection	Delta	Star
Base impedance	7.3 Ω	3.0 Ω
Stator		
- outer diameter	235 mm	310 mm
- inner diameter	145 mm	200 mm
- core length	194 mm	248 mm
- number of slots	36	48
- number of poles	4	4
- number of phases	3	3
- winding	one layer	one layer
Rotor		
- outer diameter	144.1 mm	198.4 mm
- inner diameter	53 mm	70 mm
- core length	196 mm	248 mm
- number of slots	34	40
- winding	single cage, unskewed, aluminium	double cage, unskewed, aluminium
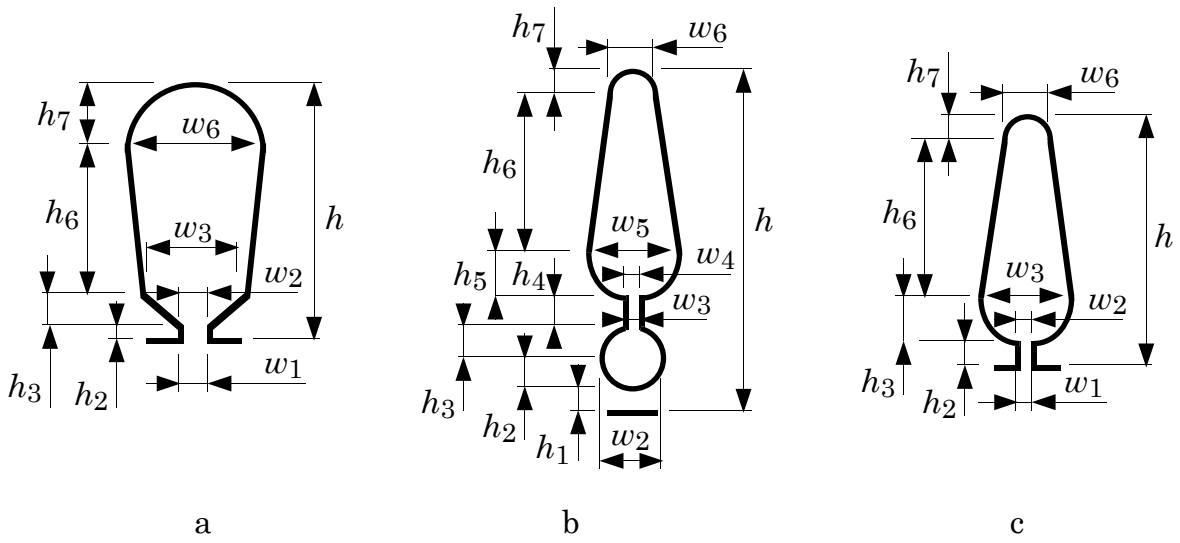
Fig. 44   Slot layouts of the analysed motors.
a) The stator slot of both motors,   b) the rotor slot of the 37 kW motor, and
c) the rotor slot of the 15 kW motor.

Table 2.   Slot dimensions of the analysed motors.

		15 kW motor		37 kW motor	
		Stator Fig. 44a [mm]	Rotor Fig. 44c [mm]	Stator Fig. 44a [mm]	Rotor Fig. 44b [mm]
	h	20.0	23.5	23.9	35.4
E_{t5}	form				segment
	h_1	–	–	–	0.7
E_{s3}	form	rectangle	rectangle	rectangle	circle
	h_2	1.3	2.47	1.0	3.0
	w_1	3.5	1.5	3.5	–
	w_2	3.5	1.5	3.5	3.0
E_{s2}	form	trapezium	circle	trapezium	circle
	h_3	0.85	2.28	1.0	2.73
	w_3	5.5	4.8	6.5	2.5
E_{s14}	form				rectangle
	h_4	–	–	–	7.0
	w_4				2.5
E_{s13}	form				circle
	h_5	–	–	–	2.62
	w_5				5.8
E_{s12}	form				trapezium
	h_6	13.9	18.0	17.5	17.8
	w_6	7.9	1.5	8.8	3.1
E_{s11}	form	circle	circle	circle	circle
	h_7	3.95	0.75	4.4	1.55

section of the slot-pitch sector, as in Chapter 2. The dimensions of the slot are given by dimension regions in the input file, specified in Chapter 8. The first dimension region is the segment of the yoke. The next regions are from the dimensions of the slot, given in Table 2. The last region for the reluctance model of the slot-pitch sector is the segment of air gap from the middle diameter of the air gap to the core.

The stator slot has four dimension regions in both the motors. They form the flux-path regions E_{s11}, E_{s12}, E_{s2} and E_{s3} of the slot, as in Fig. 45a. These flux-path regions define the flux-path regions of the tooth section E_{t11}, E_{t12}, E_{t2} and E_{t3} of the slot-pitch sector using the method of Fig. 7. The reluctivity curves of all the flux-path regions are specified taking into account an assumed direction of the flux flow. The tooth regions have the radial flux flow and the slot regions the circumferential flux flow.

In the study, the sizes of the reluctance models are reduced. In the stators, this is done by combining some of the flux-path regions in the slot and tooth, and by forming region blocks. In the stators of both the motors, the flux-path regions E_{s11} and E_{s12} of current-carrying region of the slot are joined forming the region E_{s1} and the regions E_{t11} and E_{t12} of the tooth forming the region E_{t1}, as in Fig. 45b. The reluctivity curves of the new regions are defined by the same way as the reluctivity curves of the original flux-path regions but by using the reluctivity curves and the assumed flux-flow directions of the original regions. The reluctance model and the electric model of stators are presented in Fig. 46.
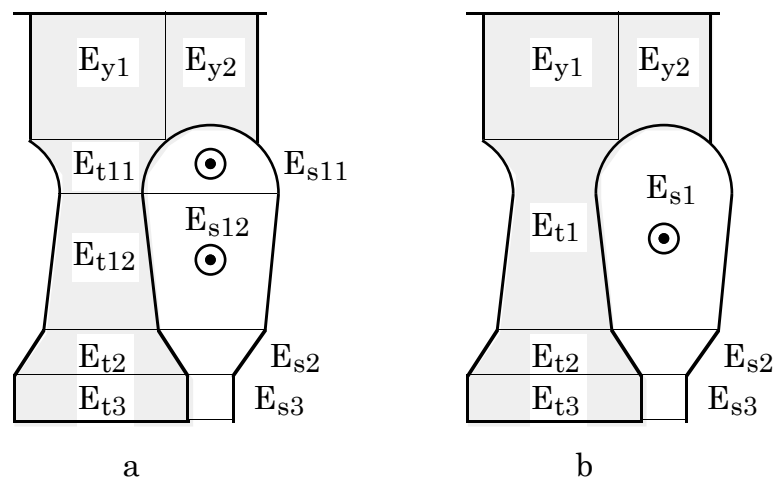

Fig. 45   Collection of the flux-path regions in the stator core of both the motors.
a) The initial collections of flux-path regions defined by the dimension regions of the input data.
b) The collections of flux-path regions used in the analysis. The regions E_{t11} and E_{t12} are replaced by the region E_{t1} in the tooth. The regions E_{s11} and E_{s12} are forming the region E_{s1}.
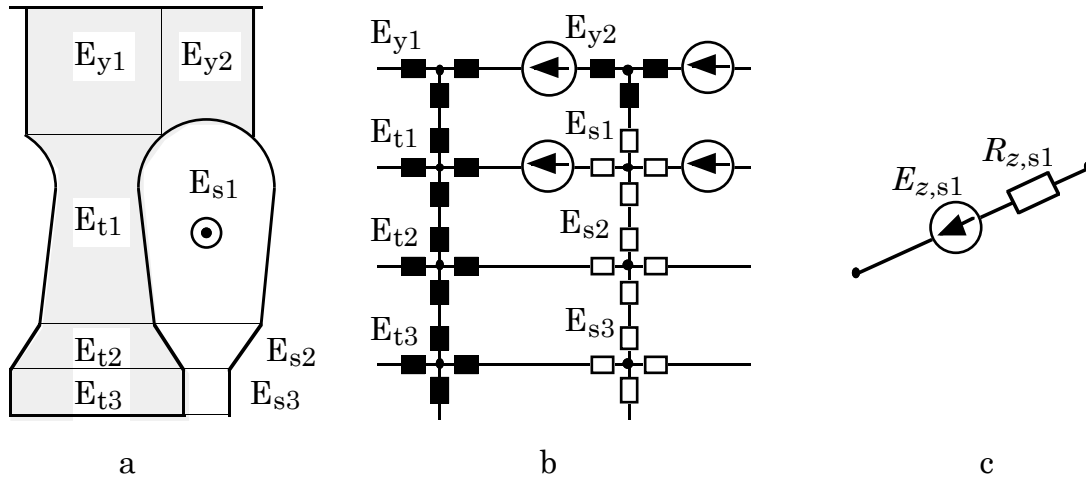
Fig. 46   The model of the stator slot-pitch sector of both the motors.
a) The division of the region, b) the reluctance model, and c) the electric model.

The rotor slot of the 15 kW motor has four dimension regions, Table 2. They form the flux-path regions E_{s11}, E_{s12}, E_{s2} and E_{s3} of the slot, as in Fig. 47a. As in the stator model, these flux-path regions define the flux-path regions of the tooth E_{t11}, E_{t12}, E_{t2} and E_{t3}. The reduction of the rotor reluctance-model is done by forming the region block E_{s1} in the slot, by combining the regions E_{s11} and E_{s12}, and the region block E_{t1} in the tooth, by combining the regions E_{t11} and E_{t12}, as in Fig. 47b. All the flux-path regions are modelled using the same methods as with the stator model.
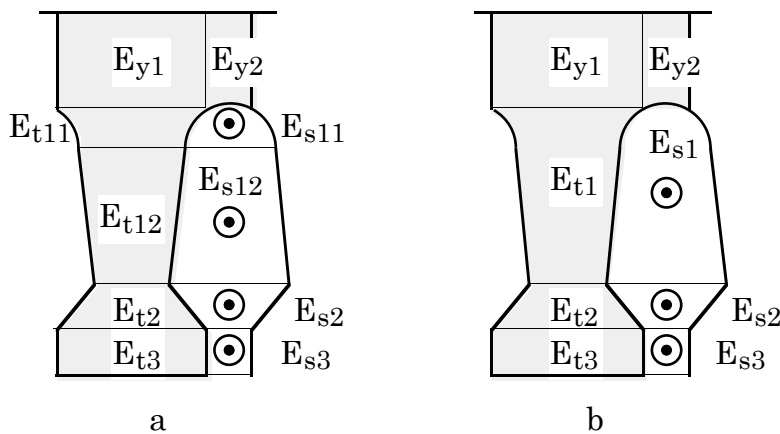

Fig. 47   Collection of the flux-path regions in the rotor core of the 15 kW motor.
a) The initial collections of flux-path regions defined by the dimension regions of the input data.
b) The collections of flux-path regions used in the analysis. The regions E_{t11} and E_{t12} are replaced by the region E_{t1} in the tooth. The regions E_{s11} and E_{s12} are forming the region E_{s1}.

The double-cage rotor slot of the 37 kW motor has seven dimension regions, Table 2. They form seven flux-path regions in the slot section of the slot-pitch sector, as in Fig. 48a. Six of the flux-path regions are in the slot, the four regions of the lower bar (farthest from the air gap), E_{s11}, E_{s12}, E_{s13} and E_{s14}, and the two regions of the upper bar (nearest the air gap), E_{s2} and E_{s3}. One of the dimension regions form the flux-path region E_{t5} named to belong to the tooth because of its material definition. The flux-path regions of the slot section define the regions of the tooth section in the slot-pitch sector using the method in Fig. 7. The regions are E_{t11}, E_{t12}, E_{t13} and E_{t14} parallel to the lower bar, E_{t2} and E_{t3} parallel to the upper bar, and E_{t4} parallel to the region E_{t5}.

In the specification of the reluctivity curves, all the flux-path regions in the slot section of the slot-pitch sector are handled on the same way. The assumed flux-flow direction is circumferential. In this model, the flux-flow definition means the regions of the yoke E_{y2}, the regions of slot E_{s11} to E_{s3}, and the tooth region E_{t5}.

In the reduction of the rotor reluctance-model, the number of the flux-path regions is decreased by forming the region blocks, E_{s1} into the slot and E_{t1} into the tooth, as in Fig. 48b. The flux-path region E_{s1} includes all the lower bar flux-path regions E_{s11} to E_{s14}. The region E_{t1} includes all the flux-path regions of the tooth parallel to the lower bar E_{t11} to E_{t14}. The reluctivity curves of the new regions are defined by using the reluctivity curves and the assumed flux-flow directions of the original regions.
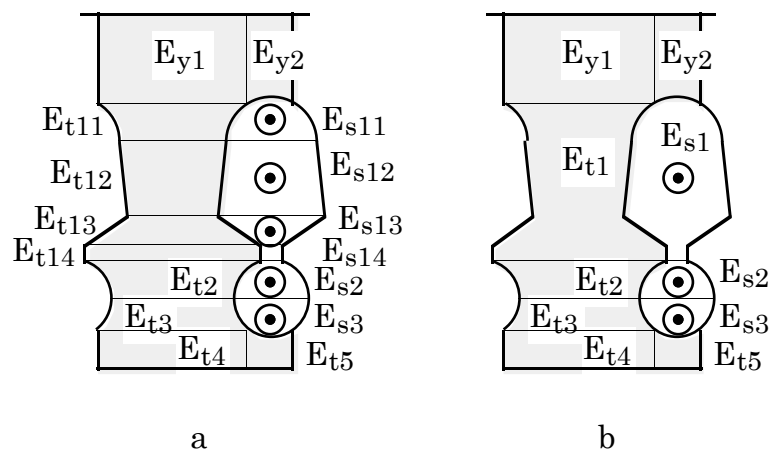

a   b

Fig. 48   Collection of the flux-path regions in the rotor core of the 37 kW motor.
a) The initial collections of flux-path regions defined by the dimension regions of the input data.
b) The collections of flux-path regions used in the analysis. The regions E_{t11} to E_{t14} are replaced by the region E_{t1} in the tooth. The regions E_{s11} to E_{s14} are forming the region E_{s1}.

The reluctance and electric models of the rotor for the 15 kW motor are presented in Fig. 49. They are constructed using the flux-path regions in Fig. 47b. The models of the rotor for the 37 kW motor are presented in Fig. 50. They are constructed using the flux-path regions in Fig. 48b.
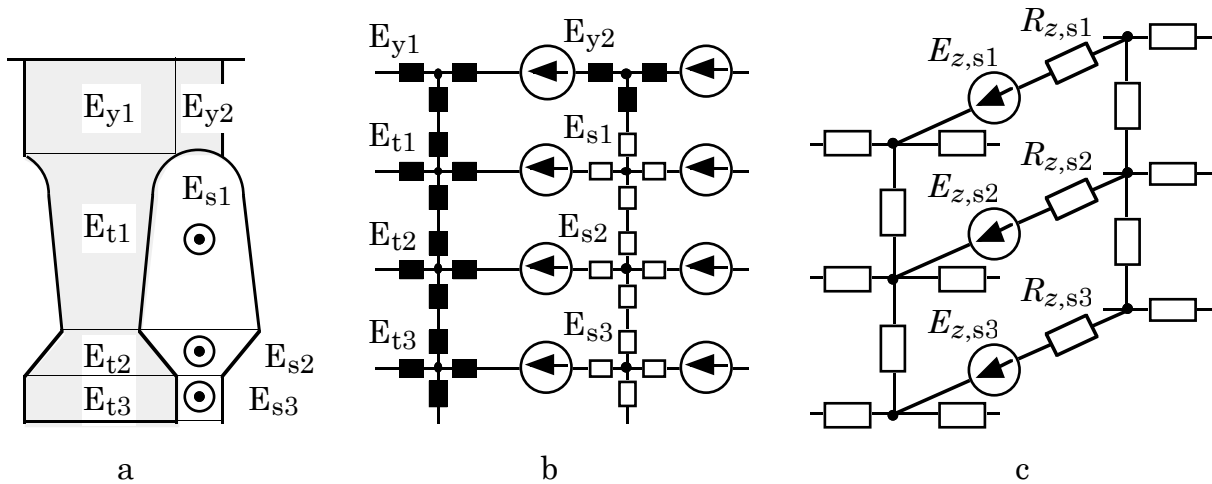

Fig. 49   The model of the rotor slot-pitch sector, the single-cage motor (15 kW).
a) The division of the region, b) the reluctance model, and c) the electric model.
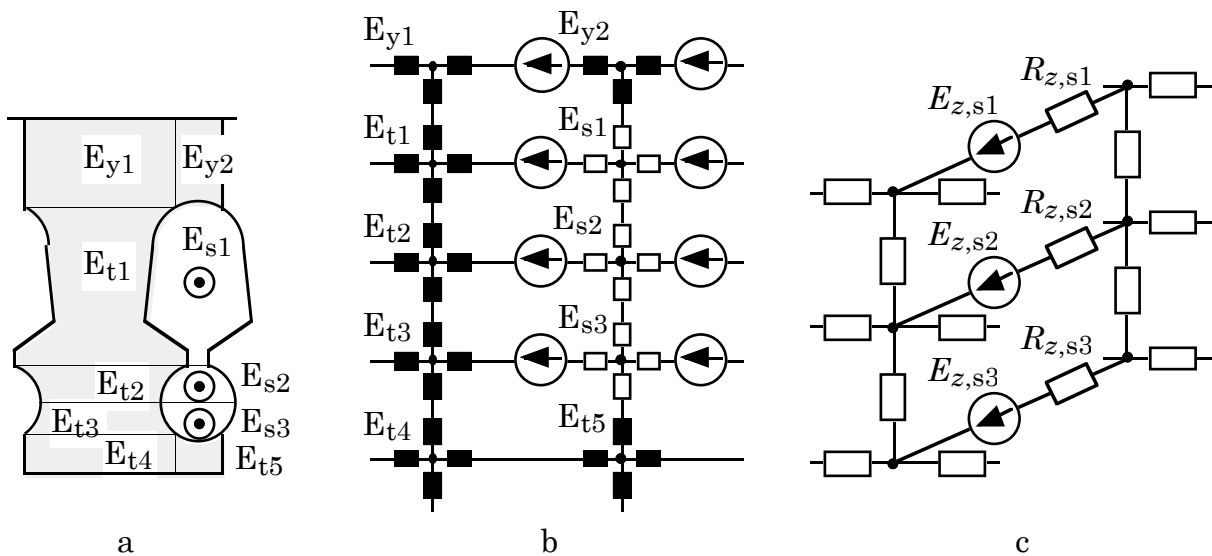

Fig. 50   The model of the rotor slot-pitch sector, the double-cage motor (37 kW).
a) The division of the region, b) the reluctance model, and c) the electric model.

9.3 15 kW motor

The reluctance and electric models used in the study are presented for the stator in Fig. 46 and for the rotor in Fig. 49.

In the stator, the reduction of the number of flux-path regions was made in the coil section of the slot and its parallel section in the tooth. Near the air gap, the stator model has reluctance elements in the wedge and opening of the slot and their parallel sections in the tooth. The reduction has a small influence to the leakage flux modelling.

In the rotor, the reduction was carried out in the lower part of the slot (farthest from the air gap) and its parallel section in the tooth. Near the air gap, the rotor model has reluctance elements for the uppermost portion of the main bar and for the opening of the slot and their parallel sections in the tooth. To model the current distribution inside the main bar, the number of bar divisions nearest the air gap is low. The number of divisions is a compromise between the accuracy and the size of the model. The reduction has a small influence to the leakage flux modelling.

In the study, the energy distribution of the reluctance network is transferred to the components of the single-phase equivalent circuit, as in Chapter 7. The single-phase equivalent circuit is presented in Fig. 42 and the equivalencies of the components in Table 3.

Table 3.   Energy components and their equivalence with the components of the single-phase equivalent circuit for the 15 kW motor, as in Fig. 42.

Components	$W_{\mathrm{m}r}$ and $W_{\mathrm{b}r}$ from regions	$W_{\mathrm{m}\varphi}$ and $W_{\mathrm{b}\varphi}$ from regions
Stator	Fig. 33	Fig. 33
X_{hS}, $R_{\mathrm{fe,hS}}$	E_{y1}, E_{y2}, E_{t1}, E_{t2}, E_{t3}	E_{y1}, E_{y2}
$X_{\mathrm{\sigma S}}$, $R_{\mathrm{fe,\sigma S}}$	E_{s1}, E_{s2}, E_{s3}	E_{t1}, E_{t2}, E_{t3}, E_{s1}, E_{s2}, E_{s3}
Rotor	Fig. 36	Fig. 36
X_{hR}, $R_{\mathrm{fe,hR}}$	E_{y1}, E_{y2}, E_{t1}, E_{t2}, E_{t3}	E_{y1}, E_{y2}
$X_{\mathrm{\sigma 1R}}$, $R_{\mathrm{fe,\sigma 1R}}$	E_{s2}, E_{s3}	E_{t2}, E_{t3}, E_{s2}, E_{s3}
$X_{\mathrm{\sigma 2R}}$, $R_{\mathrm{fe,\sigma 2R}}$	E_{s1}	E_{t1}, E_{s1}
Air gap		
$X_{\mathrm{h\delta}}$	$E_{\mathrm{\delta}}$	$E_{\mathrm{\delta}}$
	W_{e} from regions	
Rotor	Fig. 36	
R_{1R}	E_{s2}, E_{s3}	
R_{2R}	E_{s1}	

The effect of saturation on the equivalent circuit components is studied by calculating the air-gap torque, line current, starting impedance Z_{start}, and starting reactance X_{start} from the reluctance network at different sinusoidal line voltages. The starting impedance Z_{start} and the starting reactance X_{start} are defined from the equations

$$
\begin{cases}
Z_{\text{start}} = \dfrac{U}{I} \\[2ex]
X_{\text{start}} = \dfrac{mU^2 T}{W_{\text{m}}}
\end{cases}
\tag{154}
$$

In the equation, U and I are the rms-values of the fundamental harmonics of the line-to-neutral voltage and the line current, and W_{m} is the total magnetic energy of the reluctance network.

The characteristics of the starting torque and current reveal that the calculated values exhibit a relatively good agreement with the measured values, as may be seen in Fig 51. The error in the starting current is about 12% at the rated voltage. When taking into account the effect of the missing end-winding reactance of the stator (3.0%), the calculated starting-current characteristic comes closer to the measured one. Because of the relatively constant difference between the starting-current characteristics, the leakage reactance calculation is not accurate enough.
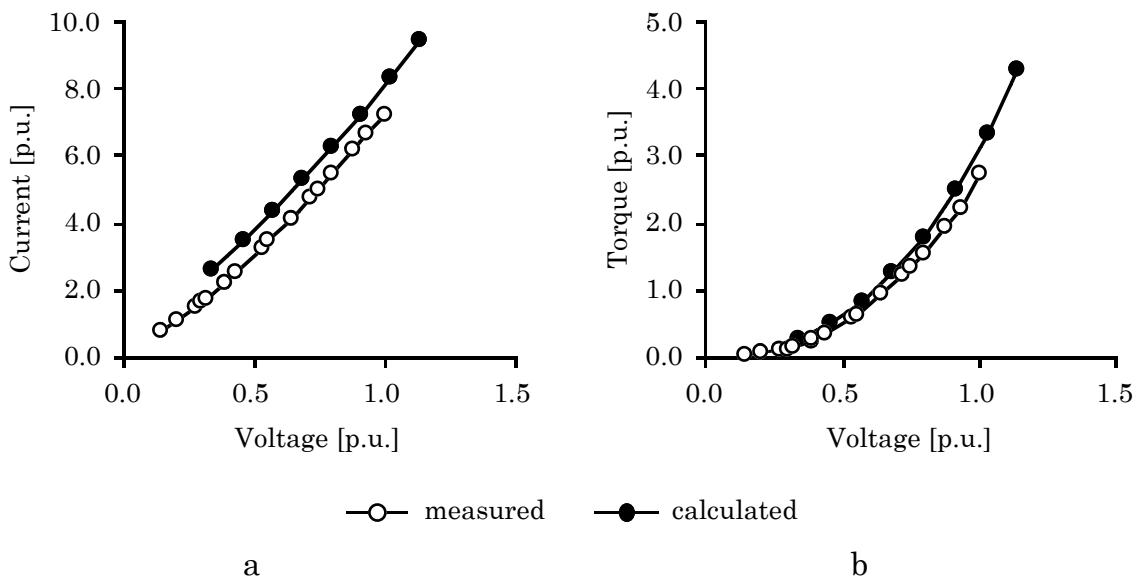

Fig. 51   The starting characteristics of the 15 kW motor.
a)   The starting current and b) torque as function of supply voltage.

The inaccuracy of the reluctance network model may be seen better from the characteristics of the starting reactance, as in Fig 52b. The measured characteristic has more gentle nature as function of voltage than the calculated one. The vertical position between the curves is larger than the value of the excluded end-winding reactance. At the lower voltages, the calculated characteristic does not represent the unsaturated state well enough. To the rated voltage, the difference between the characteristics decreases remarkably. The reason for this is that the measured reactance saturates but the level of the saturation in the calculated reactance increases more slowly. The difference between the characteristics is smaller than the excluded end-winding reactance. At the rated voltage, the difference between the characteristics is zero. This means that the saturation is not modelled accurately enough. An additional error to the characteristic of the calculated starting impedance, Fig. 52a, is caused by the resistive component and the temperature difference. The measurement was made for the motor at a stator-winding temperature of approximately 60°C, and the calculation temperature was 20°C. No temperature corrections have been made in the calculations.

To study more closely the calculated characteristic of the starting reactance, the characteristics of the significant components in the single-phase equivalent circuit, the reactances ($X_{\sigma S}$, $X_{h\delta}$, $X^*_{\sigma 1R}$ and $X^*_{\sigma 2R}$) and the rotor resistances (R^*_{1R} and R^*_{2R}), are presented in Fig. 53. All the characteristics are presented as per-unit values. The
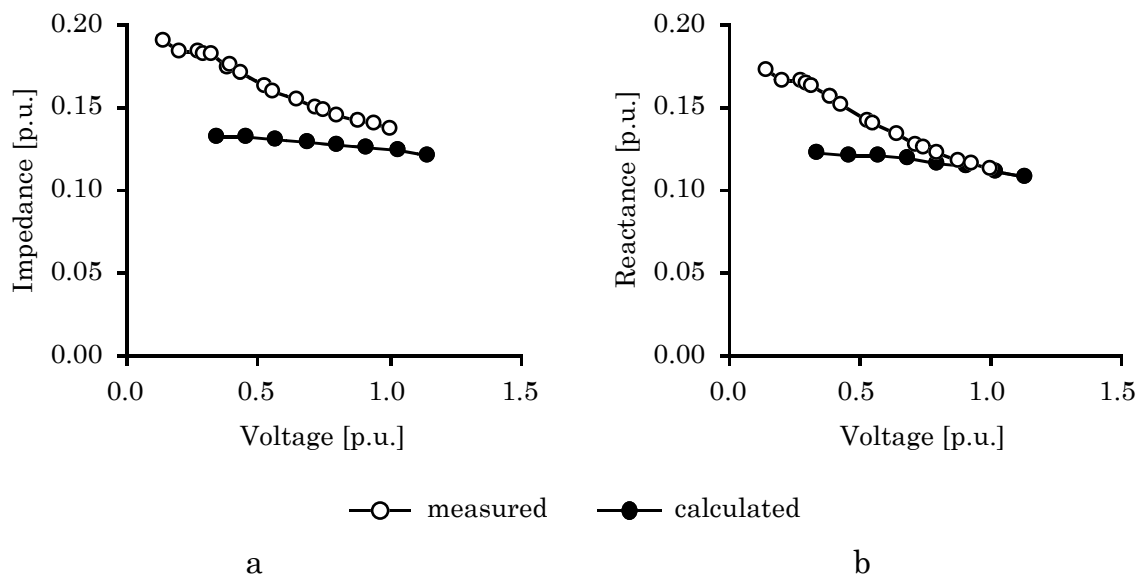

Fig. 52   The starting characteristics of the 15 kW motor.
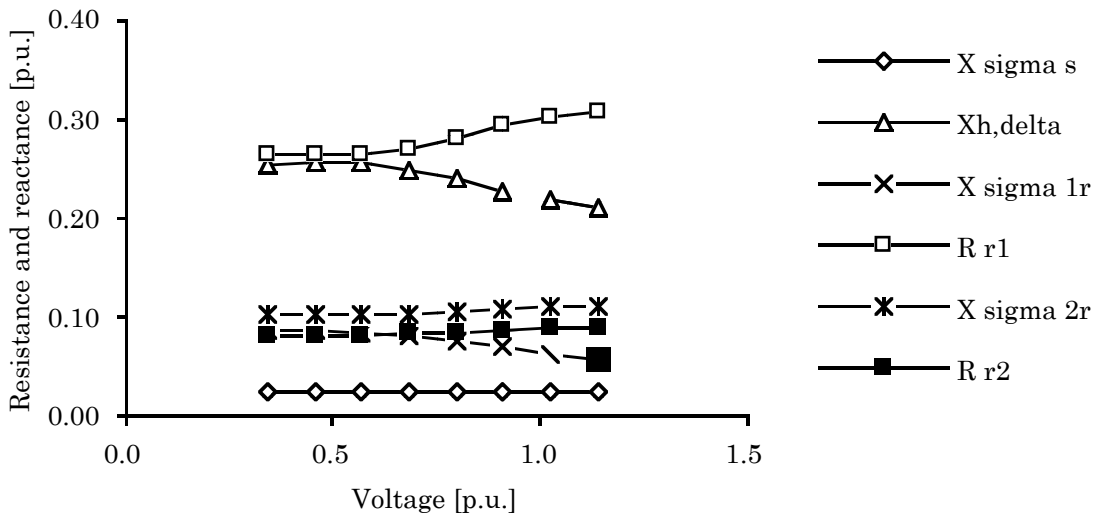*a)   The starting impedance and b) reactance as function of supply voltage.*

Fig. 53 Components of the single-phase equivalent circuit, as in Fig. 42. (15 kW)

reactances of air gap $X_{h\delta}$ and rotor slot opening $X_{\sigma1R}$ have saturating characteristics. The stator leakage reactance $X_{\sigma S}$ has an unsaturated characteristic. Its influence in the starting reactance is small. The slot opening reactances of rotor $X_{\sigma1R}$ and $X_{\sigma2R}$ have an opposite, compensating saturation-state.

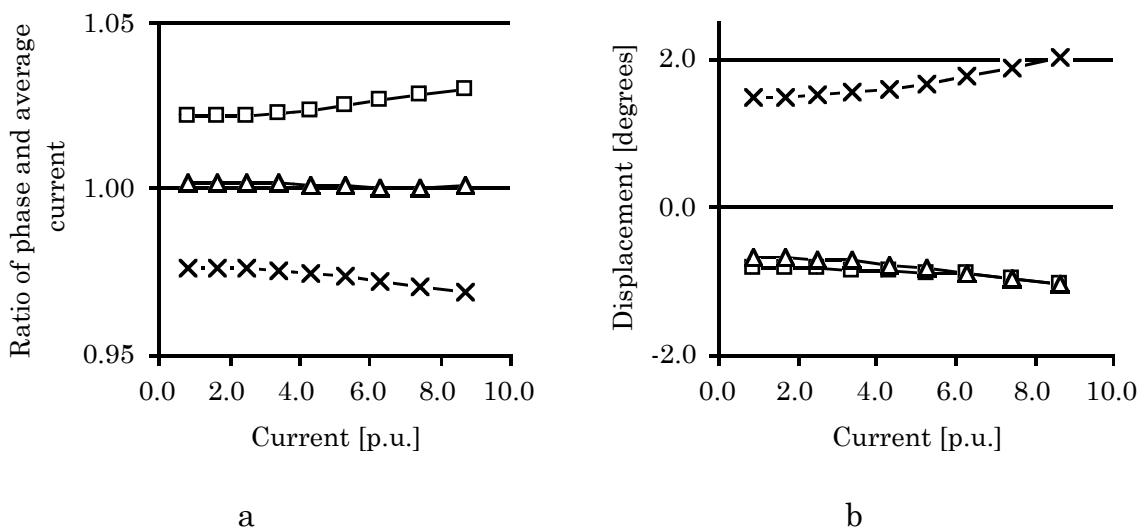The calculated winding currents, amplitudes and phase angles, are in Fig. 54.

a   b

Fig. 54 Calculation results of winding currents. (15 kW)
a) The values of the fundamental harmonic of currents in ratio to the average current.
b) The difference of the phase-shift angles of the fundamental harmonic of currents compared with the ideal 120° difference of the phases.

9.4   37 kW motor

The reluctance and electric models used in the study are presented for the stator in Fig. 46 and for the rotor in Fig. 50.

The layout of the stator model is the same as for the 15 kW motor.

In the rotor, the reduction was carried out in the lower bar of the slot (farthest from the air gap) and its parallel section in the tooth. Near the air gap, the rotor model has reluctance elements of the upper bar, the iron bridge between the slot and the air gap, and their parallel sections in the tooth. To model the current distribution inside the lower bar, the single bar division is not enough. To model the current distribution inside the upper bar, the number of bar divisions is low. The number of divisions is a compromise between the accuracy and the size of the model. The reduction has a small influence to the leakage flux modelling.

The energy distribution of the reluctance network is transferred to the components of the single-phase equivalent circuit, as in Fig. 42. The definition of components is based on Chapter 7. The equivalence of the energy component and the component in the single-phase equivalent circuit is presented in Table 4.

Table 4.   Energy components and their equivalence with the components of the single-phase equivalent circuit for the 37 kW motor, as in Fig. 42.

Components	$W_{\mathrm{m}r}$ and $W_{\mathrm{b}r}$ from regions	$W_{\mathrm{m}\varphi}$ and $W_{\mathrm{b}\varphi}$ from regions
Stator	Fig. 33	Fig. 33
$X_{\mathrm{h}S}$, $R_{\mathrm{fe,h}S}$	$E_{\mathrm{y}1}$, $E_{\mathrm{y}2}$, $E_{\mathrm{t}1}$, $E_{\mathrm{t}2}$, $E_{\mathrm{t}3}$	$E_{\mathrm{y}1}$, $E_{\mathrm{y}2}$
$X_{\sigma S}$, $R_{\mathrm{fe},\sigma S}$	$E_{\mathrm{s}1}$, $E_{\mathrm{s}2}$, $E_{\mathrm{s}3}$	$E_{\mathrm{t}1}$, $E_{\mathrm{t}2}$, $E_{\mathrm{t}3}$, $E_{\mathrm{s}1}$, $E_{\mathrm{s}2}$, $E_{\mathrm{s}3}$
Rotor	Fig. 37	Fig. 37
$X_{\mathrm{h}R}$, $R_{\mathrm{fe,h}R}$	$E_{\mathrm{y}1}$, $E_{\mathrm{y}2}$, $E_{\mathrm{t}1}$, $E_{\mathrm{t}2}$, $E_{\mathrm{t}3}$, $E_{\mathrm{t}4}$	$E_{\mathrm{y}1}$, $E_{\mathrm{y}2}$
$X_{\sigma 1R}$, $R_{\mathrm{fe},\sigma 1R}$	$E_{\mathrm{t}5}$, $E_{\mathrm{s}2}$, $E_{\mathrm{s}3}$	$E_{\mathrm{t}2}$, $E_{\mathrm{t}3}$, $E_{\mathrm{t}4}$, $E_{\mathrm{t}5}$, $E_{\mathrm{s}2}$, $E_{\mathrm{s}3}$
$X_{\sigma 2R}$, $R_{\mathrm{fe},\sigma 2R}$	$E_{\mathrm{s}1}$	$E_{\mathrm{t}1}$, $E_{\mathrm{s}1}$
Air gap		
$X_{\mathrm{h}\delta}$	E_δ	E_δ
	W_{e} from regions	
Rotor	Fig. 37	
R_{1R}	$E_{\mathrm{s}2}$, $E_{\mathrm{s}3}$	
R_{2R}	$E_{\mathrm{s}1}$	

The characteristics of the starting torque and current are presented in Figs. 55a and 55b. When taking into account the effect of the excluded end-winding reactance of the stator (3.2%) and assuming the balanced phase currents, the error in the characteristics of starting current is about 14% at the rated voltage. The inaccuracy of the calculation model may be seen from the characteristics of the starting reactance, Fig. 55d. At the lower voltages, the calculated starting reactance has higher values than measured. At the rated voltage, the characteristic approaches the measured one when taking into account the excluded end-winding reactance. In comparison with the 15 kW motor, the calculated characteristic of starting reactance has higher values in
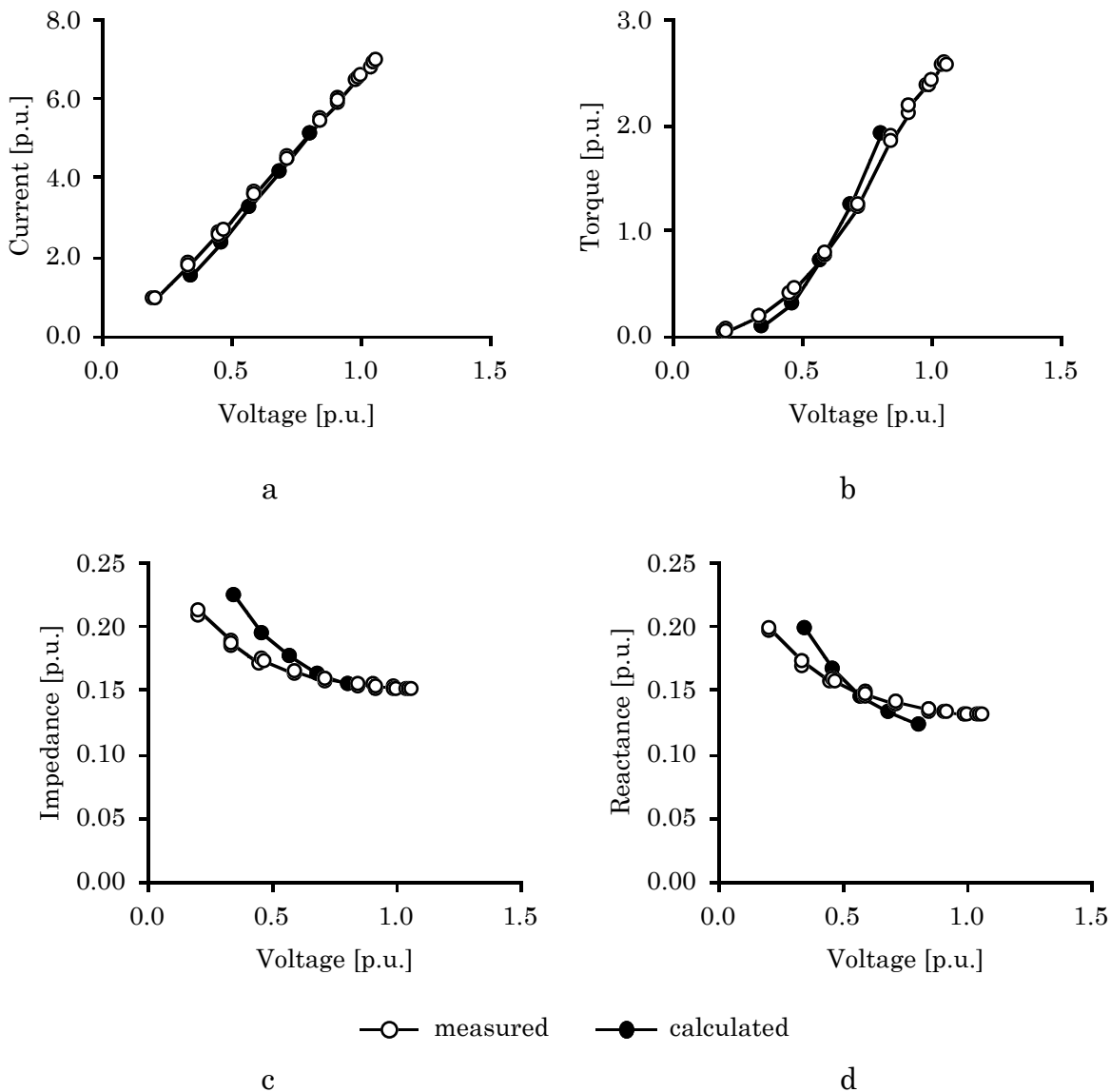

a

b

c

d

Fig. 55   The starting characteristics of the 37 kW motor.
a)   The starting current, b) torque, c) impedance, and d) reactance as function of supply voltage.

comparison with the measured characteristic. The saturation is modelled better in the 37 W motor, but the saturation is too steep. The calculated characteristic of starting impedance, Fig. 53c, has an additional error caused by the resistive component and the temperature difference. The measurement was made for the motor at a temperature of approximately 70°C and the calculation temperature was 20°C. No temperature corrections have been made.

The calculated winding currents, amplitudes and phase angles, are in Fig. 56. The currents differ from each other by amplitude and phase-shift angle. The comparison with the 15 kW motor shows that the difference is very large. It seems that only two phases give almost all the energy to the motor model. The reason for the big difference may be that the saturation directs the flux to a differently saturated flux path near to one of the phases. The reason from the modelling point-of-view may be that the "saturation" is caused by a wrong iteration value of time step or in the initial state calculation. A wrong magnetic nodal potential would direct the calculation to saturate the region. The initial state was calculated using the sinusoidal approximation for the model quantities. The unbalance of the currents was already there. No other proof of the unbalance has been found. In the measurement, there was no unbalance.

The characteristics of the significant components in the single-phase equivalent circuit, the reactances ($X_{\sigma S}$, $X_{h\delta}$, $X^*_{\sigma 1R}$ and $X^*_{\sigma 2R}$) and the resistances (R^*_{1R} and R^*_{2R}),
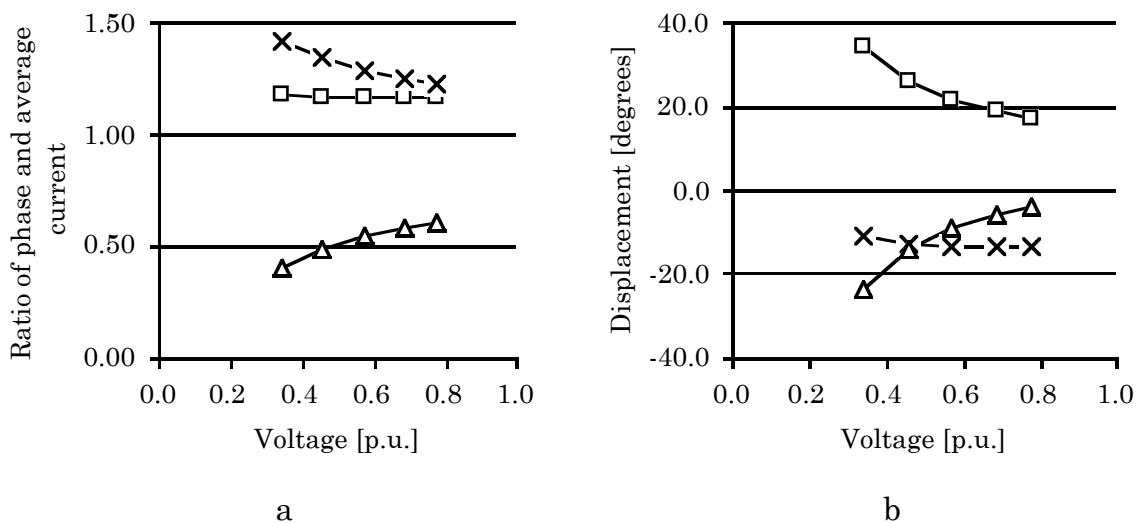

a   b

Fig. 56   Calculation results of winding currents. (37 kW)
a) The values of the fundamental harmonic of currents in ratio to the average current.
b) The difference of the phase-shift angles of the fundamental harmonic of the currents compared with the ideal 120° difference of the phases.

are presented in Fig. 57:

- The characteristics of the resistances R_{1R} and R_{2R} are decreasing as a function of voltage. The characteristics of the reactance X_{hR} is on the level 0.76 p.u. without any saturation. The resistance R_{2R} of the lower bar should be equal as a function of current with the reactance X_{hR}. That is satisfied.
- The resistance R_{1R} of the upper bar is the image of the serial connection of reactance $X_{\sigma 2R}$ and the parallel X_{hR} and R_{2R}. The decreasing of the resistance R_{1R} satisfies the considerable saturation of the reactance $X_{\sigma 2R}$ because the parallel connection is about constant. That is satisfied.
- The reason for the high saturation of the starting reactance is the high saturation of the reactance $X_{\sigma 2R}$. A question is why the reactance $X_{\sigma 2R}$ is saturating more than $X_{\sigma 1R}$. If the modelling will be correct it shouldn't. To study the characteristics more closely, the distribution of magnetic energy in the rotor is presented for the rotor reactances in Fig. 58.
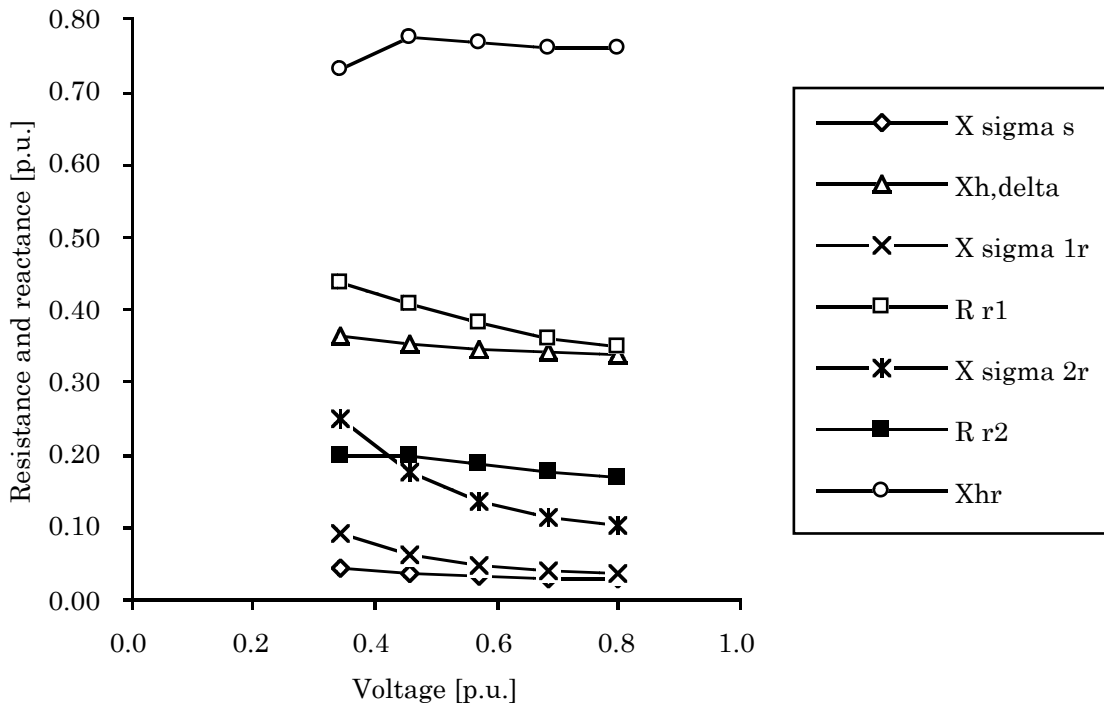

Fig. 57 Components of the single-phase equivalent circuit, as in Fig. 42. (37 kW)

The magnetic energy of the rotor is associated with the reactances $X_{\sigma 1R}$ and $X_{\sigma 2R}$, as in Fig. 58. The reactance X_{hR} has about 10 to 15% of the energy.

- The energy distribution associated with the reactance X_{hR} is presented in Fig. 59. The proportion of energy in region E_{t1} (the tooth parallel to lower bar) grows to level 86% of the total energy of reactance X_{hR}. The energy associated to the yoke is minimal, as expected. This proves that either the yoke saturates or the flux goes through the lower bar.
- The energy in reactance $X_{\sigma 2R}$ is totally associated in the lower bar and is not presented here.
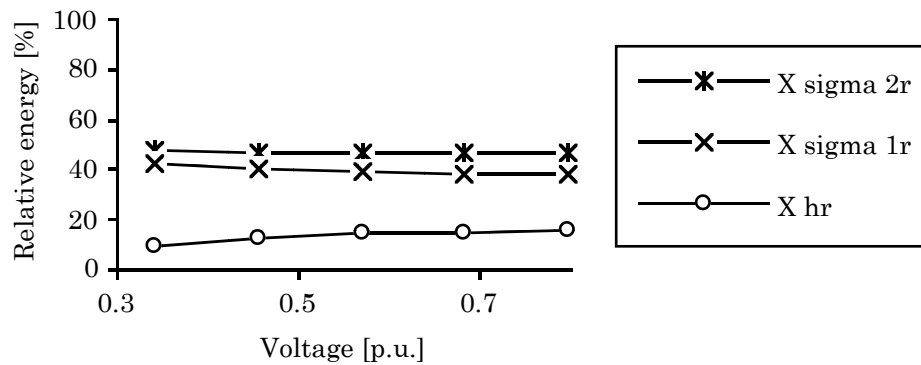

Fig. 58   The distribution of magnetic energy in the rotor. (37 kW)
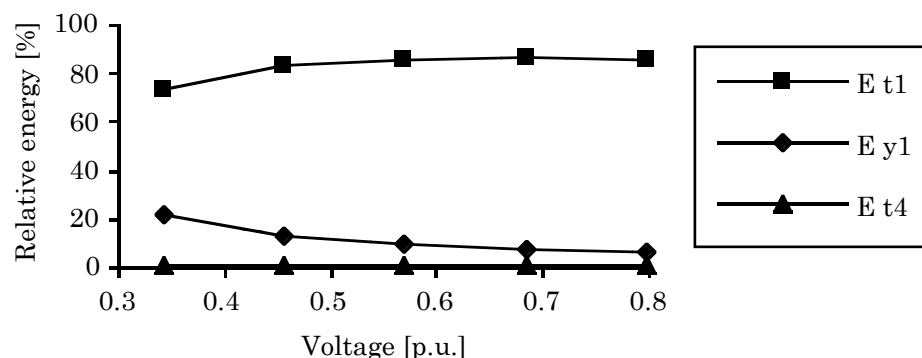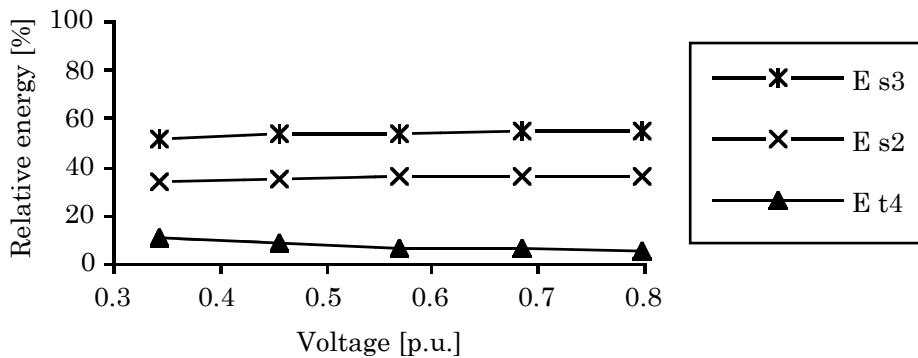*Proportions of the magnetic energy included in the components expressed as percentages.*

Fig. 59   The distribution of magnetic energy in the rotor. (37 kW)
Proportions of the magnetic energy in the flux-path regions connected to the reactance
X_{hR} expressed as percentage.

- The energy distribution associated to the reactance $X_{\sigma 1R}$ is presented in Fig. 60. The proportion of the energy associated in the region E_{t5} (bridge between the air gap and slot) is not presented because it is in range of 1 to 3%. The energy of the reactance is totally associated to the upper bar and about 70% of the bar energy to the element nearest the air gap. The flux does not flow through the region E_{t5} as it should. The flux flow near the air gap does not satisfy the experience.

It seems that the flux flow in the rotor is going along the tooth and dividing to cross both the bars. The damping of the upper cage does not direct the flux to the iron bridge near the air gap. The reason for the big difference between the stator currents cannot be that the saturation directs the flux to a differently saturated flux path near to one of the phases. The analysis of energy distribution means that the flux goes either saturating the yoke or saturating the tooth when crossing the slot. The energy distribution of the reactances $X_{\sigma 1R}$ and $X_{\sigma 2R}$ do not satisfy the tooth saturation. The flux has to flow along the yoke. The flux does not short-circuit the magnetic circuit near the stator. The reason for the unbalance may be the different air-gap reluctance for the winding phases, caused by the slotting, or the saturation model used in the reluctance elements together with some wrong potential value during the iteration.

Fig. 60   The distribution of magnetic energy in the rotor. (37 kW)
Proportions of the magnetic energy in the flux-path regions connected to the reactance $X_{\sigma 1R}$ expressed as percentage.

9.5 Conclusion

In this chapter, the reluctance network analysis was carried out for two demonstrator motors, one with a single-cage rotor and the other with a double-cage rotor. The developed computer program package of a universal reluctance network was used in the calculation. The effect of saturation was studied in both of the motors. The single-phase equivalent circuit was defined from the reluctance network results at different supply voltages. In the slotting region, the stator and rotor models of both of the motors were reduced combining the flux-path regions near the yoke. That decreased the number of tooth and slot regions used in the analysis. The accuracy near the air gap was not affected.

In the study of the 15 kW motor, the calculated torque and current showed a reasonable agreement with the measured values. The error in the starting current was about 12% at the rated voltage without taking into account the effect of the missing end-winding reactance of the stator. At the lower voltages, the calculated starting reactance was smaller than the measured reactance. The difference between the characteristics was smaller than the excluded end-winding reactance. At the rated voltage, the calculated value did not saturate enough and the difference between the characteristics disappeared. The difference was equal the end-winding reactance. The saturation was not modelled accurately enough.

In the study of the 37 kW motor, the calculated torque and current showed an error of 14% in the starting current at the rated voltage when the end-winding reactance of the stator (3.2%) was included and by assumption of balanced phase currents. At the lower voltages, the calculated starting reactance had higher values than the measured reactance. At the rated voltage, the characteristic approached the measured one when the end-winding reactance was included. In comparison with the 15 kW motor, the calculated characteristic of starting reactance had higher values in comparison with the measured characteristic. The saturation was modelled better in the 37 kW motor, but the saturation was too steep.

The phase currents had a big difference from each other by amplitude and phase-shift in the 37 kW motor in comparison with the 15 kW motor. In the measurement, there was no unbalance. The initial state for the time-stepping method was calculated using the sinusoidal approximation for the model quantities. The unbalance of the currents was already there.

The distribution of magnetic energy was studied for the rotor reactances in the 37 kW motor. The magnetic energy of the rotor was associated with the leakage reactances $X_{\sigma 1R}$ and $X_{\sigma 2R}$. The energy of the reactance was totally associated to the bars and about equally between the upper and lower bars. About 70% of the upper bar energy was associated to the bar element nearest the air gap. The flux did not flow through the iron bridge between the air gap and slot because its portion of the energy was in the range of 1 to 3%. As a conclusion, the reason for the current unbalance in stator might be the different air-gap reluctance for the winding phases, caused by the slotting, or e.g. the saturation (the derivative of the reluctivity curve) used in the reluctance elements together with some wrong potential value during the iteration.

10 SUMMARY OF CONCLUSIONS

In the study, a universal reluctance network was defined to analyse an electrical machine. The components, construction rules, and equations of the reluctance network were specified. The equations were presented to form the components of a single-phase electric equivalent circuit from the results of the reluctance network. A computer program package was developed to solve the two-dimensional reluctance network. As a demonstration, the flux and current distributions were calculated for two cage induction motors, one with a single-cage and the other with a double-cage rotor. From the analysis results, a single-phase equivalent circuit was defined to calculate the locked-rotor current in the steady-state period after the inrush current, at the moment when the rotor starts to rotate.

This study consists of ten chapters. In Chapter 1, a brief introduction about methods of modelling magnetic fields, problems of single-phase equivalent circuits and a summary of previous studies to connect special demands to the single-phase equivalent circuit was given.

In Chapter 2, the rules for the construction and the components of the universal reluctance network were specified. The basic elements of the network, the reluctance element and the electric element, were introduced.

The machine cross-section was divided to slot pitch sectors. The reluctance model for the slot pitch was constructed using the reluctance and electric elements representing the flux-path regions. The slot-pitch reluctance models of the stator and rotor, and the air-gap model form the reluctance model of the machine. The electric elements of the flux-path regions form the electric models of the windings. Together, the reluctance model and the electric models are the reluctance network of the electrical machine. The MMF sources of the reluctance model and the EMF sources of the electric model provide the energy transfer between the models.

In Chapter 3, the system equations of the universal reluctance network were specified. The system equations of the universal reluctance network were related to the electric model of the windings and the reluctance model of the machine.

For the stator winding, the voltage equations were presented connecting the electric model of the distributed winding to the electric supply. For the rotor winding, the voltage equations were presented connecting the electric elements in the cage winding.

For the reluctance model, the flux-balance equations were presented for the magnetic scalar potentials of the nodes in the reluctance element. The magnetic energy stored in the reluctance element, the flux density and air-gap torque basing on the magnetic energy, and the equations of the iron losses were presented.

In Chapter 4, the magnetic properties of the universal reluctance network were introduced. The reluctivity function using the material *BH*-characteristic and the reluctivity functions for the sinusoidal (phasor) magnetic quantities were introduced. The methods used to determine the influence of the flux-path geometry was developed for the variable width of the tooth, the uneven flux distribution of yoke, and the saturated tooth tip on the slot opening.

In Chapter 5, the magnetic capacitance for the universal reluctance network was specified. The magnetic capacitance was used as an equivalent for the eddy-current losses. The magnetic capacitance was additionally defined for the eddy-current losses in the core. The instructions for the use of magnetic capacitances were given.

In Chapter 6, the system equations for time-stepping and sinusoidal-approximation analysis were collected, and the method for matrix calculation was introduced. The reluctance model (MEC) and the finite element method (FEM) were compared according to how they solve the iterative calculation process. A discussion was presented about the sparsity of the matrix and the iteration speed.

In Chapter 7, the method was presented to construct a single-phase equivalent circuit from the results of the analysis using reluctance network. The energy distribution was specified using the time-stepping analysis of the reluctance network. The heat energy dissipated in the rotor winding was calculated from the resistive losses in the electric elements of the winding model. The iron losses were calculated using the Fourier-series of the flux-density variation in the reluctance elements. The magnetic energy distribution was calculated from the magnetic energy stored in the reluctance elements. The energy distribution of the whole reluctance model was collected in the reference slot-pitch. The components of the single-phase equivalent circuit were specified using the energy components of the reference slot-pitch. The position in which an equivalent circuit component was substituted in the single-phase equivalent circuit was dependent on the flux-path region in the reference slot-pitch where the energy was collected. Every region might have an own resistance and reactance component in the single-phase equivalent circuit.

In Chapter 8, the developed computer program package of the universal reluctance network was introduced. The input data was in three input files. The details of the stator and rotor construction were in the stator and rotor files. The operating instructions were in the third file. The program constructed the reluctance network and solved the system equations. The output of the program was saved in the files and controlled by the user. According to operating instructions, the results for the initial state, for the last time step, and for the time-stepping were saved to their own files. The list of the optional output files was given.

In Chapter 9, the reluctance network analysis was carried out for two demonstrator motors, one with a single-cage rotor and the other with a double-cage rotor. The developed computer program package of a universal reluctance network was used in the calculation. The effect of saturation was studied in both of the motors. The single-phase equivalent circuit was defined from the reluctance network results at different supply voltages. In the slotting region, the stator and rotor models of both the motors were reduced combining the flux-path regions near the yoke. That decreased the number of tooth and slot regions used in the analysis. The accuracy near the air gap was not affected.

In this study, the reluctance network was limited so as to model only two-dimensional flux distributions. The three-dimensional leakage-flux paths of the end-windings were outside the scope of this study. The reactances of these paths might be included as extra leakage inductances to the single-phase equivalent circuit.

In the study of the 15 kW motor, the calculated torque and current showed a reasonable agreement with the measured values. The error in the starting current was about 12% at the rated voltage without taking into account the effect of the missing end-winding reactance of the stator. At the lower voltages, the calculated starting reactance was smaller than the measured reactance. The difference between the characteristics was smaller than the excluded end-winding reactance. At the rated voltage, the calculated value did not saturate enough and the difference between the characteristics disappeared. The was equal the end-winding reactance. The saturation was not modelled accurately enough.

In the study of the 37 kW motor, when the excluded end-winding reactance of the stator (3.2%) was included, there was an error of 14% in the starting current at the rated voltage. At the lower voltages, the calculated starting reactance had higher values than the measured reactance. At the rated voltage, the characteristic approached the measured one when the end-winding reactance was included. In

comparison with the 15 kW motor, the calculated characteristic of starting reactance had higher values in comparison with the measured characteristic. The saturation was modelled better in the 37 kW motor, but the saturation was too steep.

The phase currents had a big difference from each other by amplitude and phase-shift in the 37 kW motor in comparison with the 15 kW motor. In the measurement, there was no unbalance. The initial state for the time-stepping method was calculated using the sinusoidal approximation for the model quantities. The unbalance of the currents was already there.

The distribution of magnetic energy was studied for the rotor reactances in the 37 kW motor. The magnetic energy of the rotor was associated with the leakage reactances of rotor. The energy of the reactance was totally associated to the bars and about equally between the upper and lower bars. About 70% of the upper bar energy was associated to the bar element nearest the air gap. The flux did not flow through the iron bridge between the air gap and slot because its portion of the energy was in the range of 1 to 3%. As a conclusion, the reason for the current unbalance in stator might be the different air-gap reluctance for the winding phases, caused by the slotting, or e.g. the saturation (the derivative of the reluctivity curve) used in the reluctance elements together with some wrong potential value during the iteration.

The reluctance network represents the geometry of the machine cross-section. It saves the information of geometry into the reluctances. The reluctances can be connected in parallel or in series to make a block having only one common reluctance. Nevertheless, the information of the geometry remains. The reluctance network may have a future as an analysing tool in research, particularly in the operational simulation of an electrical machine. A simple network can solve accurately enough the simulation more quickly than a small model using FEM.

In spite of that the results in the analysis were not satisfactory in the saturation modelling, the analysis indicated the possibilities of the reluctance network in the analysis of cage induction motors.

REFERENCES

Agarwal P., Alger P., 1961. Saturation factors for leakage reactance of induction motors. *Transaction of AIEE*, February 1961, pp. 1037-1042.

Ah-Jaco A., Makki A., Yahoui H., Grellet G., 1998. Modelling of the three phase asynchronous motor. Application to magnetic faults diagnostic. *Proceedings of ICEM*, Istanbul, Turkey, 2-4 September 1998, pp. 443-447.

Akbaba M., Fakhro S., 1987. Saturation effects in three-phase induction motors. *Electrical Machines and Power Systems*, 1987, No. 12, pp. 179-193.

Andresen E., Müller W., 1983. Berechnung der Anlaufdaten von Asynchron-Käfigläufermotoren verschiedener Stabformen mit der Methode der finiten Differenzen. *Archiv für Elektrotechnik*, 1983, Vol. 66, pp. 179-185.

Andresen E., Kruckow W., Pfeiffer R., 1986. The effect of air gap increase on mains and inverter supplied induction machines. *Proceedings of International Conference on Evolution and Modern Aspects on Induction Machines*, Torino, Italy, 8-11 July 1986, pp. 203-209.

Andria G., Dell'Aquila A., Salvatore L., 1986. Effect of saturation on harmonic impedances of inverter-fed induction motors. *Proceedings of International Conference on Evolution and Modern Aspects on Induction Machines*, Torino, Italy, 8-11 July 1986, pp. 115-122.

Angst G., 1963. Saturation factors for leakage reactance of induction motors with skewed rotors. *IEEE Transactions on Power Apparatus and Systems*, October 1963, pp. 716-725.

Arnold E., laCour J. L., 1909. Die Asynchronen Wechselstrommaschinen IV. Teil I. Verlag von Julius Springer, Berlin, Germany, 1909, 601 p.

Atallah K., Zhu Z., Howe D., 1992. The prediction of iron losses in brushless permanent magnet DC motors. *Proceedings of ICEM*, Manchester, United Kingdom, 15-17 September 1992, pp. 814-818.

Athani V., Walivadekar V., 1994. Equivalent circuit for switched reluctance motor. *Electrical Machines and Power Systems*, 1994, No. 22, pp. 533-543.

Atkins W., 1958. An improved electromagnetic analogue. *Proceedings of IEE*, 1958, Vol. 105C, pp. 151-154.

Beier E., 1964. Die Vorausberechnung der Betriebskennlinien der Asynchronmaschine unter Berücksichtigung der Eisensättigung. Dissertation, München, Germany, 1964, 155 p.

Bolte E., 1981. Berechnung von Ausgleichsvorgängen beim Asynchronmotor mit Hochstabläufer unter Berücksichtigung der Stromverdrängung. *Archiv für Elektrotechnik*, 1981, Vol. 63, pp. 233-245.

Brown J., Kovacs K., Vas P., 1983. A method of including the effects of the main flux path saturation in the generalized equations of AC machines. *IEEE Transactions on Power Apparatus and Systems*, 1983, Vol. 102, No. 1, pp 96-103.

Chalmers B., Richardson J., 1966. Investigation of high-frequency no-load losses in induction motors with open stator slots. *Proceedings of IEE*, 1966, Vol. 113, No. 10, pp. 1597-1605.

Chalmers B., Dodgson R., 1969. Saturated leakage reactance of cage induction motors. *Proceedings of IEE*, 1969, Vol. 116, No. 8, pp. 1395-1404.

Ciosk K., Gierczak E., 1998. Analysis of electromagnetic field in a disk induction motor with double-sided stator and twin rotors using a 3-D reluctance network method. *Proceedings of ICEM*, Istanbul, Turkey, 2-4 September 1998, pp. 286-289.

Dudzikowski I., 1994. Method of calculating magnetic circuit of DC machines excited by permanent magnets. *Proceedings of ICEM*, Paris, France, 5-8 September 1994, pp. 571-576.

Ferreira de Jesus J., 1988. A model for saturation in induction machines. *IEEE Transactions on Energy Conversion*, 1988, Vol. 3, No. 3, pp. 682-687.

Fritz W., 1989. Magnetische Spannung im Ständerjoch von Drehfeldmaschinen - Prüfung einer klassischen Theorie mit Hilfe eines numerischen Programms. *ETZ Archiv*, 1989, Vol. 11, No. 11, pp. 343-349.

Fujimaki T., Miyashita O., 1985. Calculation of characteristics of the inverter-fed squirrel-cage induction motor. *Proceedings of* EPE, Brussels, Belgium, 16-18 October 1985, pp. 3.357-3.362.

Gagnon R., Viarouge P., Kamwa I., Le-Huy H., 1993. Calculation method of saturated magnetic circuits for the CAD of electrical machines. *Proceedings of* IMACS-TCI, Montreal, Canada, 7-9 July 1993, pp. 613-618.

Ganji A., Guillaume P., Pintelon R., Lataire P., 1996. Identification of the induction motor dynamic and static inductance with regard to saturation. *Proceedings of IEE - Power Electronics and Variable Speed Drives*, 1996, pp. 42-47.

Gibbs W., 1947. Tooth-ripple losses in unwound pole-shoes. *Journal of IEE*, 1947, Vol. 94, Part 2, pp. 2-12.

Gibbs W., 1948. Induction and synchronous motors with unlaminated rotors. *Journal of IEE*, 1948, Vol. 95, pp. 411-420.

Gynt S., Schuisky W., 1958. Berechnung der magnetischen Spannung für Joch und Zähne. *ETZ-A*, 1958, Vol. 79, No. 20, pp. 780-784.

Gyselinck J., Vandevelde L., Melkebeek J., 1998. Coupling finite elements and magnetic and electrical networks in magnetodynamics. *Proceedings of ICEM*, Istanbul, Turkey, 2-4 September 1998, pp. 1431-1436.

Hamels D., 1984. Application of different equivalent circuits in determining induction machine performance in practical situations. *Proceedings of ICEM*, Lausanne, Switzerland, 18-21 September 1984, pp. 380-383.

Hasuike K., 1984. A study of the reduction of harmonic rotor copper losses of the three-phase squirrel cage induction motor driven by inverter. *Electrical Engineering in Japan*, 1984, Vol. 104, No. 4, pp. 124-129.

Healey R., Williamson S., Smith A., 1994. Improved rotor models for vector controllers. *IEEE IAS annual conference*, Denver, 2-5 October 1994, pp. 1-10.

Hrusovsky F., Hrabovcova V., 1995. Investigation of iron loss and magnetic field distribution in inverter fed induction motor. *Proceedings of Transcom*, Zilina, Slovakia, 28-30 June 1995, pp. 153-156.

Iwata K., 1984. Influences of cast rotor slot size on a slot constant and motor characteristics. *Electrical Engineering in Japan*, 1984, Vol. 104, No. 5, pp. 65-74.

Jagiela K., 1985. Le facteur de deplacement d'un courant du moteur asynchrone profondement encoche alimente par l'onduleur thyristorique voltmetrique. *Proceedings of EPE*, Brussels, Belgium, 16-18 October 1985, pp. 3.81-3.87.

Jimoh A., Findlay R., Poloujadoff M., 1985. Stray losses in induction machines. Part I, definition, origin and measurement. Part II, calculation and reduction. *IEEE Transactions on Power Apparatus and Systems*, 1985, Vol. 104, No. 6, pp. 1500-1511.

Kamoun M., Poloujadoff M., 1986. Accounting for saturation and cross-saturation in a dynamic stability study. *Electrical Power Systems Research*, 1986, No. 10, pp. 55-61.

Levi E., 1997. General method of magnetising flux saturation modelling in d-q axis models of double-cage induction machines. *Proceedings of IEE - Electrical Power Applications*, 1997, Vol. 144, No. 2, pp. 101-109.

Li J-C., 1996. Analytical model of cross-magnetizing effect in saturated synchronous machines. *Electric Power Systems Research*, 1996, Vol. 37, pp. 19-28.

Luomi J., Niemenmaa A., Arkkio A., 1986. On the use of effective reluctivities in magnetic field analysis of induction motors fed from a sinusoidal voltage source. *Proceedings of ICEM*, München, Germany, 8-10 September 1986, pp. 706-709.

Löser F., Sattler Ph., 1986. Additional losses of induction motors - experimental results and better theoretical approach. *Proceedings of ICEM*, München, Germany, 8-10 September 1986, pp. 324-327.

Moriyasu S., Endo K., 1980. The ripple loss at the rotor surface of synchronous machines. *IEEE Transactions on Power Apparatus and Systems*, 1980, Vol. 99, November/December, pp. 2393-2399.

Mouly V., Subrahmanyam V., Rao G., 1983. Fluxes and currents in a skewed rotor induction motor. *Electrical Machines and Power Systems*, 1983, No. 8, pp. 233-245.

Mukherjee S., Adams G., Hoft R., 1989. FEM analysis of inverter-induction motor, rotor conduction losses. *IEEE Transactions on Energy Conversion*, 1989, Vol. 4, No. 4, pp. 671-680.

Oberretl K., 1963. Die Ermittlung von magnetischen Feldern, Wirbelströmen und Kräften in komplizierten Fällen durch Simulation an Gittermodellen. *Archiv für Elektrotechnik*, 1963, Vol. 48, No. 5, pp. 297-313.

Ostovic V., 1989a. Dynamic of Saturated Electric Machines. Springer-Verlag, New York, USA, 1989, 445 p.

Ostovic V., 1989b. A novel method for evaluation of transient states in saturated electric machines. *IEEE Transactions on Industry Applications*, 1989, Vol. 25, No. 1, pp. 194-199.

Paszek W., 1981. Transientes Verhalten der Induktionsmaschine mit Hochstabläufer. *Archiv für Elektrotechnik*, 1981, Vol. 63, pp. 77-86.

Paszek W., Pawelek Z., 1984. Ersatzschaltung für transiente Vorgänge der Induktionsmaschine mit Keilstabläufer. *Archiv für Elektrotechnik*, 1984, Vol. 67, pp. 259-264.

Perho J., 1993. Oikosulkumoottorin sijaiskytkennän laskeminen reluktanssiverkolla. (Calculation of an equivalent circuit of cage-induction motor by reluctance network method, in Finnish). Licentiate Thesis, Helsinki University of Technology, Laboratory of Electromechanics, Espoo, Finland, Report 40, 1993, 74 p., (In Finnish).

Perho J., Ritchie E., 1995. A Motor operation analysis using reluctance net. *Proceedings of Stockholm Power Tech Conference, Electrical Machines and Drives*, Stockholm, Sweden, 18-22 June 1995, pp. 356-361.

Perho J., Ritchie E., 1996. Analysis of a permanent magnet machine using reluctance network. *Proceedings of ICEM*, Vigo, Spain, 10-12 September 1996, Vol. I, pp. 44-48.

Qishan G., 1986. Saturation harmonics in induction machines. *Proceedings of International Conference on Evolution and Modern Aspects on Induction Machines*, Torino, Italy, 8-11 July 1986, pp. 264-271.

Rasmussen C. B., 1996. Modelling and simulation of surface mounted PM motors. PhD Thesis, Aalborg University, Institute of Energy Technology, Denmark, 1996, 206 p.

Rasmussen C., Ritchie E., 1997. Improved reluctance-mmf network for calculation of magnetic field distribution in surface-mounted permanent-magnet motors. *Electromotion*, 1997, No. 4, pp. 55-61.

Richter E., Chari M., Tandon S., 1981. Studies of magnetic fields in electrical machines by means of finite element analysis. *Electric Machines and Electromechanics*, 1981, No. 4, pp. 297-306.

Richter R., 1936. Electrische Maschinen IV. Verlag von Julius Springer, Berlin, Germany, 1936, 440 p.

Richter R., 1951. Elektrische Maschinen I. Zweite Auflage, Verlag Birkhäuser, Basel, Germany, 1951, 630 p.

Roberts J., 1960. Analogue treatment of eddy-current problems involving two-dimensional fields. *Proceedings of IEE*, 1960, Vol. 107C, pp. 11-18.

Roberts J., 1962. Analogue treatment of eddy-currents and magnetic flux penetration in saturated iron. *Proceedings of IEE*, 1962, Vol. 109C, pp. 406-411.

Rogers G., Benaragama D., 1978. An induction motor model with deep-bar efect and leakage inductance saturation. *Archiv für Electrotechnik*, 1978, Vol. 60, pp. 193-201.

Savelainen J., 1980. Analytical calculation of saturable leakage reactances of an induction motor. *Electric Machines and Electromechanics*, 1980, No. 5, pp. 211-224.

Sewell P., Bradley K., Clare J., Wheeler P., Ferrah A., Magill R., Sunter S., 1998. Dynamic reluctance mesh modelling of induction motors. *Proceedings of ICEM*, Istanbul, Turkey, 2-4 September 1998, pp. 1324-1329.

Silvester P., 1967. Network analog solution of skin and proximity effect problems. *IEEE Transactions on Power Apparatus and Systems*, 1967, Vol. 86, No. 2, pp. 241-247.

Sliwinski T., 1987. Electromagnetic field in slots of electrical machines. *Journal of Prace Institutu Electrotechniki*, 1987, Vol. 147, pp. 99-109.

Udayagiri M., Lipo T., 1989. Simulation of inverter fed induction motors including core losses. *Proceedings of IEEE Industrial Electronics Conference*, Philadelphia, USA, 6-10 November 1989, Vol. I, pp. 232-237.

Vandevelde L., Gyselinck J., Melkebeek J., 1998. Electromechanical analysis of vibrations and noise of squirrel-cage induction motors. *Proceedings of ICEM*, Istanbul, Turkey, 2-4 September 1998, pp. 496-501.

Vogt K., 1983. Elektrische Maschinen. VEB Verlag Technik, Berlin, Germany, 1983, 500 p.

Wang R., Gieras J., 1998. Analysis of characteristics of a permanent magnet hybrid linear stepping motor. *Proceedings of ICEM*, Istanbul, Turkey, 2-4 September 1998, pp. 833-838.

Weh H., 1957. Über die Berechnung magnetischer Spannungen in hochgesättigten Jochen von Drehstrommaschinen. *Archiv für Electrotechnik*, 1957, Vol. 43, pp. 77-94.

Xiaogang C., Shixiang N., Jin H., 1995. Study of saturated squirrel cage induction machine by means of MEC method. *Proceedings of CICEM*, Hangzhou, China, 31 August - 2 September 1995, pp.912-915.